CHAPTER 6

CASE STUDY

A magnetotelluric (MT) survey was conducted along the road between Sishen and Keimoes in the Northern Cape Province of South Africa. It followed the route of a deep seismic reflection survey that was carried out during 1989 on behalf of the Geological Survey and the National Geophysics Programme by Geoseis (Pty) Ltd. of South Africa. The aim of the MT survey was twofold:

- Compare the results obtained by the two methods to determine whether it would be beneficial to do a magnetotelluric survey prior to a deep reflection seismic survey in order to locate areas of interest. This would be of economic interest since a deep reflection seismic survey costs considerably more than a magnetotelluric survey.
- Shed light on a number of interesting features that is visible on the reflection data.

The statistical techniques discussed in the previous chapter were applied to the data.

6.1. SURVEY LOCATION

Eleven sounding stations were positioned along the Sishen - Keimoes road at roughly 20km intervals. Figure 6.1 shows the location of the survey area in South Africa.

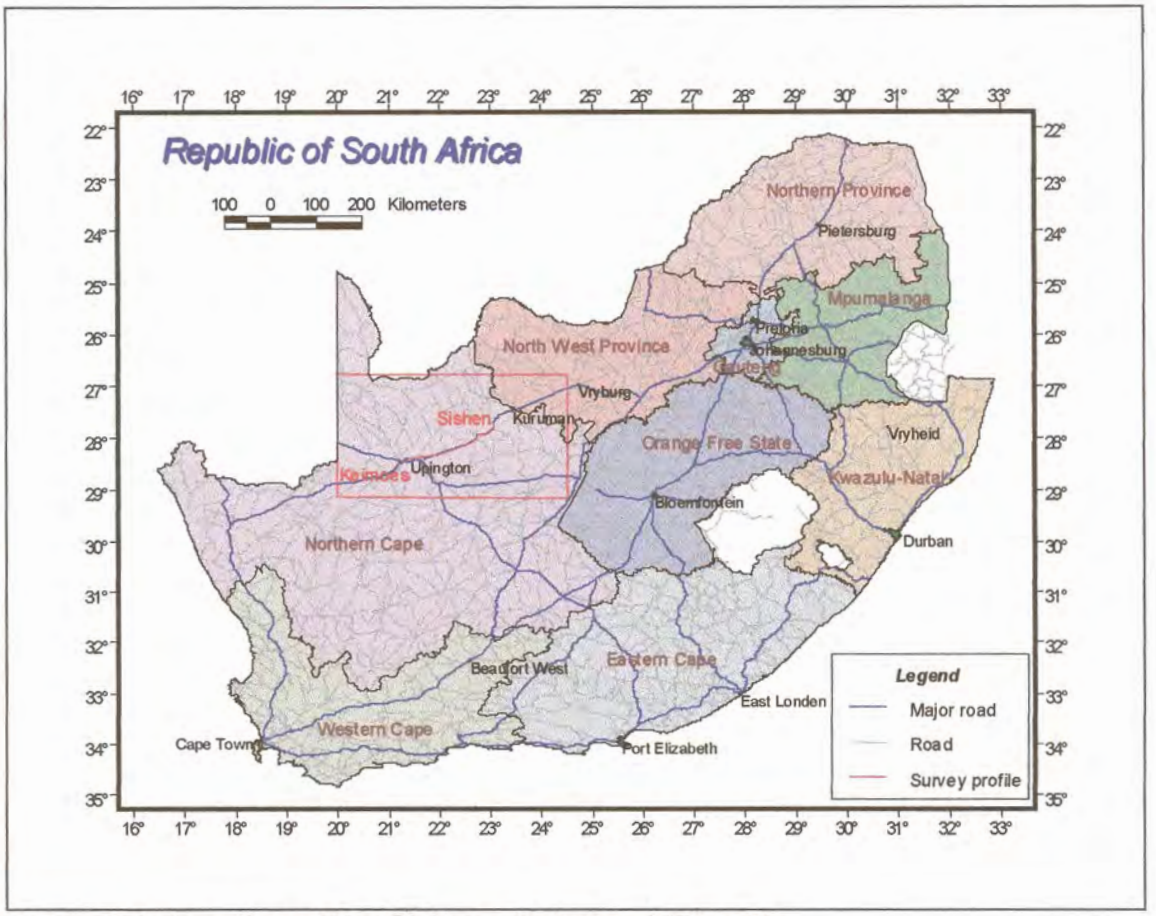

Figure 6.1. Location of the Sishen - Keimoes MT profile.

The Northern Cape Province is an arid region inhabited mainly by farming communities. Many of the farms near Upington and Keimoes are cultivated by vineyards and use electricity as power source for their irrigation systems. This acts as a source of artificial noise on the magnetotelluric data. A large open cast iron ore mine located at Sishen ships ore to Saldanha on the west coast via an electrical railway line. The railway line produces noise with a frequency of 15.6 Hz.

6.2. GENERAL GEOLOGY OF THE STUDY AREA

Figure 6.2 shows the general geology of the study area extracted from the 1:1 000 000 geological map (Keyser, 1997).

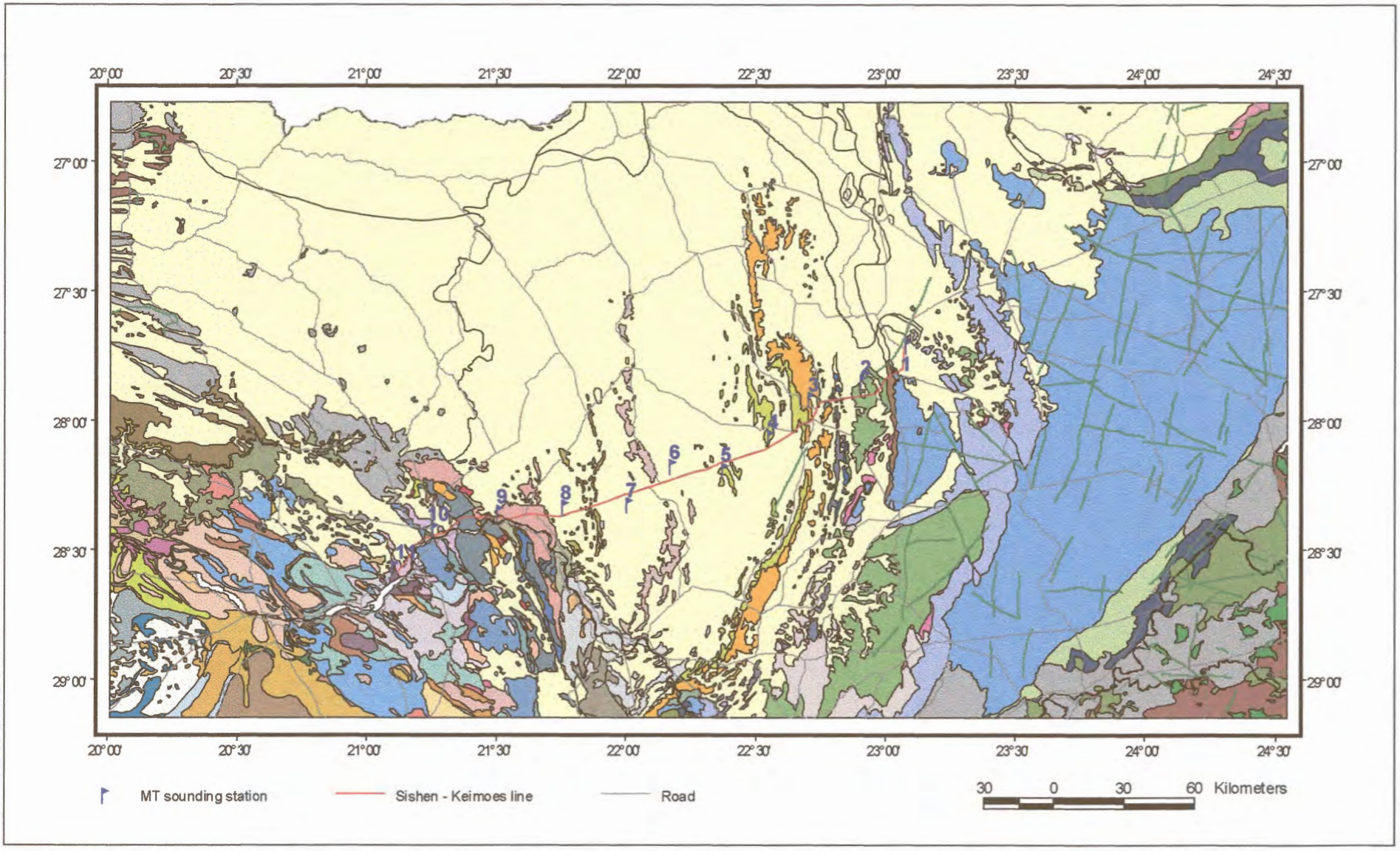

Figure 6.2. Geology of the study area from the 1:1 000 000 geological map (Keyser, 1997) with the location of the MT sounding stations indicated.

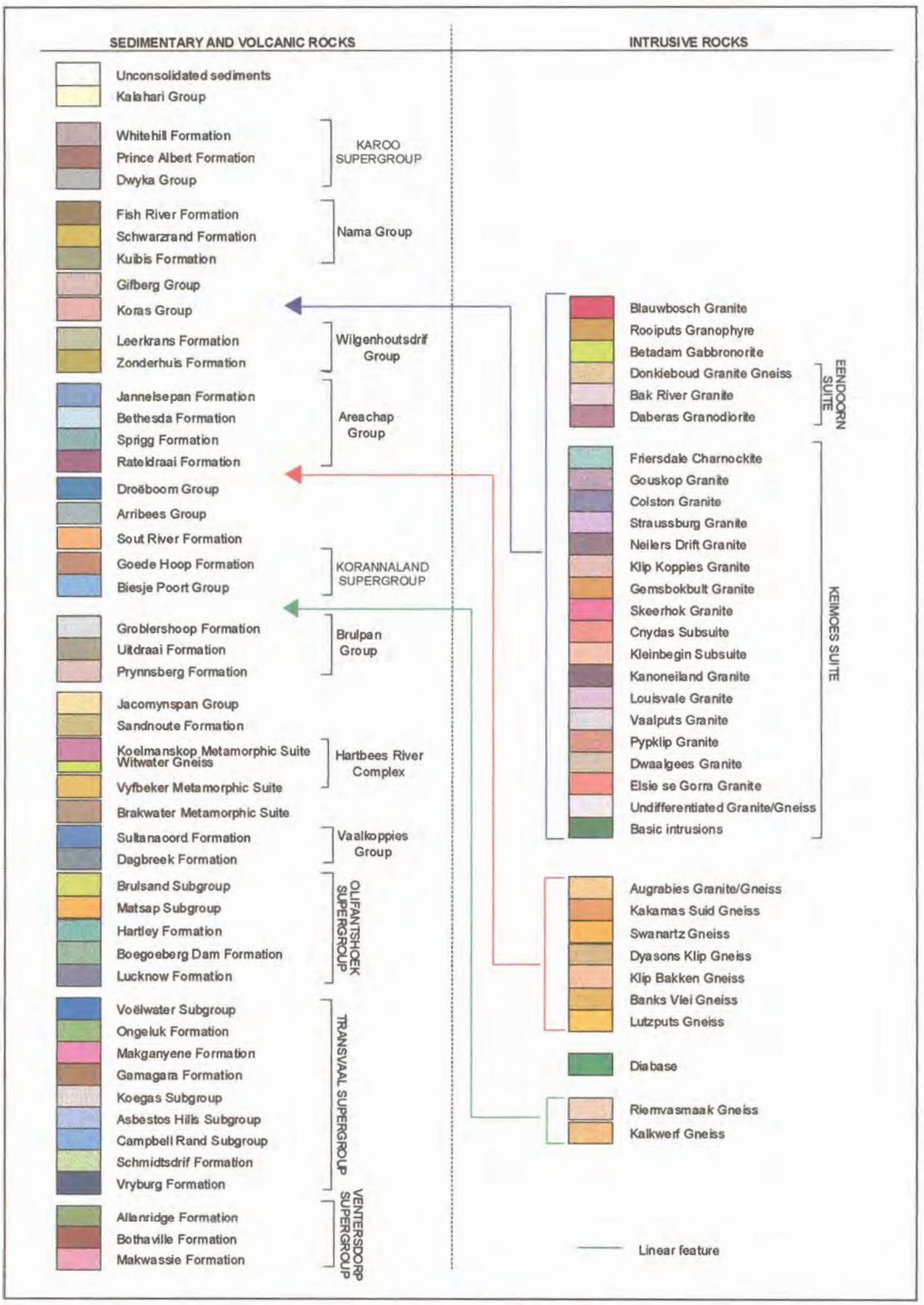

Figure 6.2 (continued). Legend for the geological map.

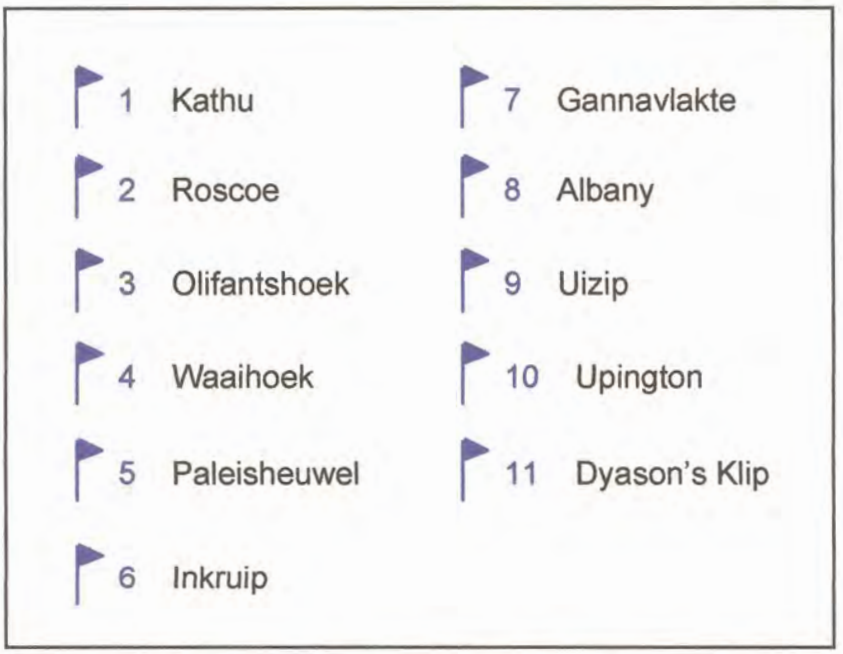

Figure 6.2 (continued). MT stations depicted on the geological map.

The study area (Figure 6.2) has a very complex tectonic history. At least three different terranes constitute the basement material on which geological formations were deposited.

The stations gradually move from Transvaal Supergroup material in the east, across Olifantshoek-, Brulpan- and Vaalkoppies sediments onto mainly intrusive granitic rocks in the west.

6.2.1. Transvaal Supergroup

The Transvaal Supergroup rocks in Griqualand West were deposited in a basin on the western edge of the Kaapvaal Craton. Extensive faulting and folding deformed the western edge of the basin. Beukes (1986) identifies a chemical sedimentary unit (the Ghaap Group) unconformably overlain by a mixed volcanic-chemical rock unit. Beukes and Smit (1987) report the following thicknesses for the different subgroups and formations (from top to bottom):

- Schmidtsdrif Formation (dolomite, shale, limestone, sandstone) : 10 – 250m

- Campbellrand Subgroup (mainly carbonaceous rocks) : 1500 – 1700m
- Asbestos Hills Subgroup : Kuruman Formation (banded ironstone, crocidolite, jaspilite, chert) 150 – 750m; Griquatown Formation (jaspilite with crocidolite, amphibolite, shale) 200 – 300m
- Koegas Subgroup (mudstone, amphibolite, quartzite, jaspilite and conglomerate at the base, jaspilite, quartzite, dolomite and banded ironstone at the top) : 240 – 600m
- Gamagara Formation (shale, quartzite, conglomerate) : 290m
- Makganyene Formation (diamictite with subordinate sandstone, conglomerate, limestone and mudstone) : 40 – 150m
- Ongeluk Formation (andesitic lava with zones of red jasper and agglomerate) : 900m
- Voëlwater Subgroup (dolomite, jaspilite, lava) : 250m

A deep borehole drilled at Kathu penetrated the Campbellrand Subgroup at a depth of 325m and was sunk to a depth of 3672m without reaching the base of the Schmidtsdrif Subgroup (Altermann and Siegfried, 1997). Altermann and Siegfried (1997) give the fact that the borehole was located on the northern flank of the Maremane Dome as a possible reason for the apparently increased thickness of the strata at the drill site.

Beukes (1986) states that the deposition of the lower part of the Transvaal Supergroup in the Griqualand West area was controlled by three tectono-sedimentary elements, namely a shallow water platform, a platform edge and a deeper basin to the west and southwest of the continent. He envisions the following scenario: sediments of the Schmidtsdrif Formation were derived from the Kaapvaal Craton and were fluvially deposited; carbonates of the Schmitsdrif Formation and Campbell Rand Subgroup were deposited in a carbonate platform sequence on a platform edge; transgression put an end to shallow water carbonate deposition; banded iron formation making up the Asbestos Hills Subgroup was deposited in deeper water and the Koegas Subgroup was deposited in a fresh water lake. The presence of stromatolites lead

Altermann and Herbig (1991) to believe that the Campbell Rand Subgroup was deposited in a shallow marine environment rather than on a platform edge.

De Villiers and Visser (1977) propose that there can be no doubt about the glacial origin of the diamictite of the Makganyene Formation. They suggest a sequence of events that started with glaciation in the north and transportation of glacial debris from the north towards the south into a water body, resulting in glaciomarine/glaciolacustrine deposits. Periodic retreats of the ice caused build-up of sedimentary piles along the basin margin that subsequently slumped into the basin, forming sandstone and subgraywacke deposits. Volcanism started during the waning stages of the ice period and clastic sedimentation stopped completely when the Ongeluk lava covered the area. Pillow lava indicates outpouring before the basin was filled with sediment.

6.2.2. Olifantshoek Supergroup

This Supergroup comprises mainly clastic sediments and volcanic rocks. The Mapedi Formation (included with the Lucknow Formation on the 1:1 000 000 map) follows disconcordantly on the Voëlwater Formation. It consists of quartzite and conglomerate at the base followed by phyllitic shale and a few layers of lava. Quartzite with a few layers of dolomitic limestone makes up the Lucknow Formation. This formation forms the foothills of the Langeberg east of Olifantshoek (Visser, 1989). The Hartley Formation, that is almost completely composed of andesitic lava, follows paraconcordantly on the Lucknow Formation.

The Matsap and Brulsand Subgroups constitute the Volop Group that follows on the Hartley Formation. Quartzite, conglomerate, greywacke and sandstone of this group strike roughly north-south and dip 30°-60° to the west (Visser, 1989).

6.2.3. Vaalkoppies Group

The Vaalkoppies Group comprises the Dagbreek and Sultanaoord Formations. The Dagbreek Formation consists of quartz-sericite schist, quartzite and amphibolite. It is characterised by a layer of quartzose schist with high aluminium content at the top (Visser, 1989). The Sultanaoord Formation follows concordantly on this Formation and consists mainly of quartzite.

6.2.4. Brulpan Group

This Group contains the Uitdraai and Groblershoop Formations. Banded and massive quartzite make up the Uitdraai Formation. The Groblershoop Formation is composed of quartz-sericite schist, with lenticular layers of greenstones and quartzite.

6.3. MAGNETOTELLURIC SOUNDING STATIONS

In this section the data at each of the sounding stations will be discussed individually. These discussions will include comparisons between apparent resistivity and phase curves obtained from the different statistical reduction techniques.

6.3.1. Katu

For this sounding station data were only obtained in the limited frequency range of 0.01 Hz to 1 Hz due to a lack of natural electromagnetic energy. The electrode spacing was 80m.

Results of statistical reduction

Figures 6.3 (a) to (f) show the data curves obtained for this station with the statistically estimated results overlain. The quality of the ρ_{yx} data is especially bad and the curves fitted through them are equally poor. Curves estimated for the ρ_{xy} with the different statistical techniques are

very similar, but it seems as though the adaptive L_p – norm using Sposito's equation (Figure 6.3e) yields the best results for both the ρ_{xy} and ρ_{yx} data. The phase data are of very poor quality. As a result the fitted curves are not realistic at all. This can be attributed to a low signal to noise ratio.

Interpretation

The apparent resistivity increases with depth, starting at approximately 10 Ωm at the highest frequency and increasing to 1000 Ωm at the lowest frequency. Since the curves obtained for both directions are very similar, it can be assumed that the underlying electrical structure is one-dimensional. Figure 6.4 shows a one-dimensional model for this sounding.

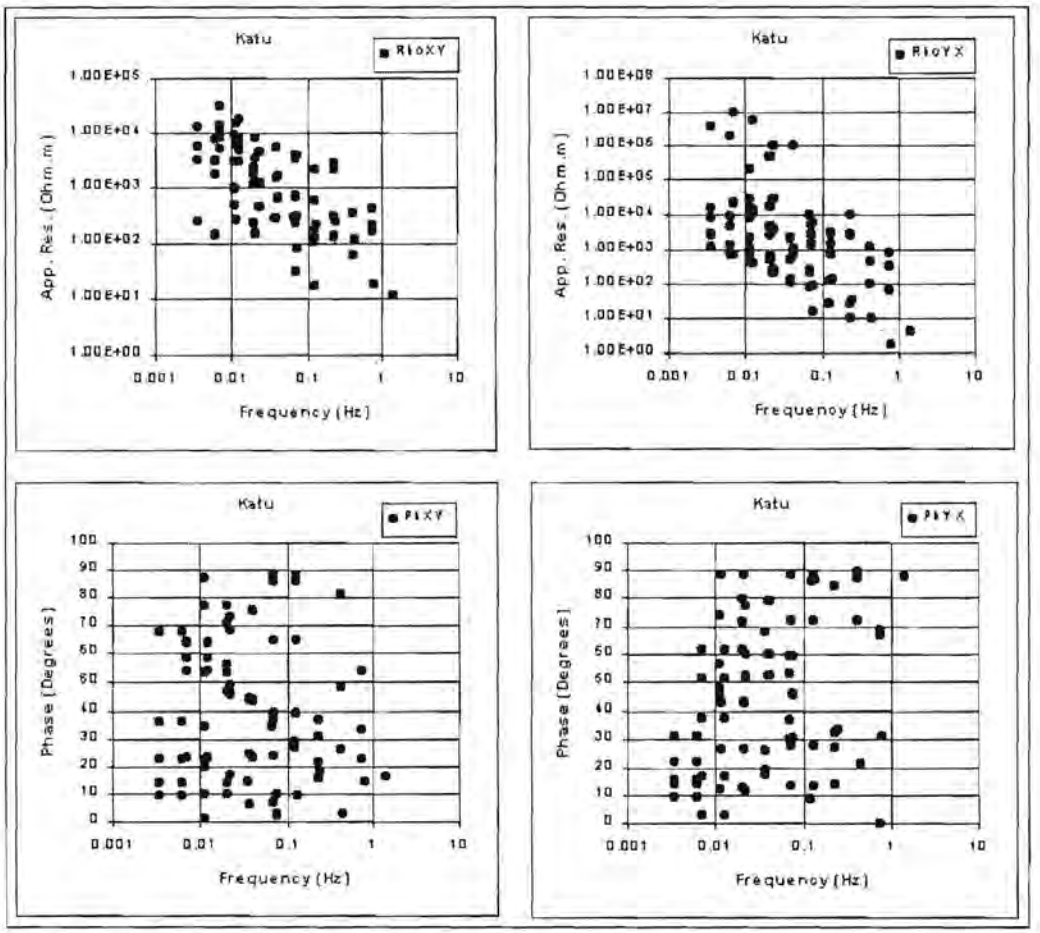

Figure 6.3(a). Apparent resistivity and impedance phase versus frequency curves for Katu.

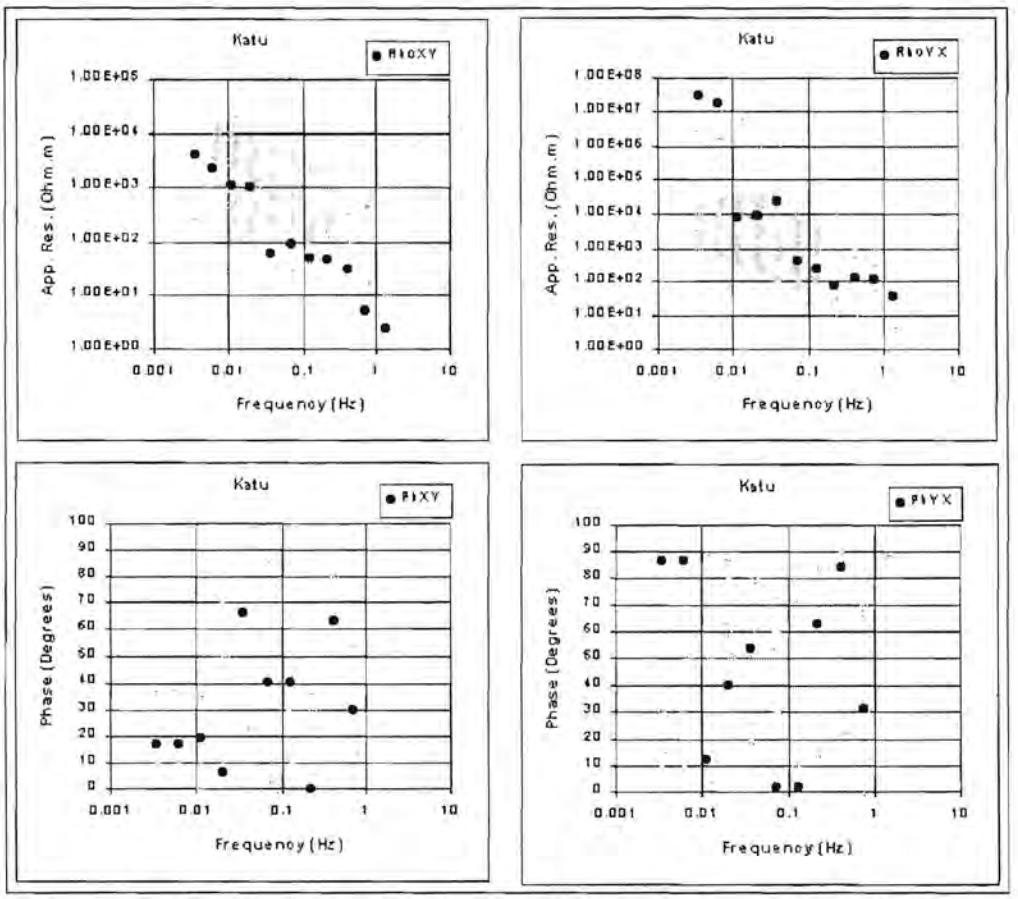

Figure 6.3(b). Curves estimated for Katu using L_1 -norm reduction.

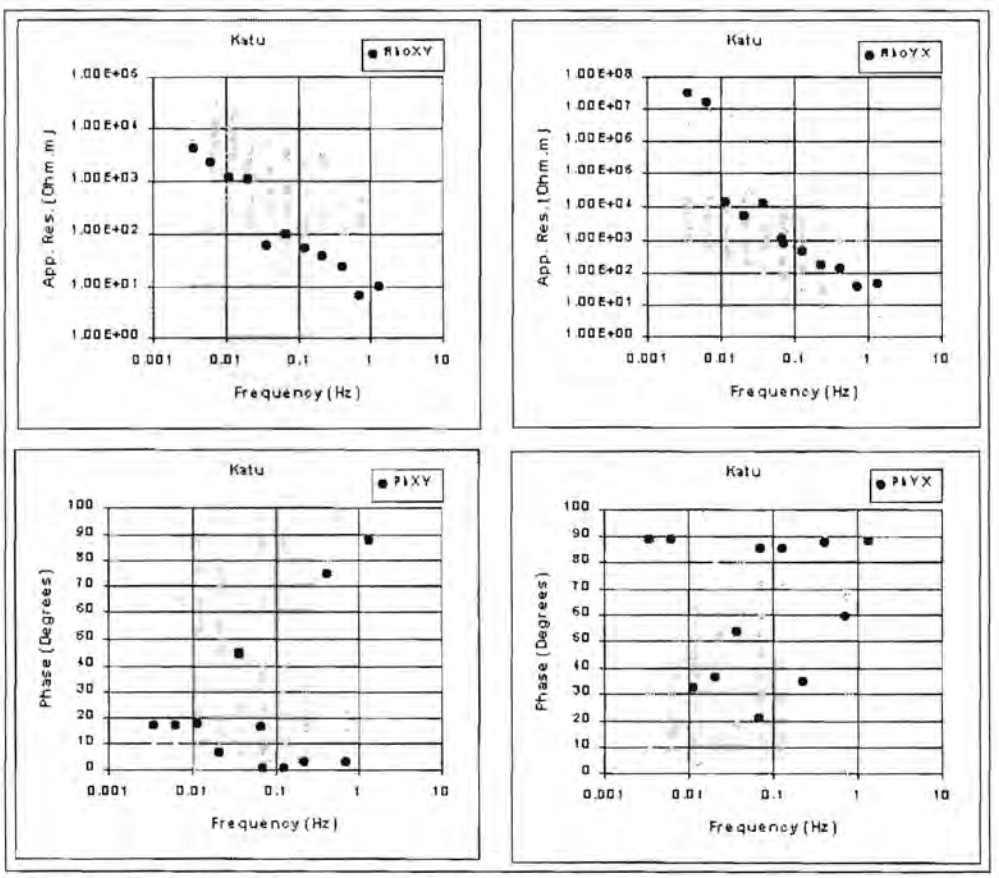

Figure 6.3(c). Curve estimated for Katu using least squares reduction.

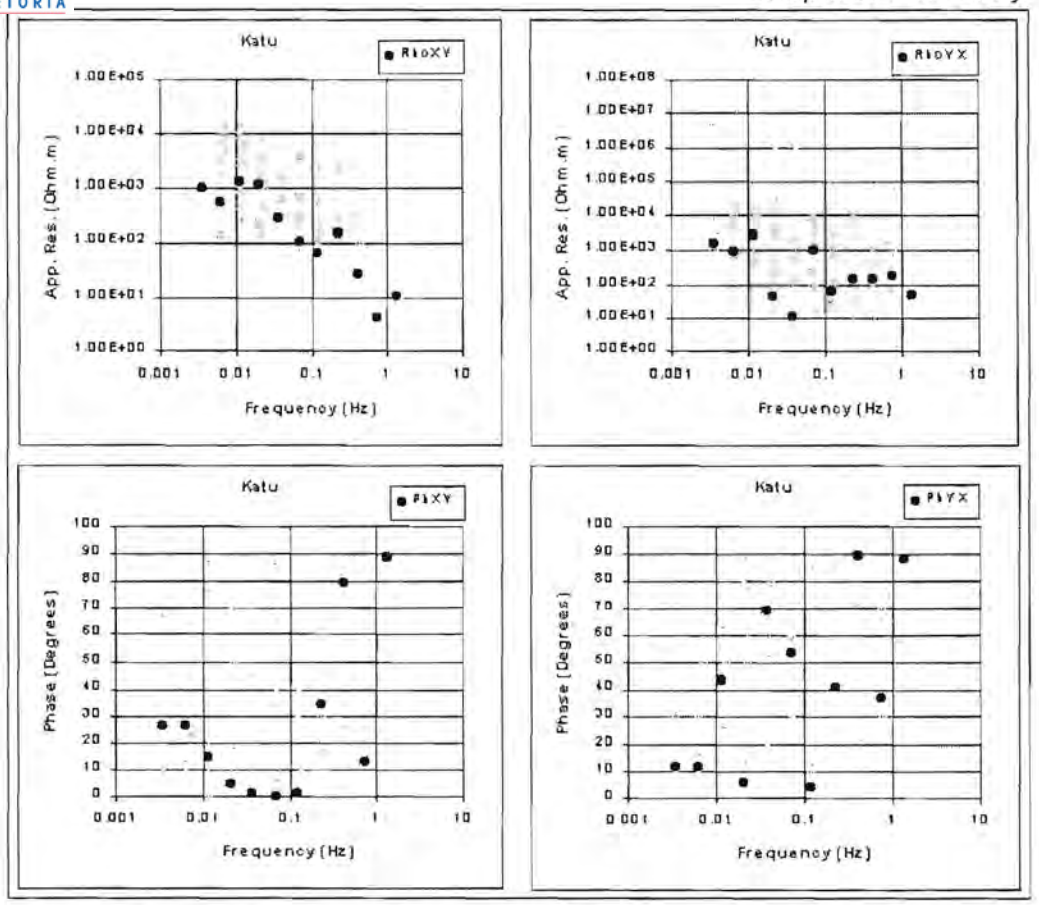

Figure 6.3(d). Curves estimated for Katu using robust M-estimation.

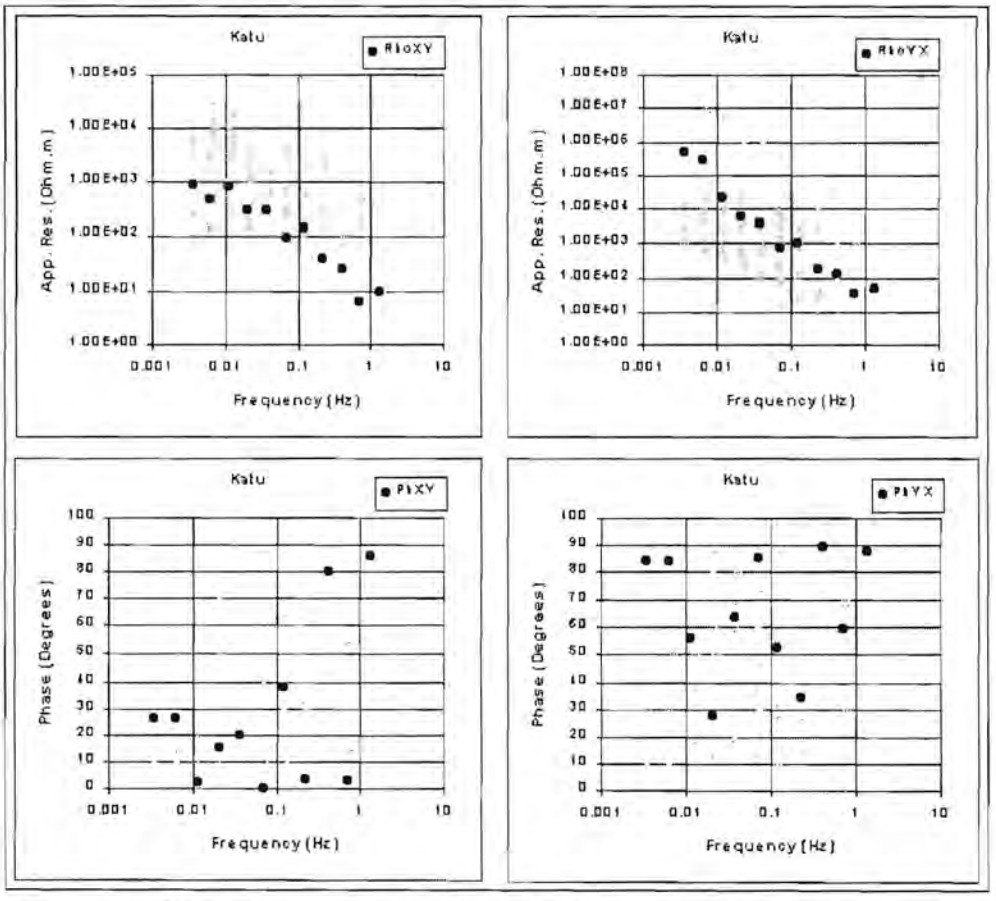

Figure 6.3(e). Curves estimated for Katu using adaptive L_p norm reduction (Sposito et al., 1983).

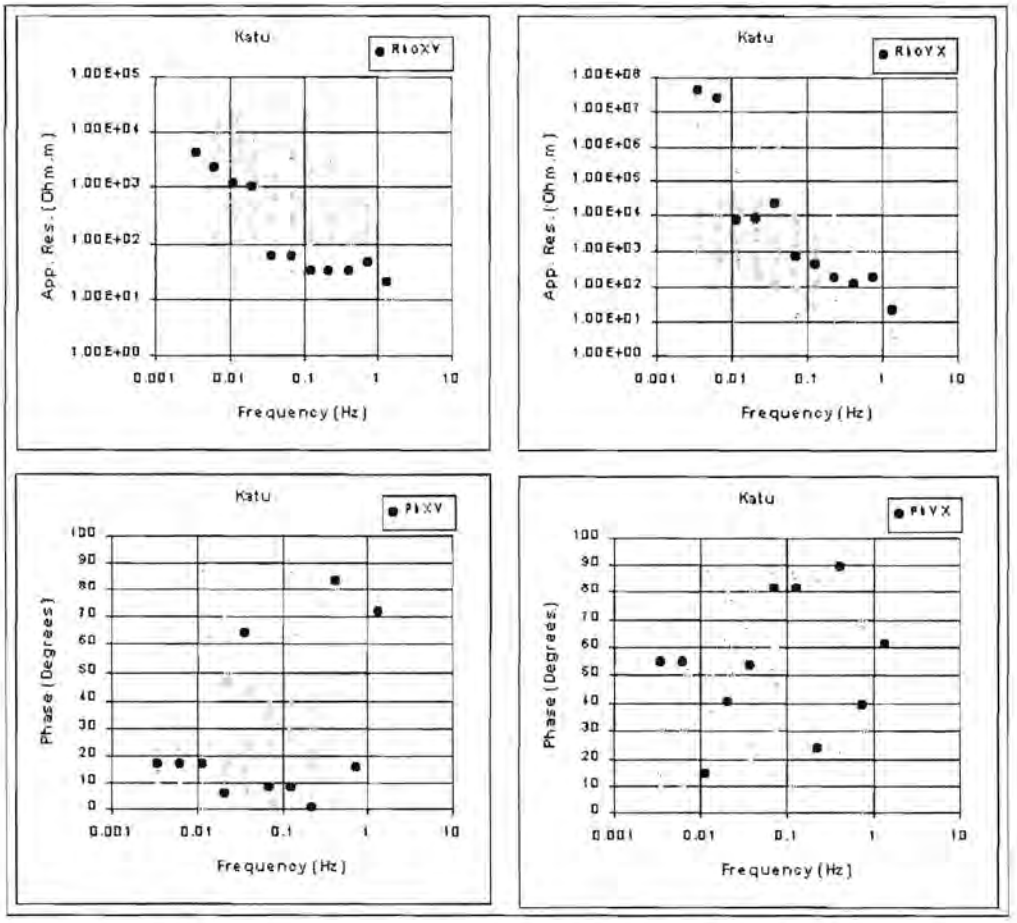

Figure 6.3(f). Curves estimated for Katu using adaptive L_p norm reduction (Money et al., 1982).

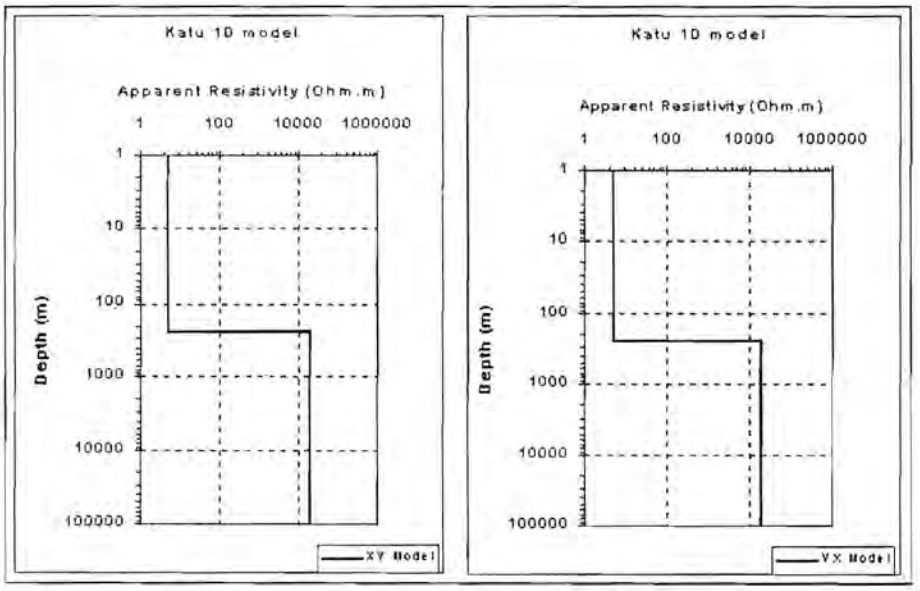

Figure 6.4. One dimensional models for Katu.

6.3.2. Roscoe

At Roscoe data were collected between 0.01 Hz and 2000 Hz. The quality of the apparent resistivity and phase data in the xy-direction is quite good, although there is a jump in the ρ_{xy} curve at 0.3 Hz (Figure 6.5(a)). The reason for this jump is unclear. It is not visible in the yx-direction and is therefore probably not caused by calibration errors.

A number of outliers appear on the ρ_{yx} data. The phase data in this direction is severely scattered indicating serious noise problems.

Results of statistical reduction

Figures 6.5(b) to (f) show the fitted curves overlain on the data. In this case, the robust M-estimation technique yields the best result for the data in both directions. The adaptive L_p-norm and least squares methods (Figure 6.5(c), (e) and (f)) were severely affected by outliers for the yx-direction data. Results obtained with the L1 norm (Figure 6.5(b)) compares quite well with the robust M-estimation curves.

Interpretation

For the xy-direction the apparent resistivity increases with decreasing frequency until roughly 0.3 Hz where the curve turns. This turn is very suspect since it coincides with the sudden jump in the data at this specific frequency.

The ρ_{yx} curve is more complex than the ρ_{xy} curve. At high frequencies the Earth is very conductive. The apparent resistivity increases with depth, but at approximately 20 Hz the curve flattens, pointing to the possible presence of a conductor. As the frequency decreases, the apparent resistivity increases to roughly 400 Ωm. At 0.3 Hz the curve flattens and starts to turn downwards.

The apparent resistivity curves in the xy- and yx-directions differ quite substantially. This indicates that the underlying geology is becoming more complex than at Katu and two- and three-dimensional structures are playing a role. Figure 6.6 depicts the layered earth one-dimensional models for each of the apparent resistivity curves.

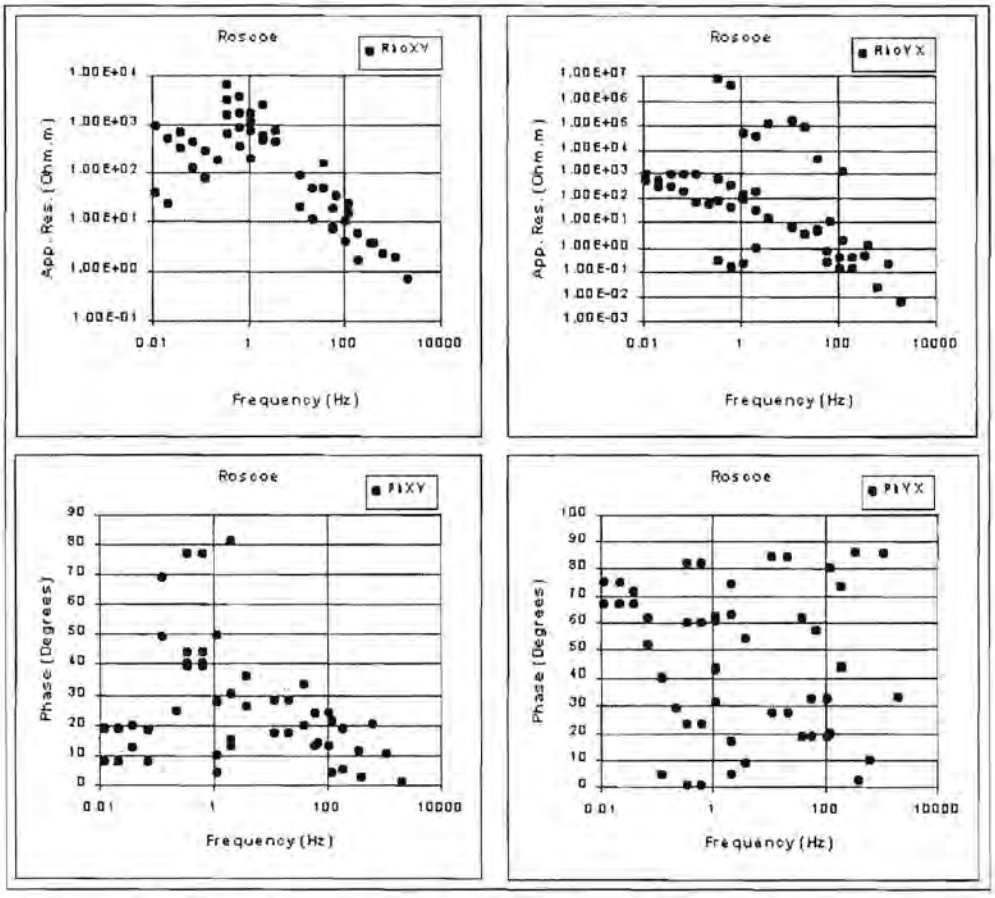

Figure 6.5(a). Apparent resistivity and impedance phase versus frequency curves for Roscoe.

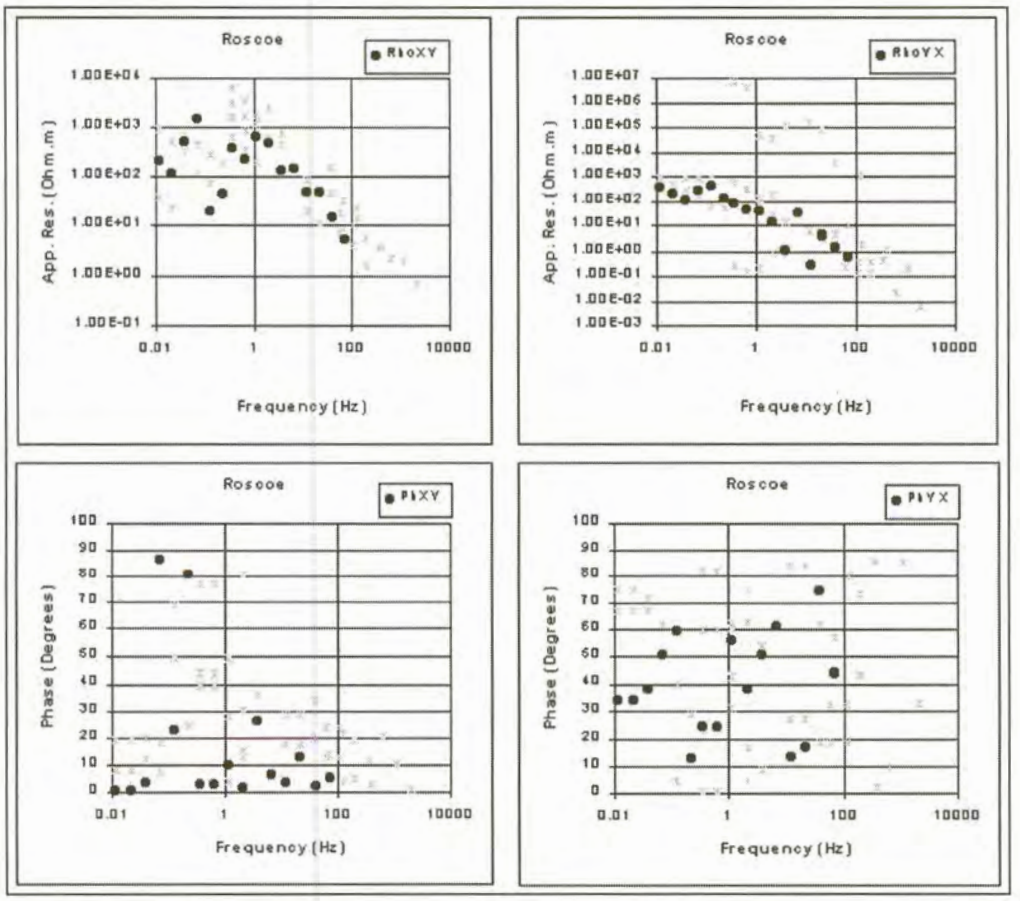

Figure 6.5(b). Curves estimated for Roscoe using L_1 norm reduction.

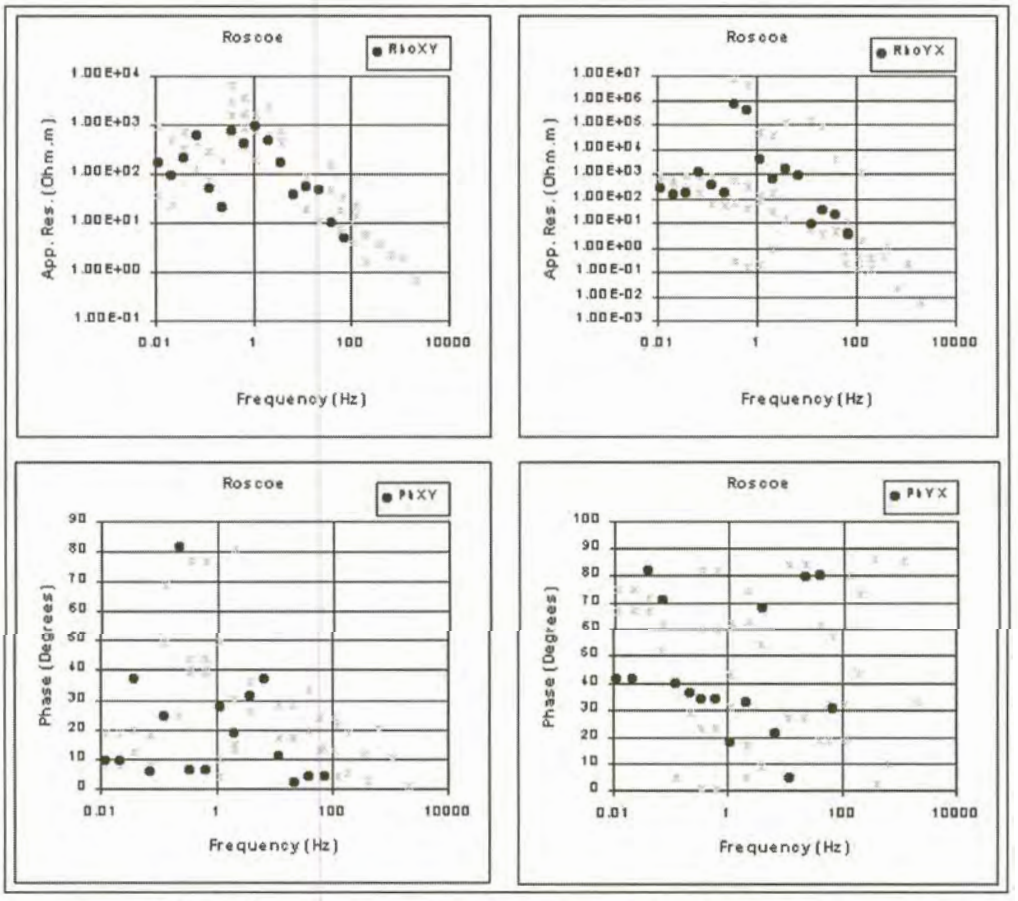

Figure 6.5(c). Curves estimated for Roscoe using least squares reduction.

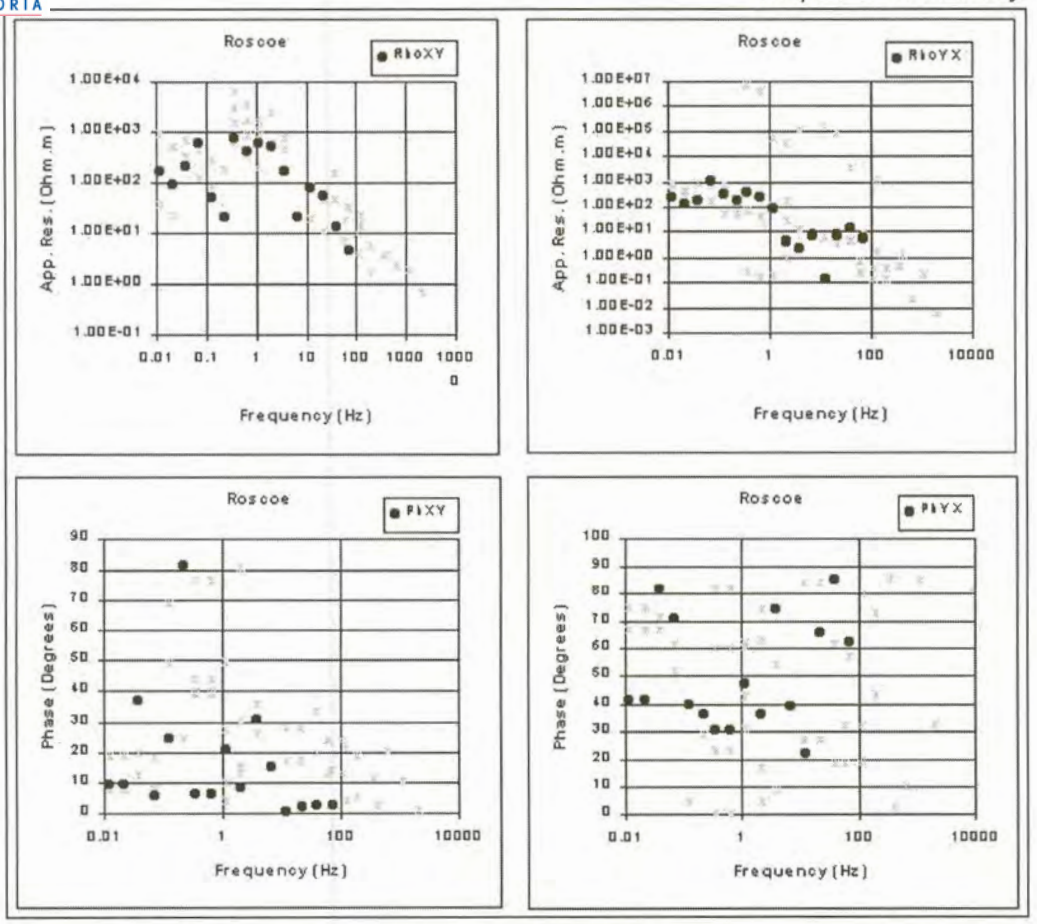

Figure 6.5(d). Curves estimated for Roscoe using robust M-estimation.

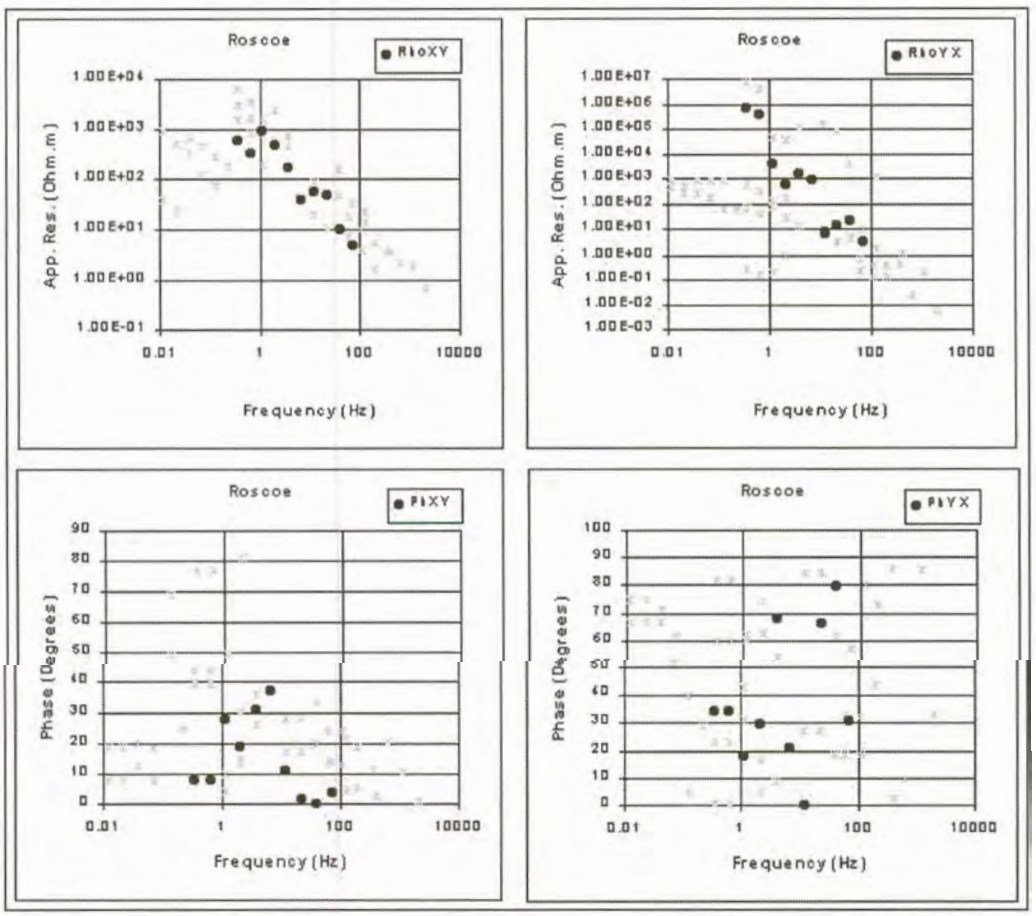

Figure 6.5(e). Curves estimated for Roscoe using adaptive L_p norm reduction (Sposito et al., 1983).

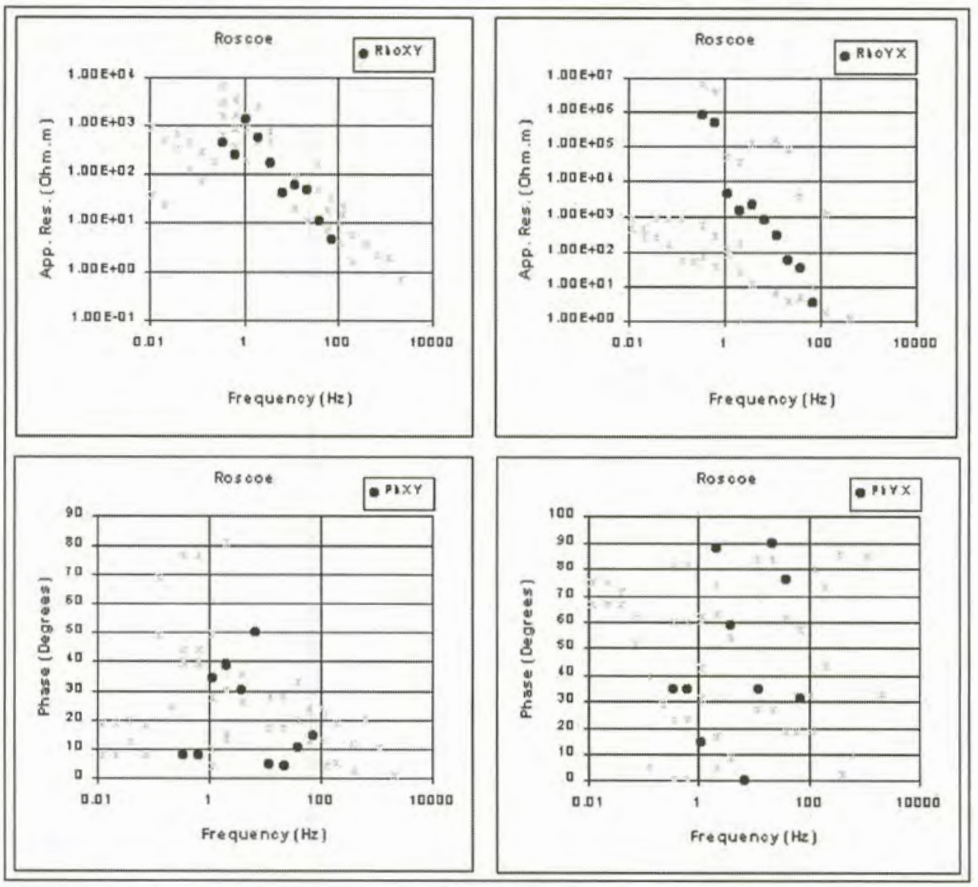

Figure 6.5(f). Curves estimated for Roscoe using adaptive L_p norm reduction (Money et al., 1982).

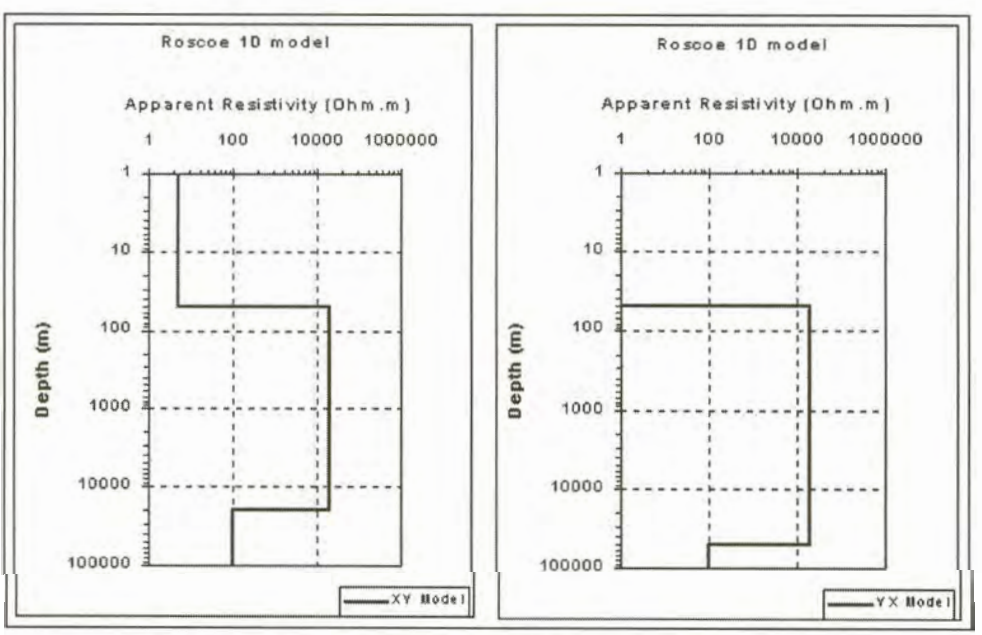

Figure 6.6. One dimensional models for Roscoe.

6.3.3. Olifantshoek

Data at this station were obtained between 0.01Hz and 10000Hz, with a gap between 0.1Hz and 2Hz where no data were collected (Figure 6.7(a)). The phase data are once again of very poor quality. On the xy-direction apparent resistivity data, some values fall on a straight line at higher frequencies. This is definitely caused by noise.

Results of statistical reduction

All of the statistical reduction techniques were severely biased by the noise that appears in the high frequency range of the xy-direction apparent resistivity data. None of the curves estimated for the apparent resistivity data in the yx direction yields a good fit.

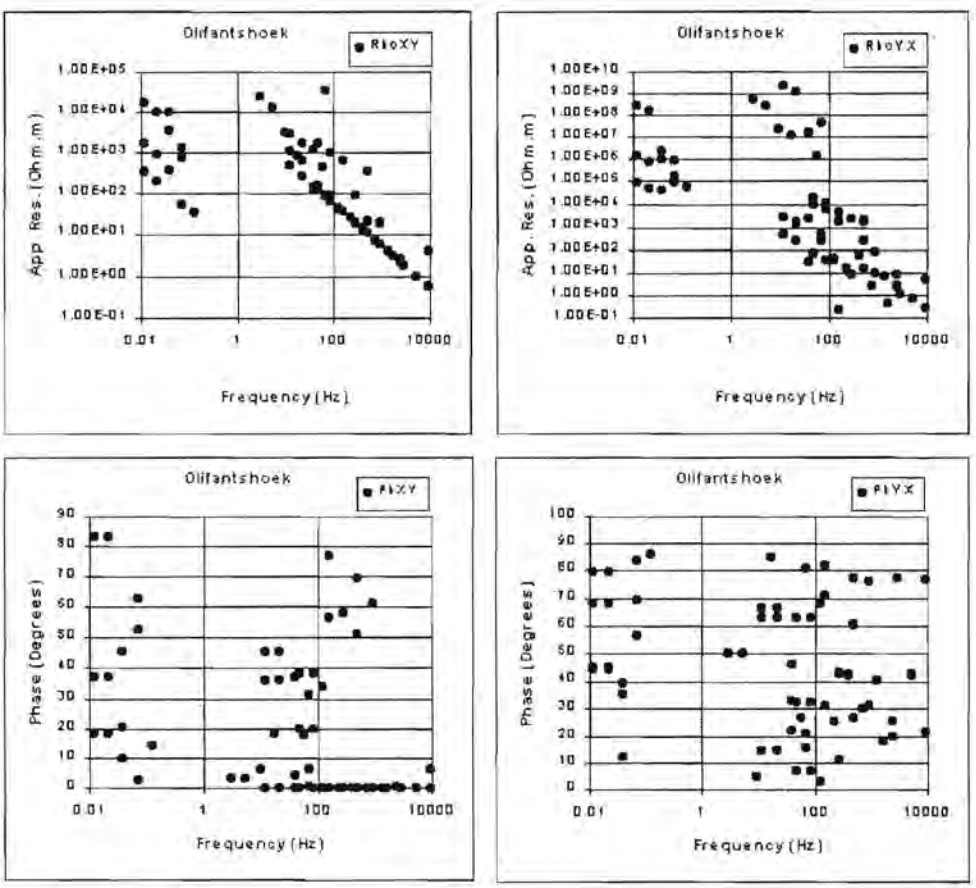

Figure 6.7(a). Apparent resistivity and impedance phase versus frequency curves for Olifantshoek.

Interpretation

The one-dimensional model calculated for the xy-direction shows an increase in resistivity as frequencies change from 1000 Hz to 10 Hz (Figure 6.8). Indications are that the curve turns somewhere between 10 Hz and 0.1 Hz and flattens to roughly 1000 ohm.m at 0.01 Hz. The data in the yx-direction increase steadily with decreasing frequency. The difference between the two curves suggest that the earth is probably anisotropic beneath this station.

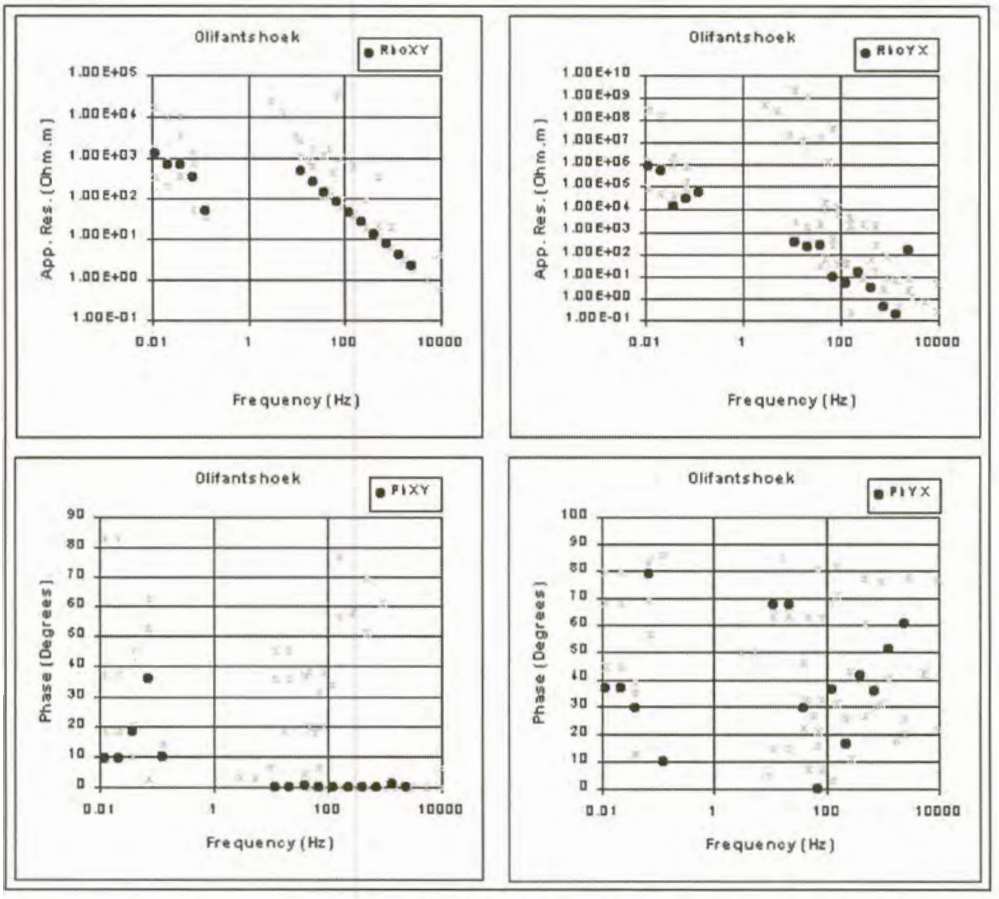

Figure 6.7(b). Curves estimated for Olifantshoek using L_1 norm reduction.

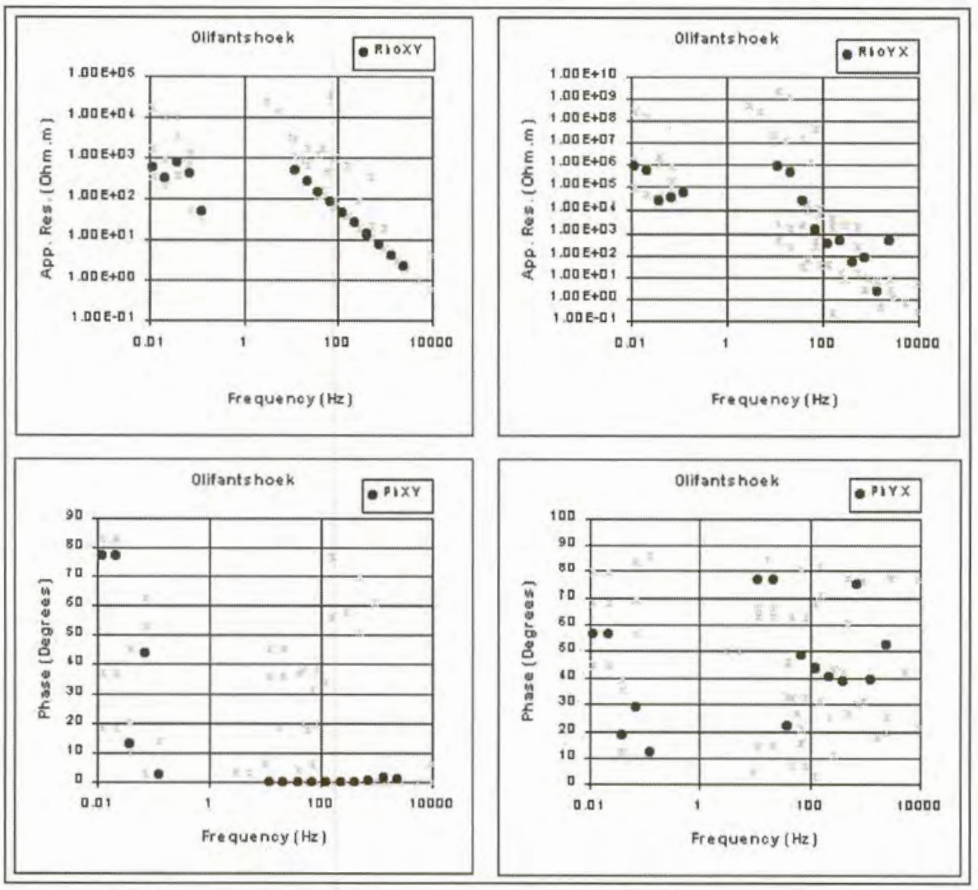

Figure 6.7(c). Curves estimated for Olifantshoek using least squares reduction.

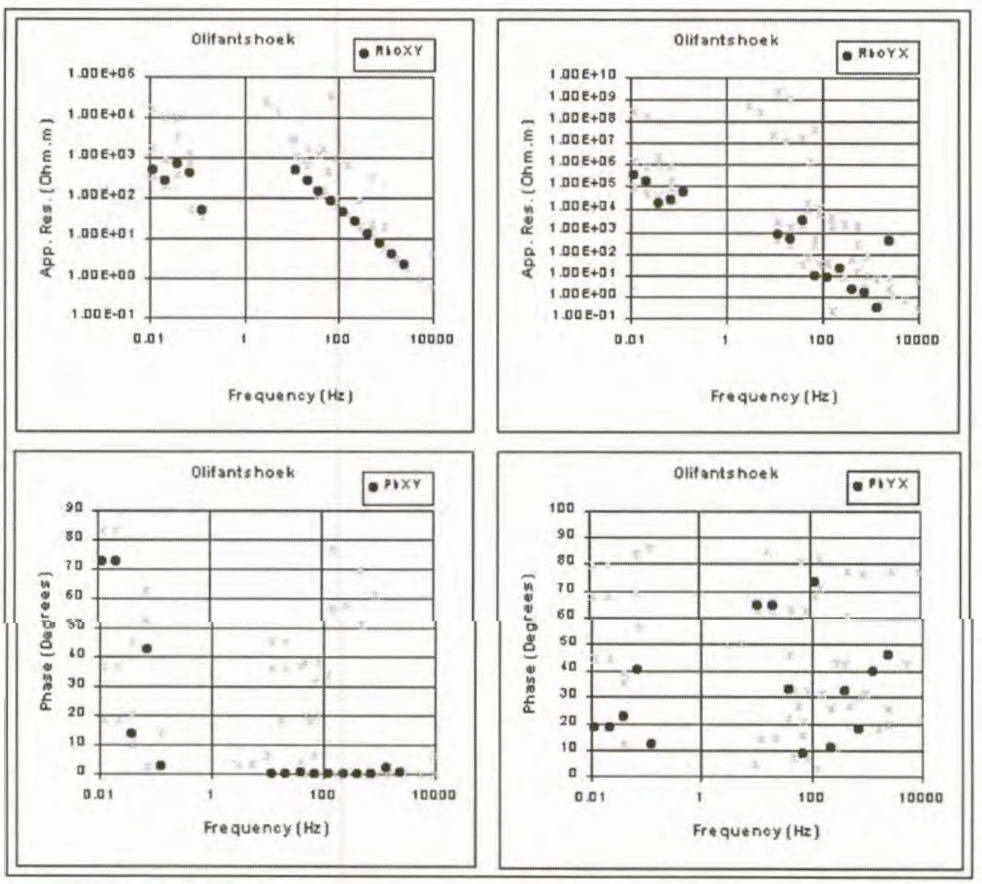

Figure 6.7(d). Curves estimated for Olifantshoek using robust M-estimation.

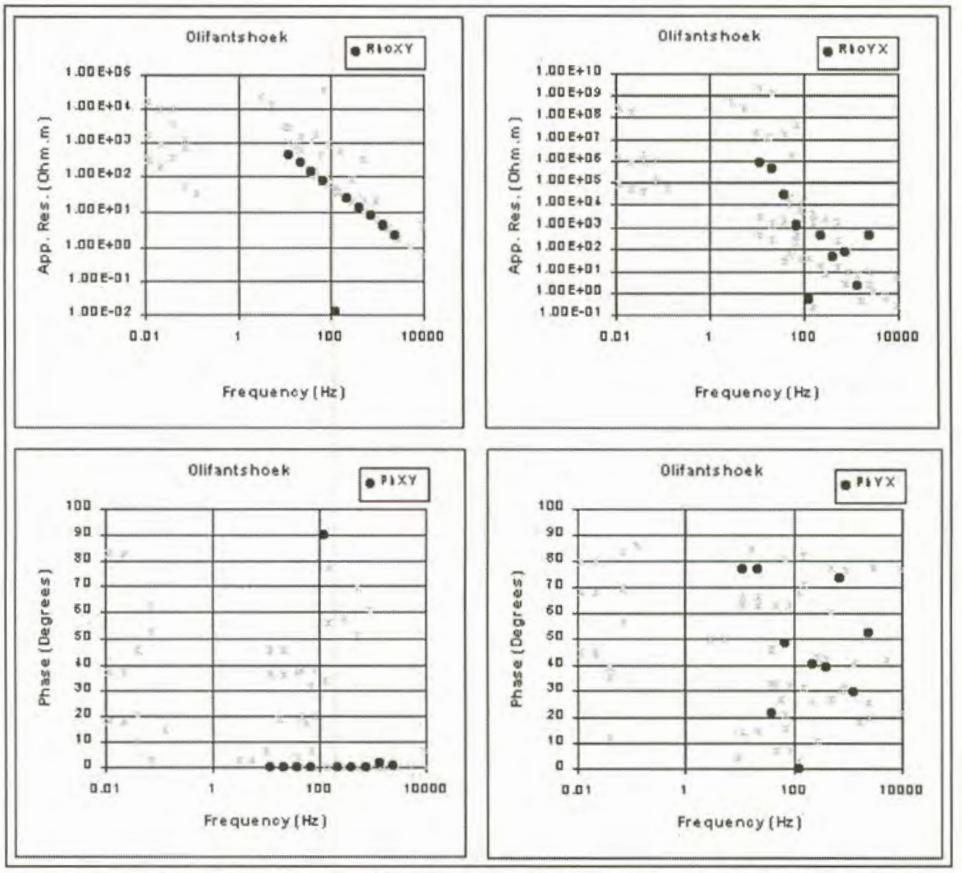

Figure 6.7(e). Curves estimated for Olifantshoek estimated using adaptive L_p norm reduction (Sposito et al., 1983).

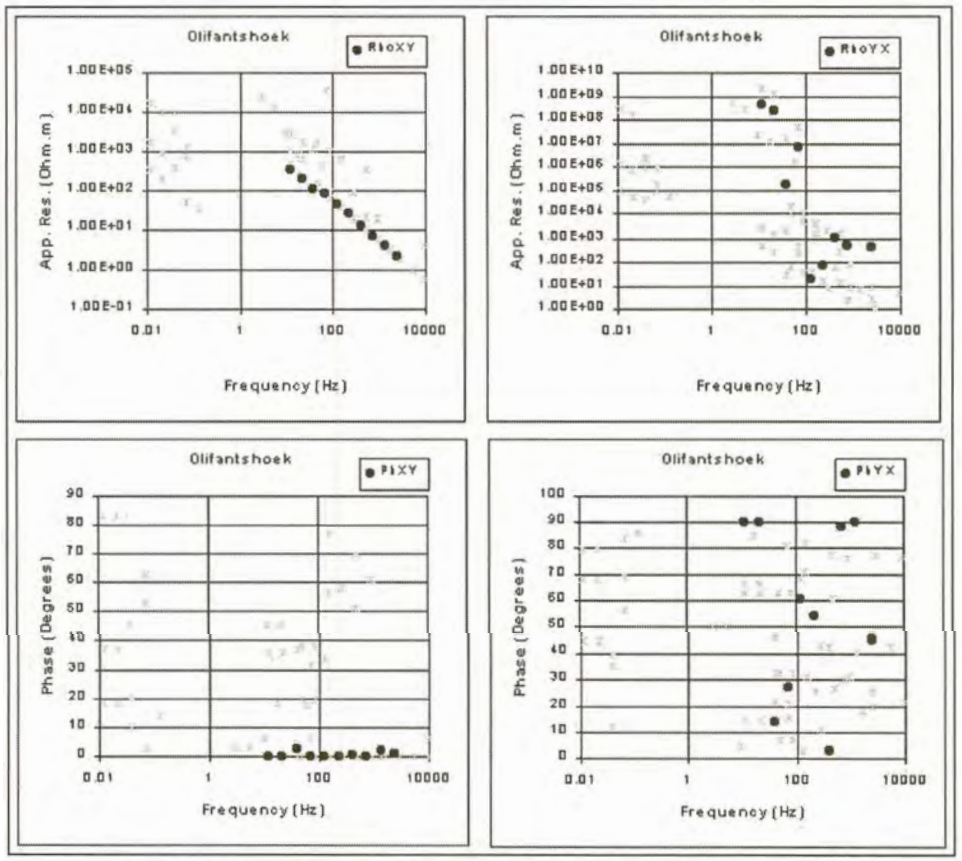

Figure 6.7(f). Curves estimated for Olifantshoek using adaptive L_p norm reduction (Money et al., 1982).

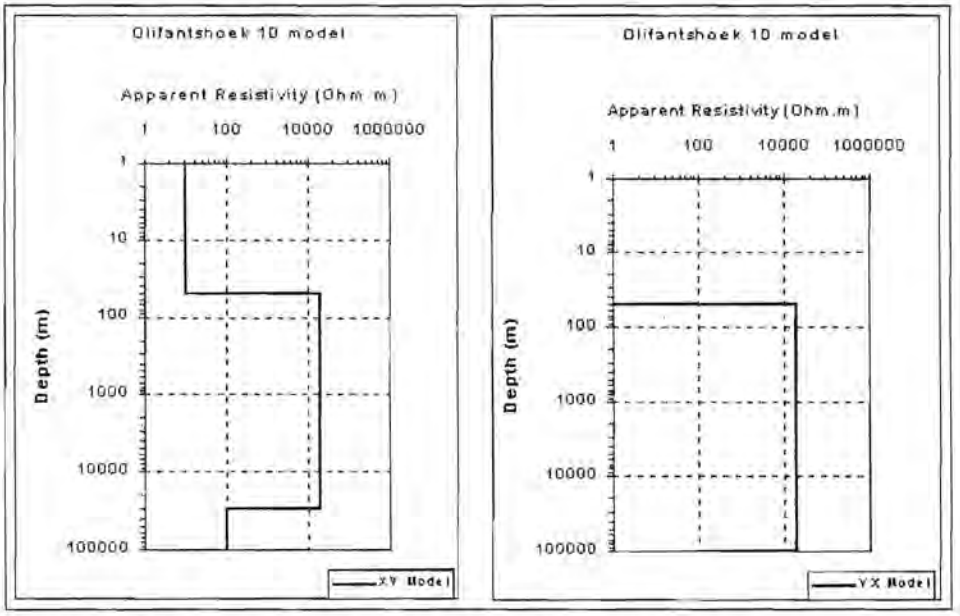

Figure 6.8. One dimensional models for Olifantshoek.

6.3.4. Waaihoek

Figure 6.9(a) shows data collected at this station. The quality of the data is much better for the xy-direction data than for the yx-direction data. Even the phase data in the xy-direction have a higher quality than at any of the previous stations.

Results of statistical reduction

All the statistical techniques, with the exception of the L1 norm (Figure 6.9(b)), yield good results for the data in the xy-direction. The curve determined by the adaptive L_p norm technique using Money's equation (Figure 6.9(f)) shows some deterioration at 55 Hz. The best results for the phase data are obtained by the L2-norm and robust M-estimation methods (Figures 6.9(c) and (d)).

More outliers are present in the yx-direction. This causes a marked deterioration in the quality of the fitted curves, especially at higher frequencies. The curve calculated using the L_p-norm method and Money's equation gives the best result in the higher frequency range.

Interpretation

The apparent resistivity curves are nearly identical in the two measurement directions. This suggests a lack of two- and three-dimensional structures at this station.

The curves start at approximately 10 Ωm at high frequencies and increases to roughly 1000 Ωm at 11 Hz. It then flattens and remains at this for lower frequencies. There is a subtle increase in apparent resistivity at the lowest frequencies. Figure 6.10 shows the one-dimensional model deduced from these curves.

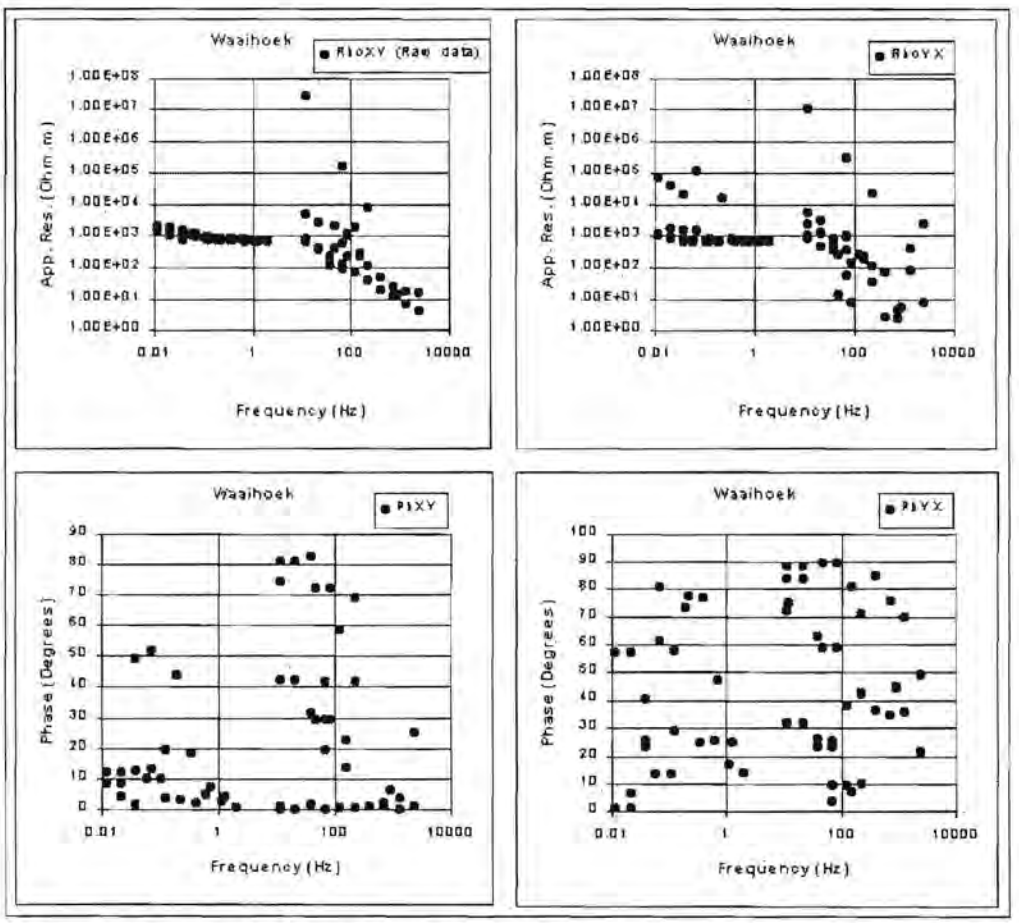

Figure 6.9(a). Apparent resistivity and impedance phase versus frequency curves for Waaihoek.

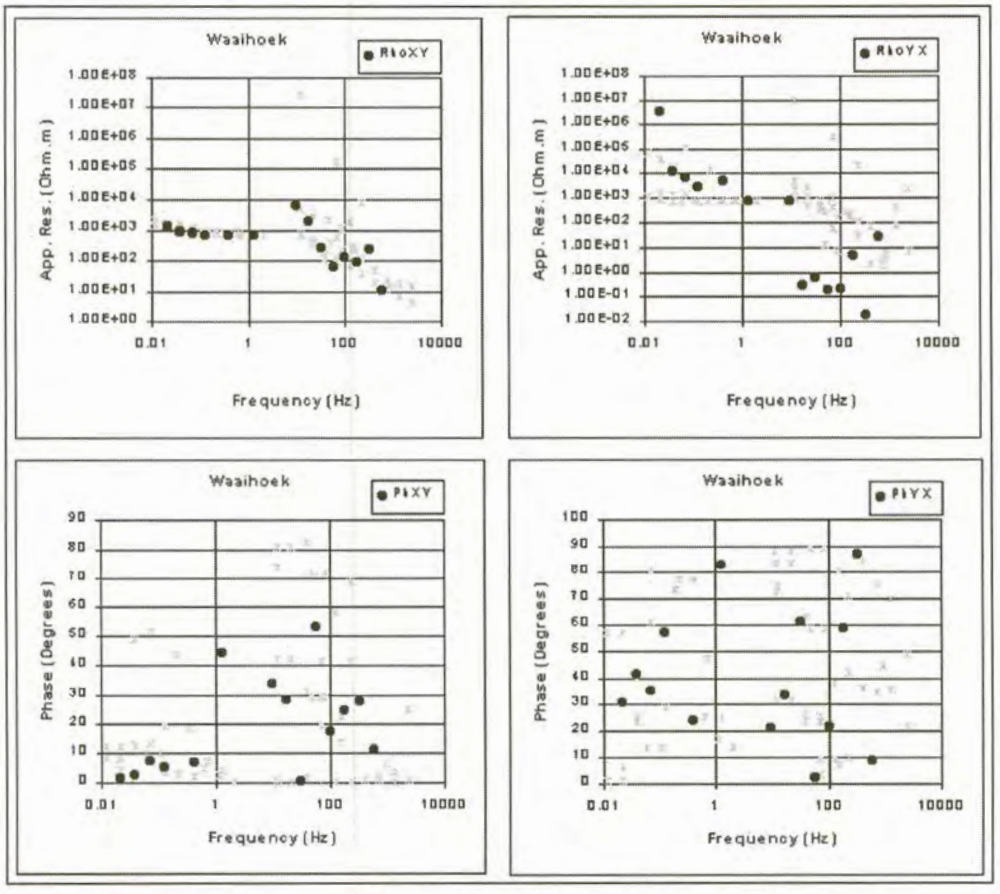

Figure 6.9(b). Curves estimated for Waaihoek using L_1 norm.

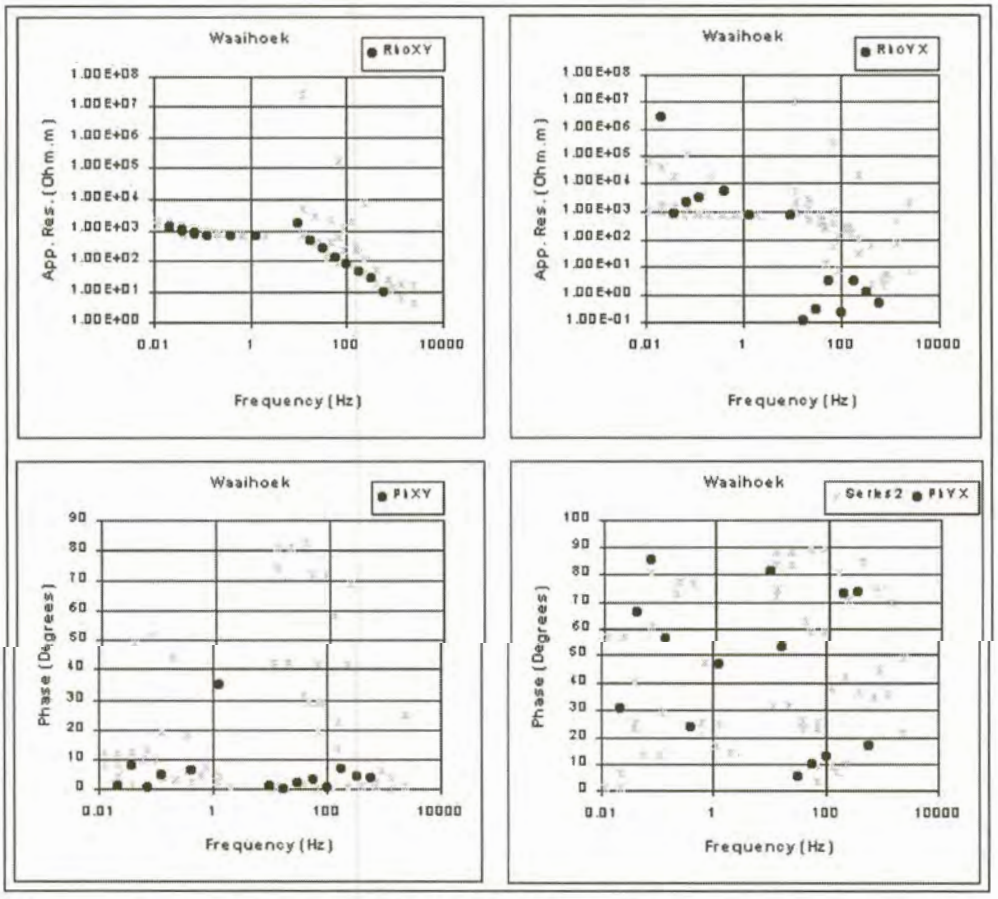

Figure 6.9(c). Curves estimated for Waaihoek using least squares reduction.

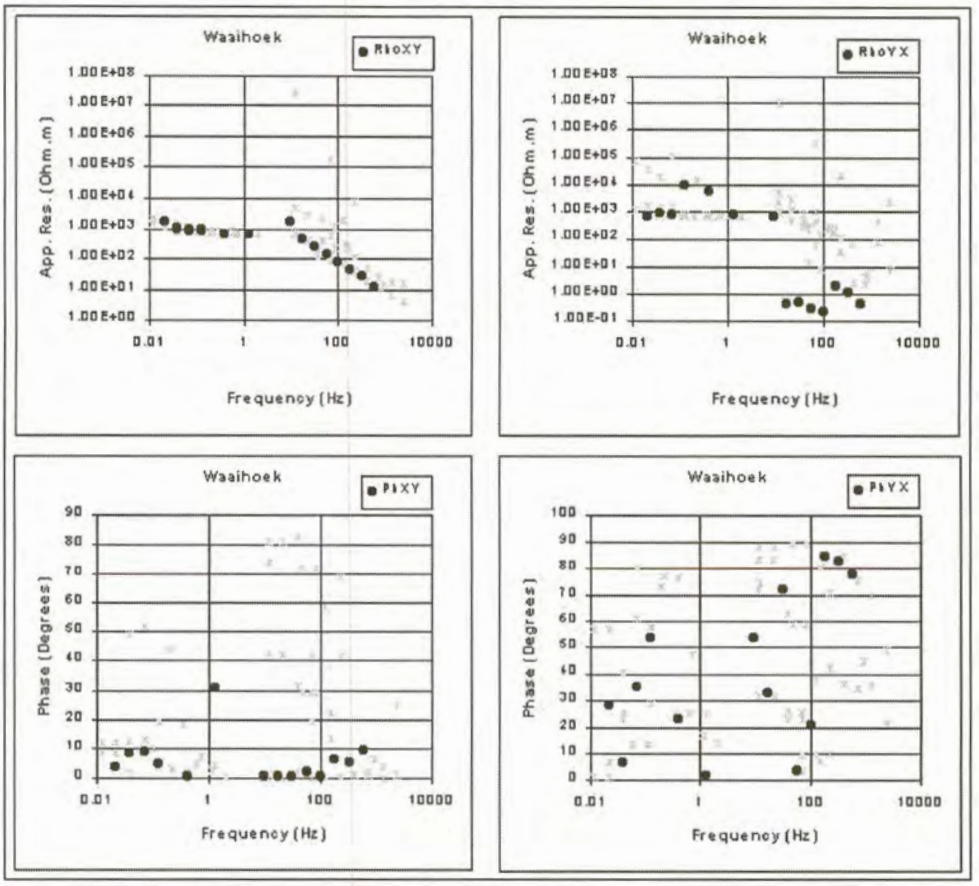

Figure 6.9(d). Curves calculated for Waaihoek using robust M-estimation.

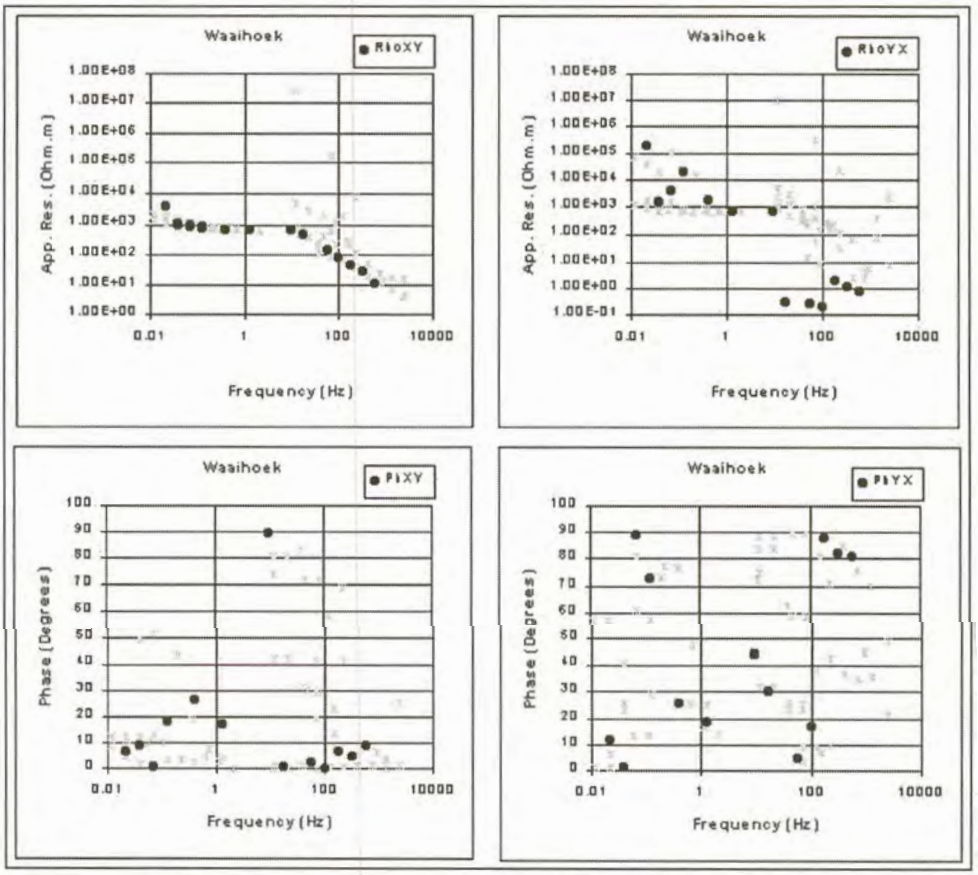

Figure 6.9(e). Curves calculated for Waaihoek using adaptive L_p norm reduction (Sposito et al., 1983).

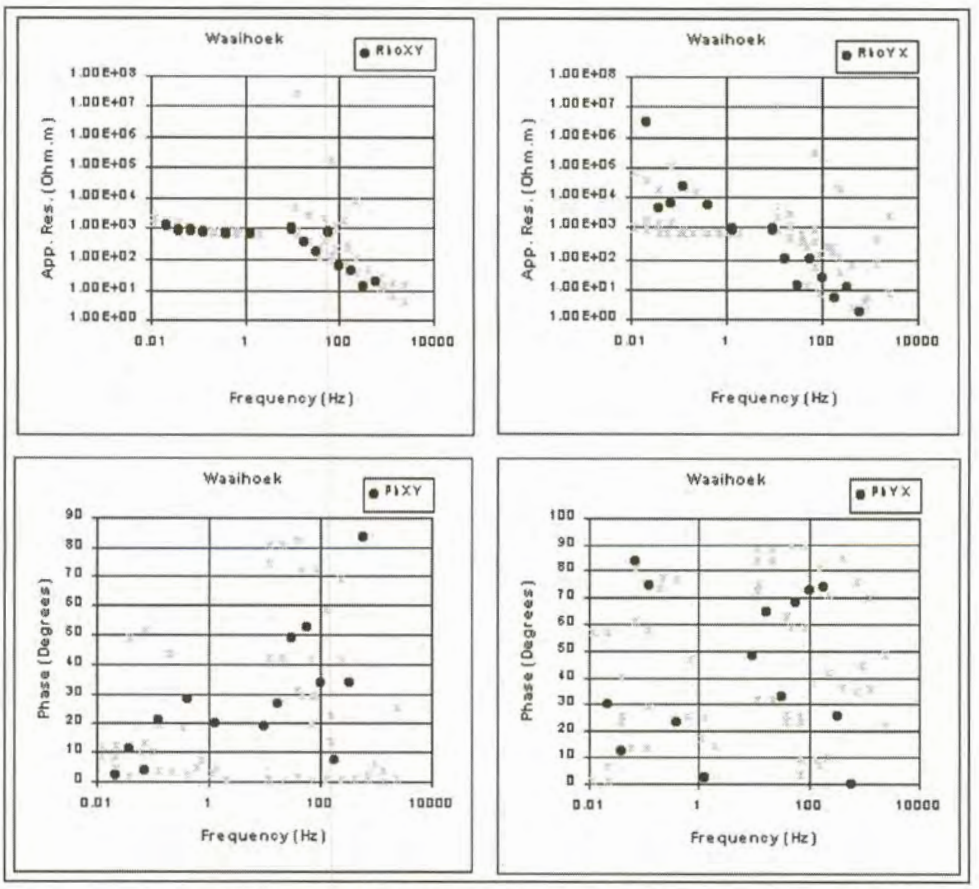

Figure 6.9(f). Curves calculated for Waaihoek using adaptive L_p norm reduction (Money et al., 1982).

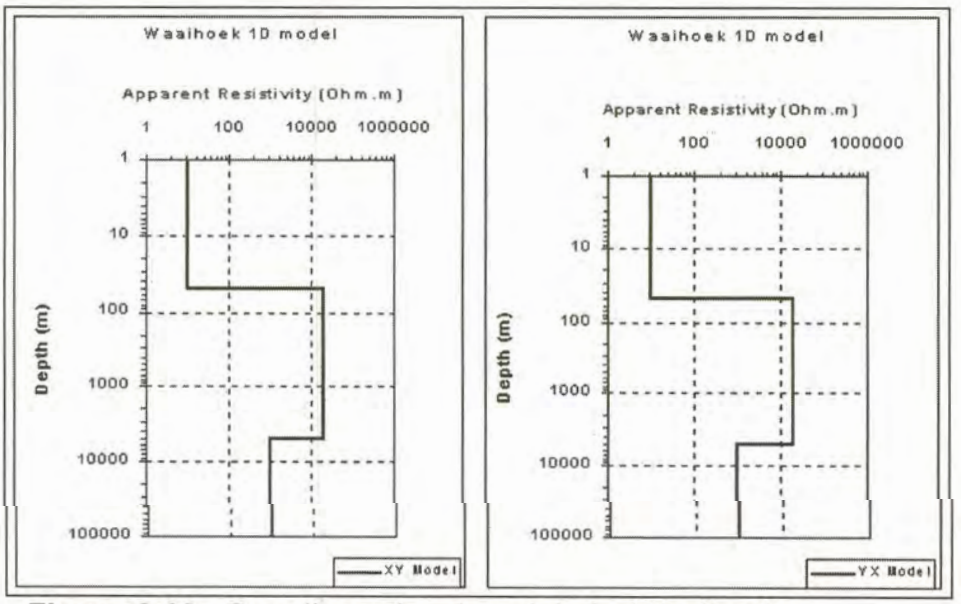

Figure 6.10. One dimensional models for Waaihoek.

6.3.5. Paleisheuwel

The data curves for this station are very scattered, although it is possible to see some trend in the apparent resistivity curves (Figure 6.11(a)). Data were only obtained up to 115 Hz. Although data in both directions are scattered, a number of outliers occur on the ρ_{yx} curve.

Results of statistical reduction

All the statistical reduction methods yield very poor results for this data set. The curves estimated for the yx-direction data yield better results than for the xy-direction. The adaptive L_p norm technique using Sposito's equation produces the best fit to the data (Figure 6.11(e)). Curves obtained for the xy-direction vary quite significantly depending on the statistical method used.

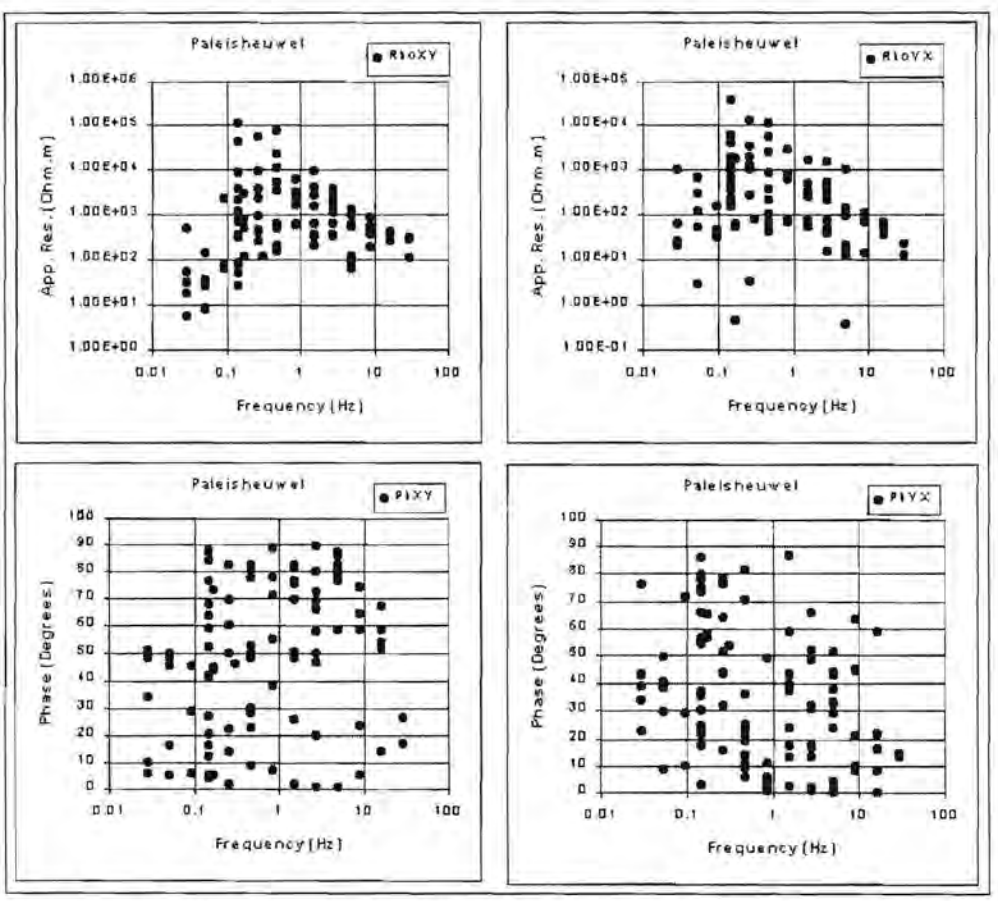

Figure 6.11(a). Apparent resistivity and impedance phase versus frequency curves for Paleisheuwel.

Interpretation

The apparent resistivity curves in both directions have basically the same trend, but values for the ρ_{xy} curve are almost an order of magnitude larger than those for the yx-direction. Both curves start with low resistivities at high frequencies, increasing with a decrease in frequency. At approximately 0.25 Hz the resistivities start to decrease. The one-dimensional models for this station are shown in Figure 6.12.

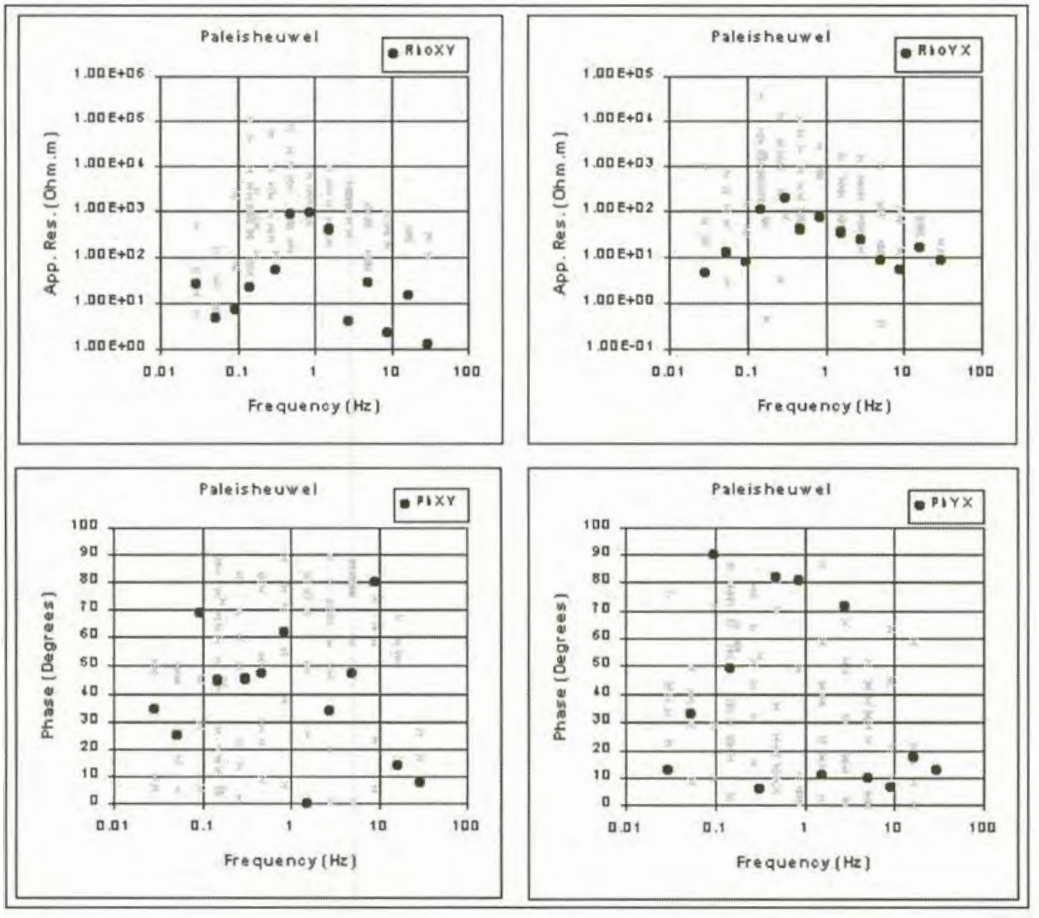

Figure 6.11(b). Curves estimated for Paleisheuwel using L_1 norm reduction.

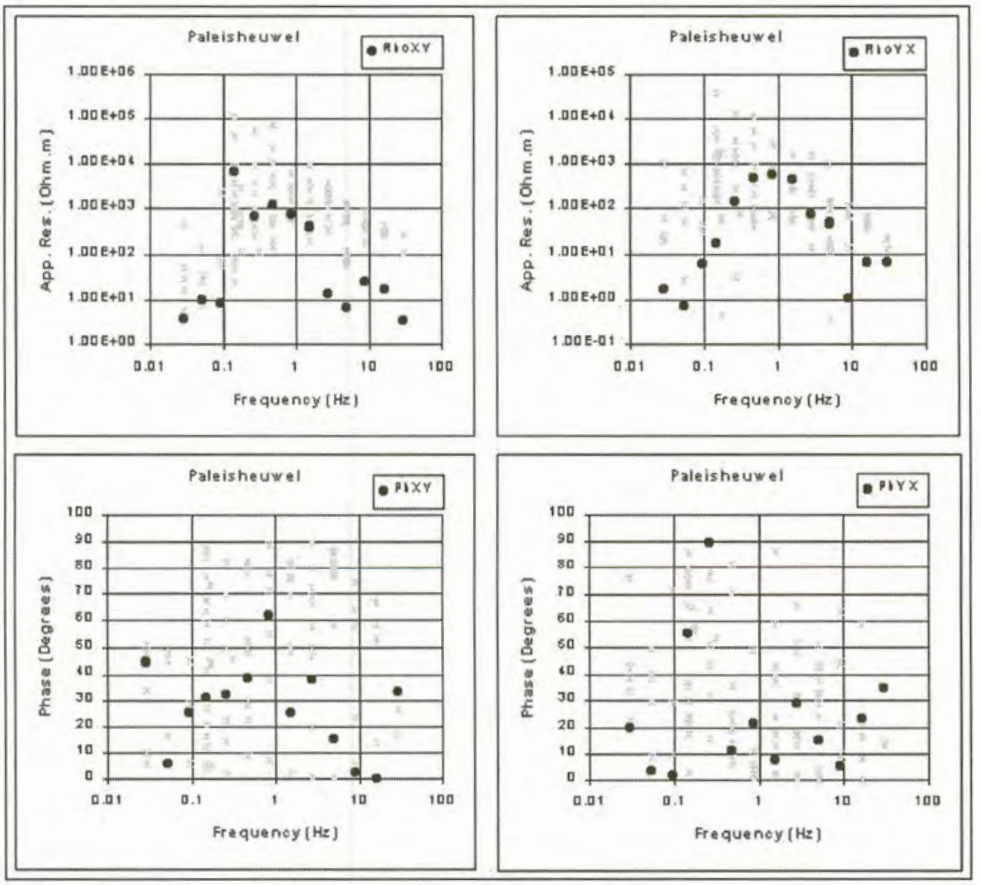

Figure 6.11(c). Curves estimated for Paleisheuwel using least squares reduction.

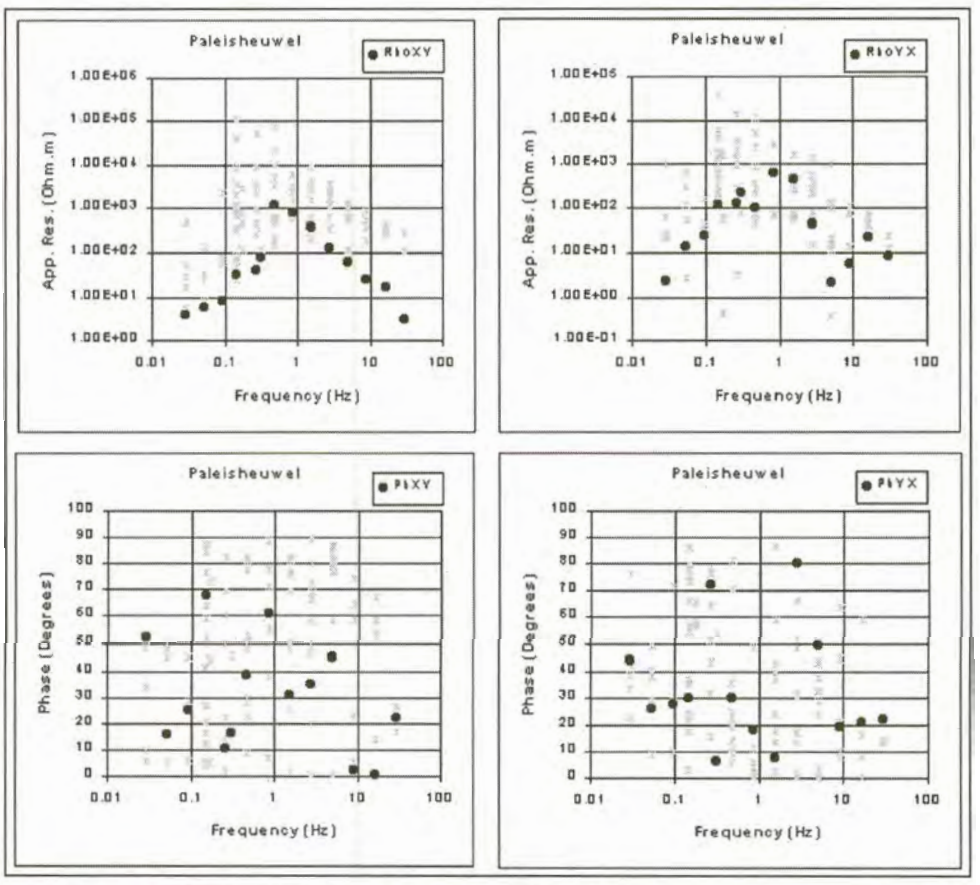

Figure 6.11(d). Curves calculated for Paleisheuwel using robust M-estimation.

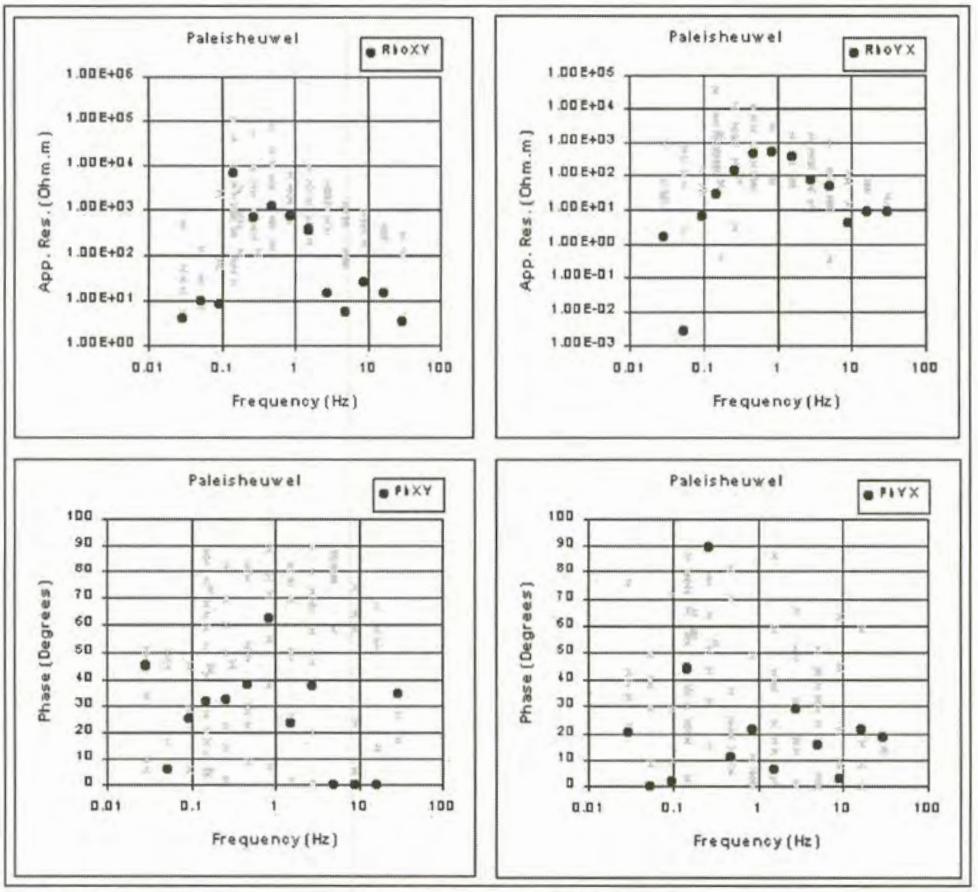

Figure 6.11(e). Curves estimated for Paleisheuwel using adaptive L_p norm reduction (Sposito et al., 1983).

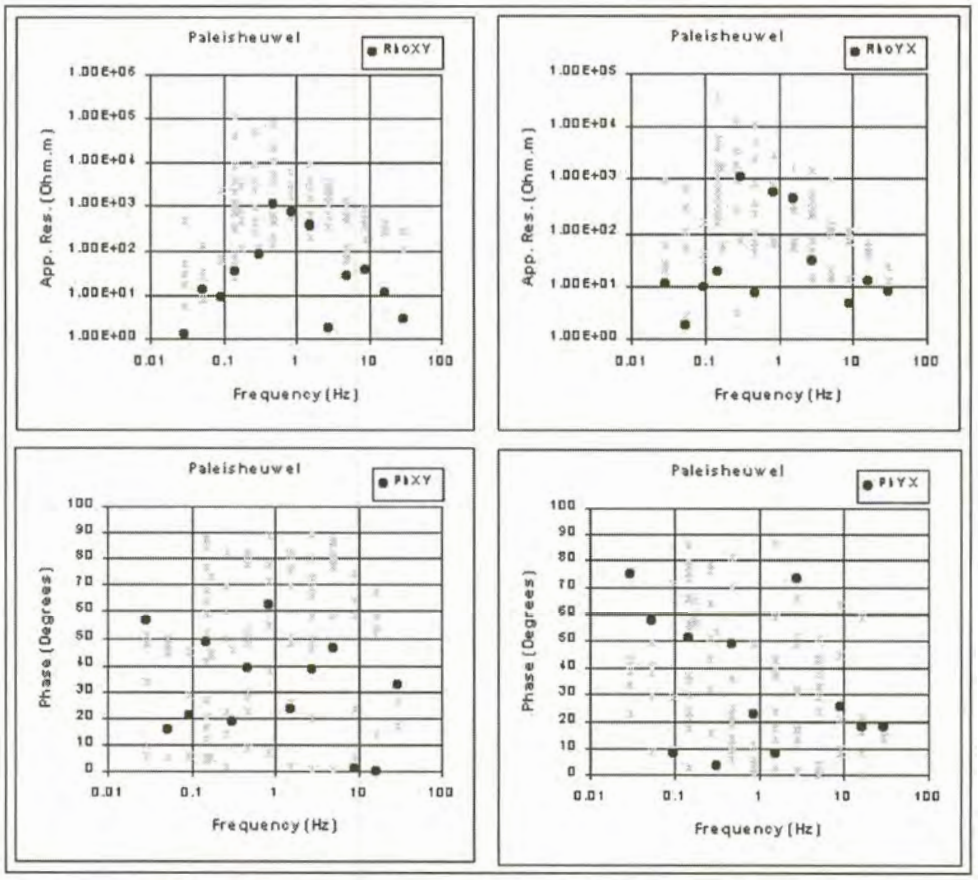

Figure 6.11(f). Curves estimated for Paleisheuwel using adaptive L_p norm reduction (Money et al., 1982).

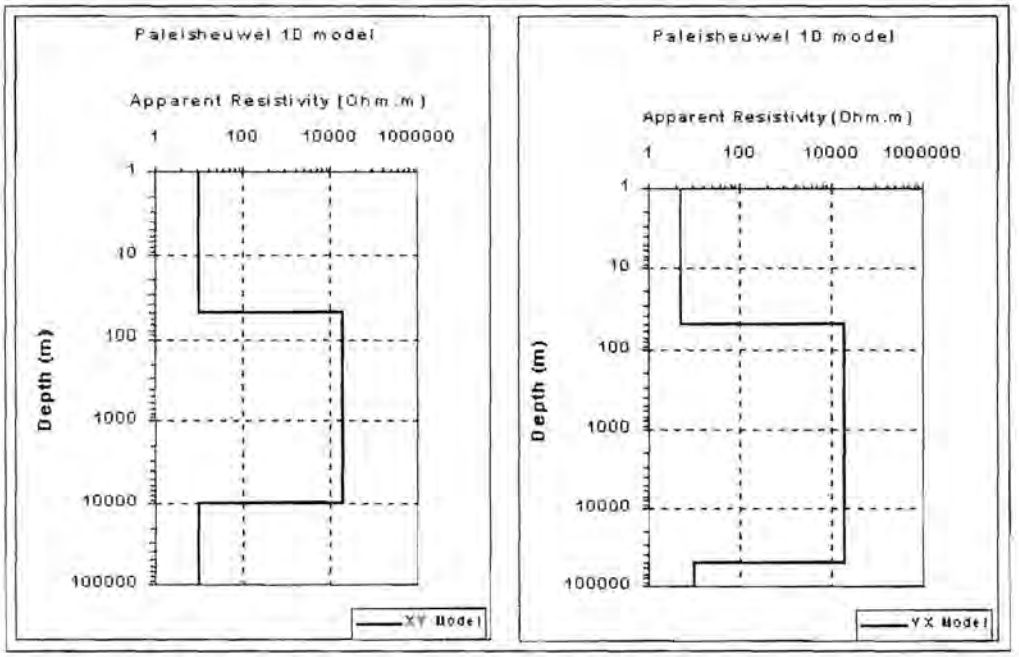

Figure 6.12. One dimensional models for Paleisheuwel.

6.3.6. Inkruip

The data for this station are scattered, but it is possible to distinguish a trend for both the ρ_{xy} and ρ_{yx} data sets (Figure 6.13(a)). Data were obtained between 0.15 Hz and 167 Hz.

Results of statistical reduction

Curves fitted through the data with the different statistical reduction methods are all of quite good quality (Figure 6.13(b) to (f)). Better results are obtained at frequencies where more data could be obtained. At the lowest freqeuncies where only a few data points occur the quality of the curves deteriorates drastically.

For data in both directions the least squares technique yields the poorest results (Figure 6.13(c)). Curves calculated by the robust M-estimation- and adaptive L_p norm methods are very similar.

Interpretation

The apparent resistivity curves in the two directions differ quite substantially. In the xy-direction the apparent resistivity increases with

decreasing frequency. The curve flattens out a little in the vicinity of 5 Hz, but from about 2 Hz it increases again. At high frequencies the ρ_{yx} curve increases with decreasing frequency, but at roughly 20 Hz it turns and the apparent resistivity steadily decreases with decreasing frequency.

The large difference between the two curves indicates a very anisotropic electrical substructure at this station. One dimensional models for this station (Figure 6.14) are very different for the two measurement directions.

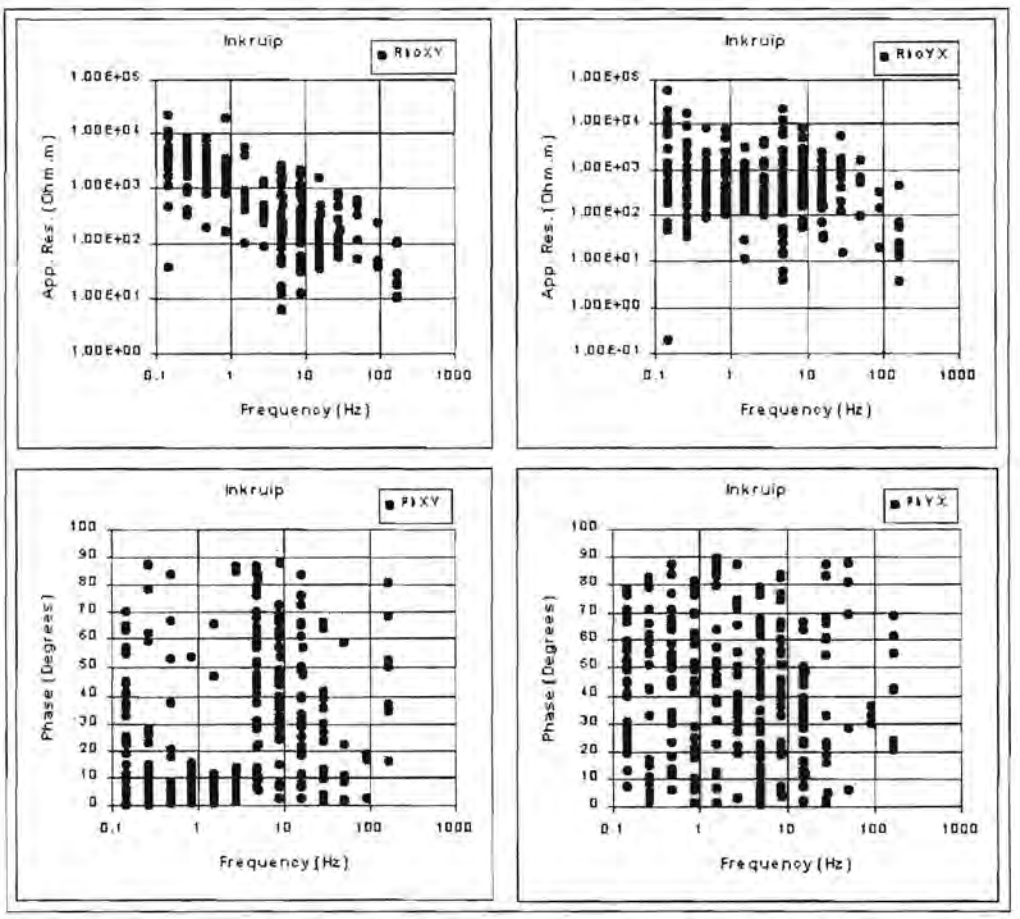

Figure 6.13(a). Apparent resistivity and impedance phase versus frequency curves for Inkruip.

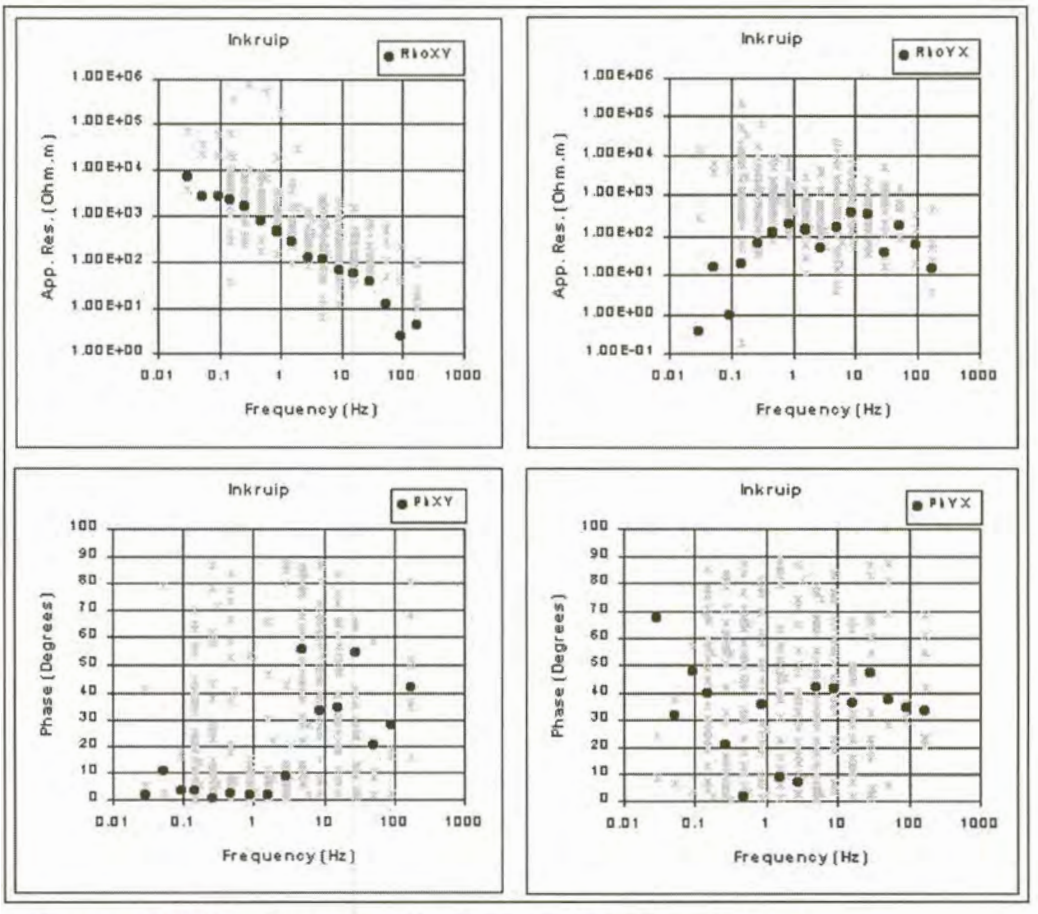

Figure 6.13(b). Curves estimated for Inkruip using L_1 norm reduction.

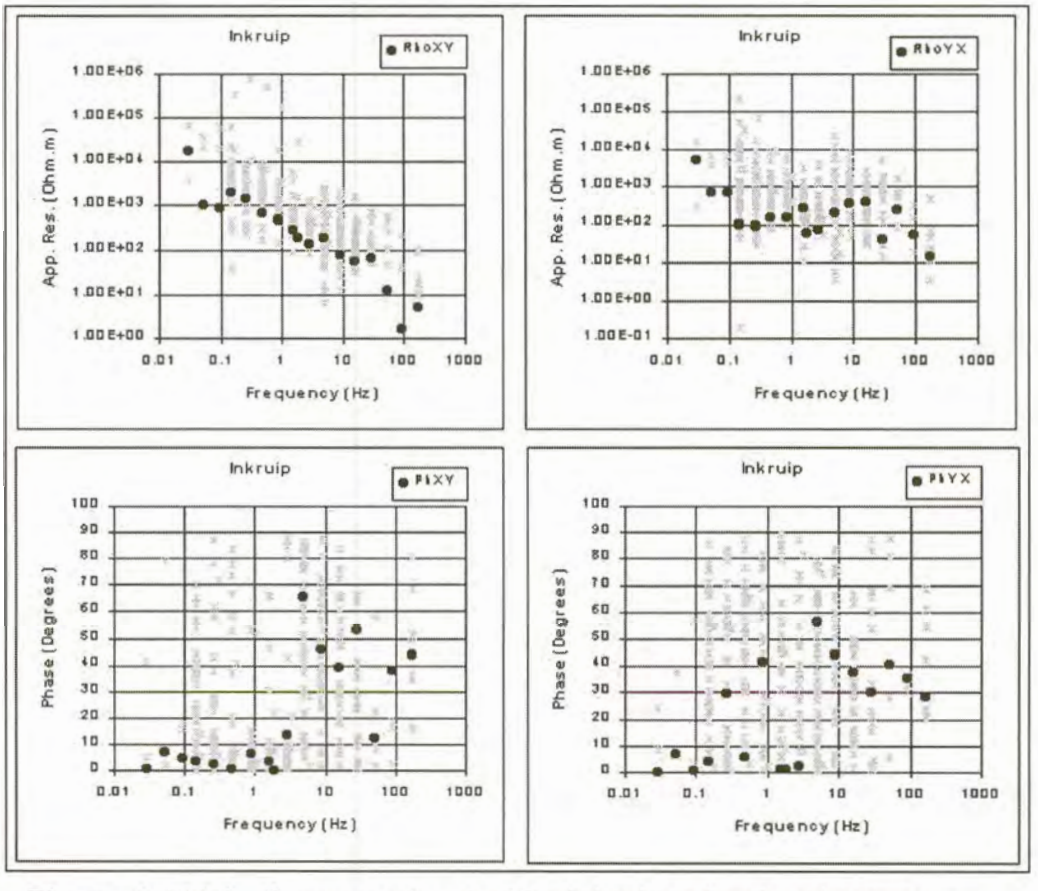

Figure 6.13(c). Curves estimated for Inkruip using least squares reduction.

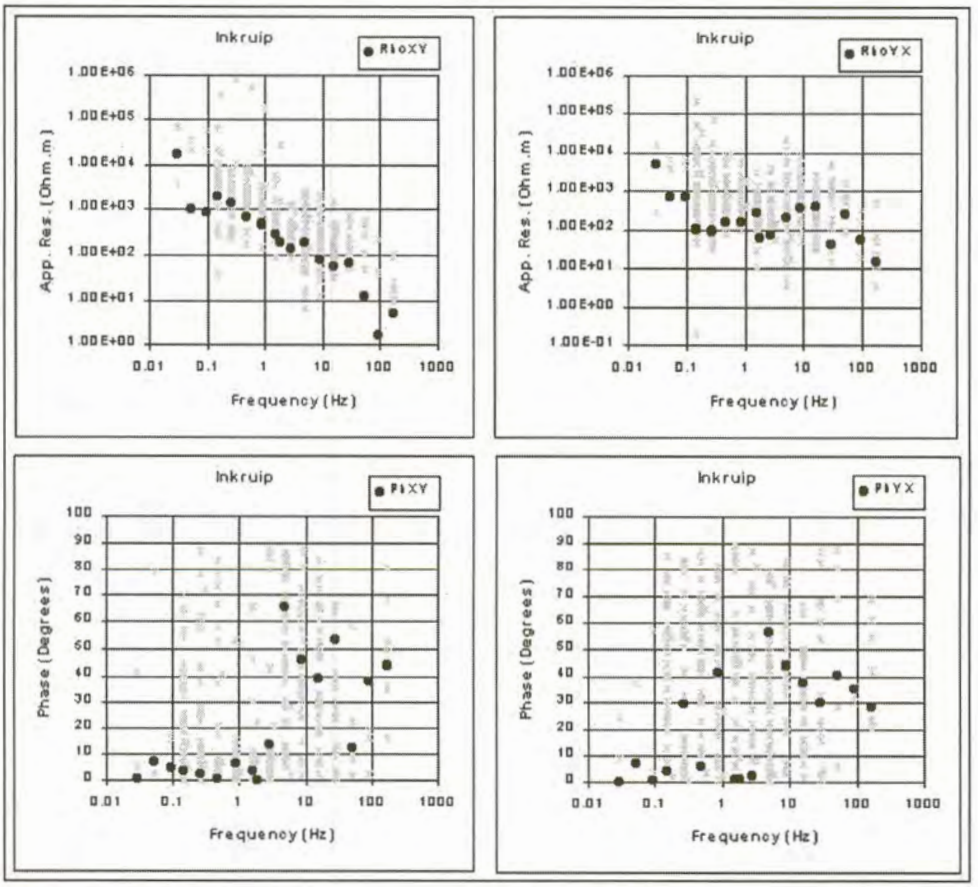

Figure 6.13(d). Curves estimated for Inkruip using robust M-estimation.

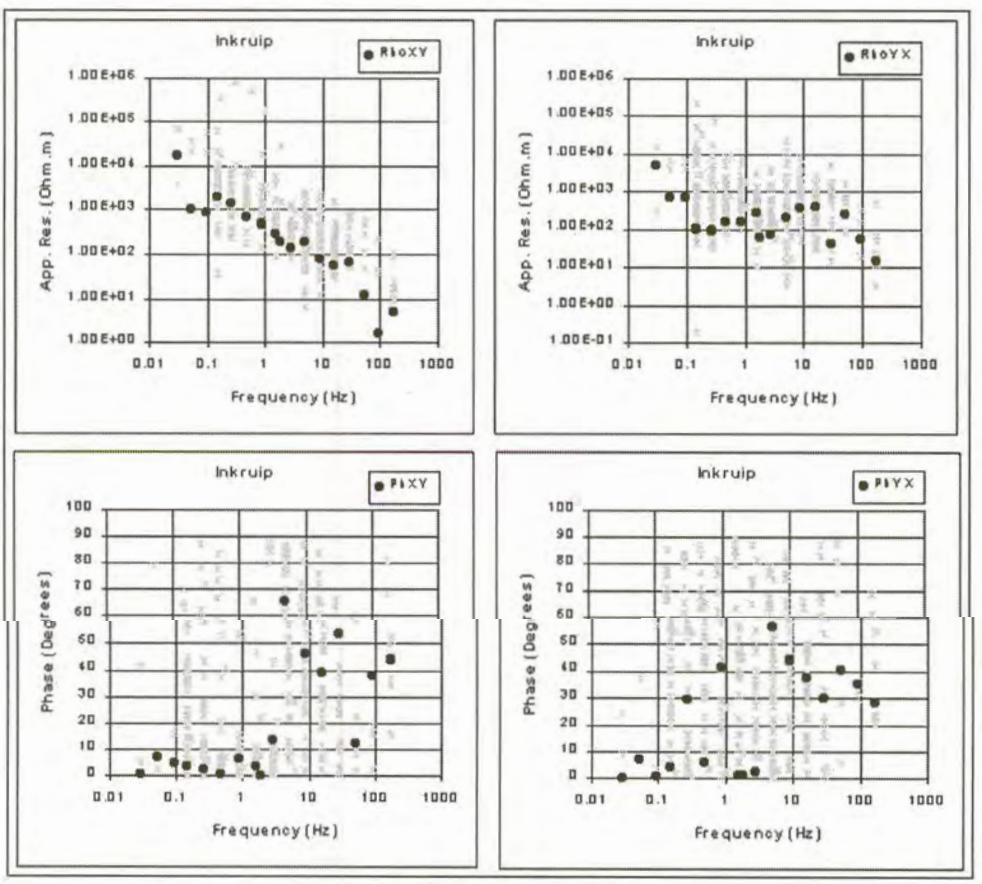

Figure 6.13(e). Curves estimated for Inkruip using adaptive L_p norm reduction (Sposito et al., 1983).

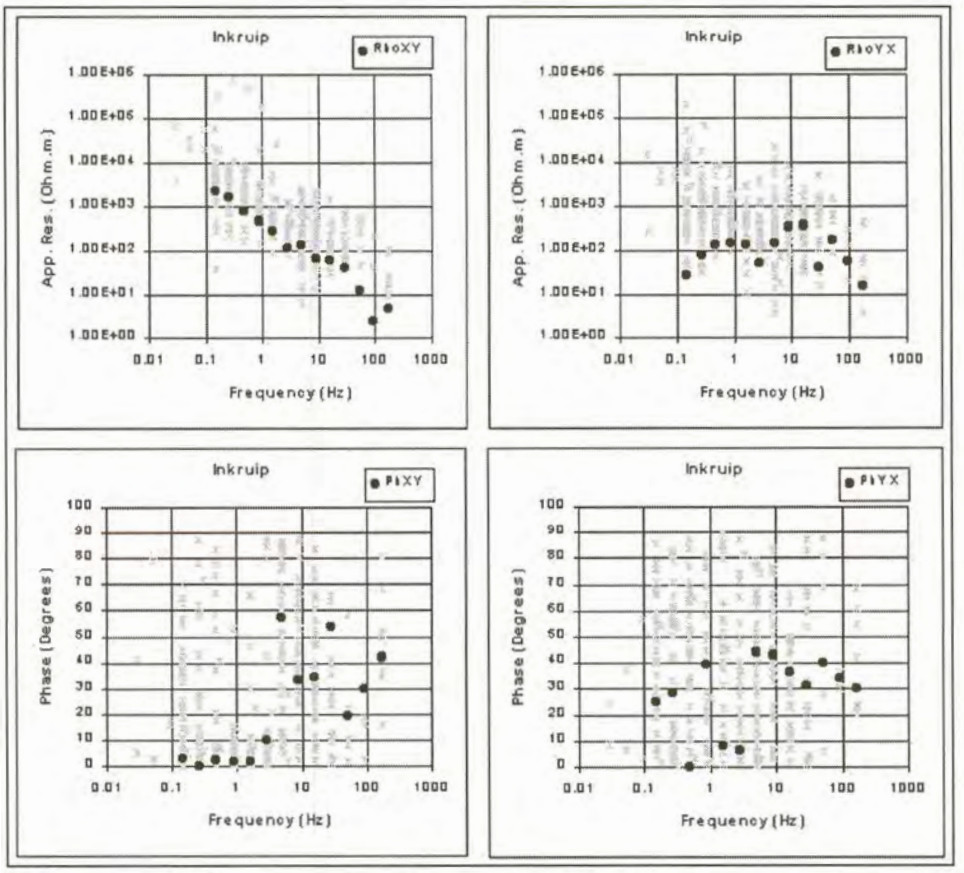

Figure 6.13(f). Curves estimated for Inkruip using adaptive L_p norm reduction (Money et al., 1982).

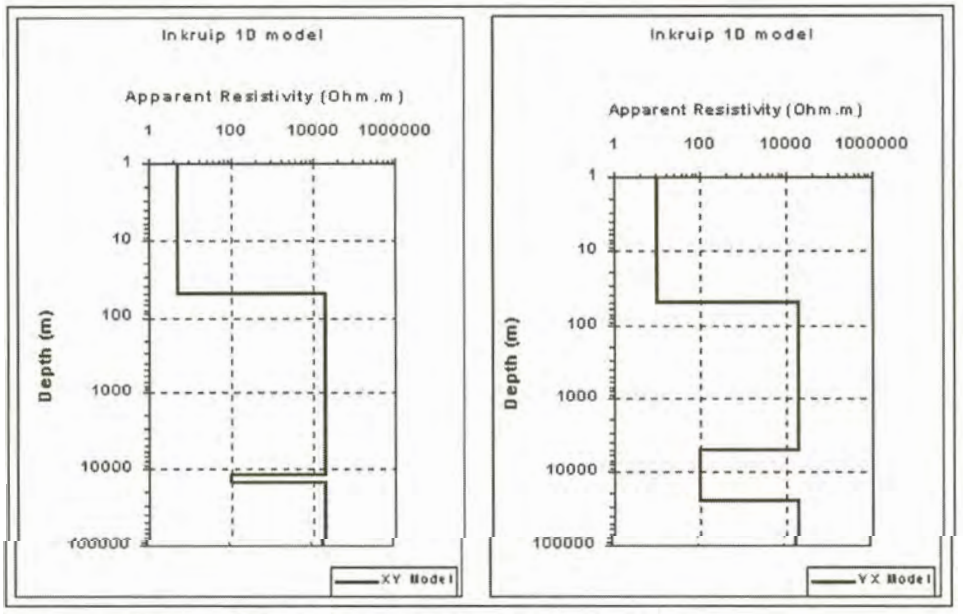

Figure 6.14. One dimensional models for Inkruip.

6.3.7. Gannavlakte

Data were collected between 0.1 Hz and 1000 Hz at this station (Figure 6.15(a)). The quality of the data is very low for both measurement directions.

Results of statistical reduction

None of the statistical methods yielded good fits (Figures 6.15(b) to (f)).

Interpretation

The data at this station follow the same trend as for Inkruip. Apparent resistivity values in the xy-direction increase with decreasing frequencies, with a possible conductor present at 10 Hz. In the yx-direction the resistivity values also increase with decreasing frequency at higher frequencies. At 10 Hz the curve flattens out. From 1 Hz and lower the resistivies start to increase again. Figure 6.16 shows the one-dimensional models for this station.

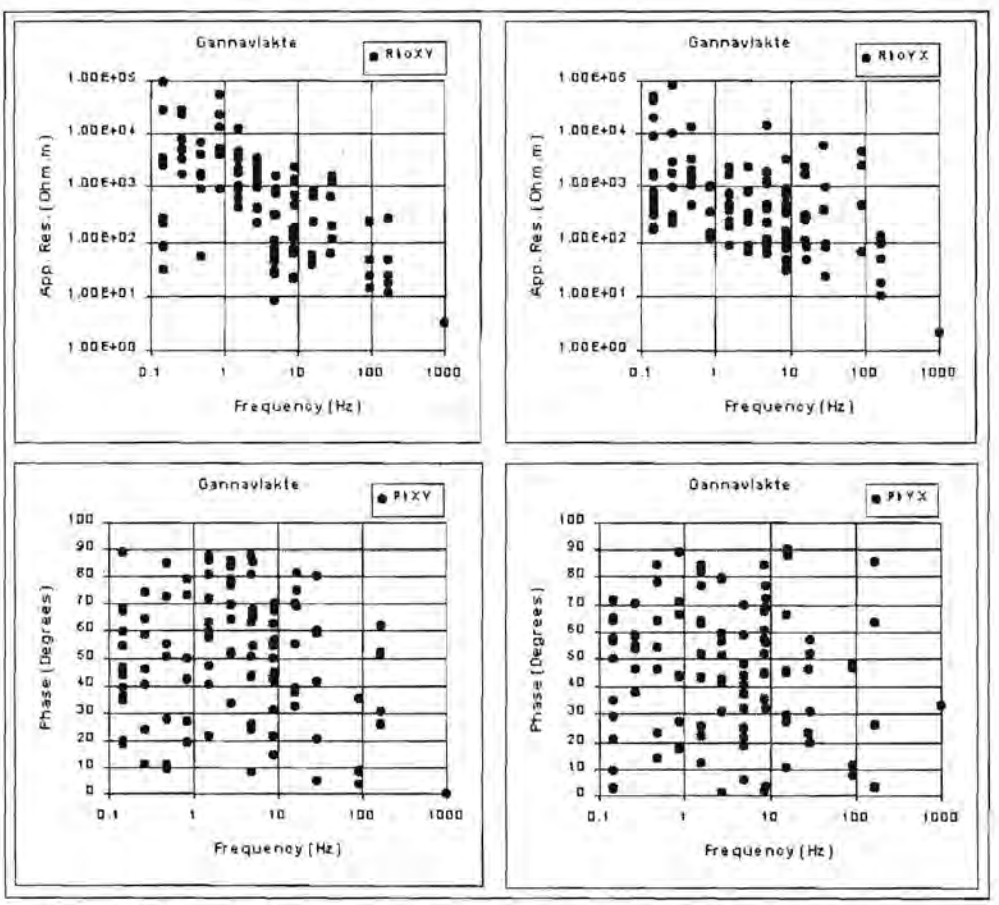

Figure 6.15(a). Apparent resistivity and impedance phase versus frequency curves for Gannavlakte.

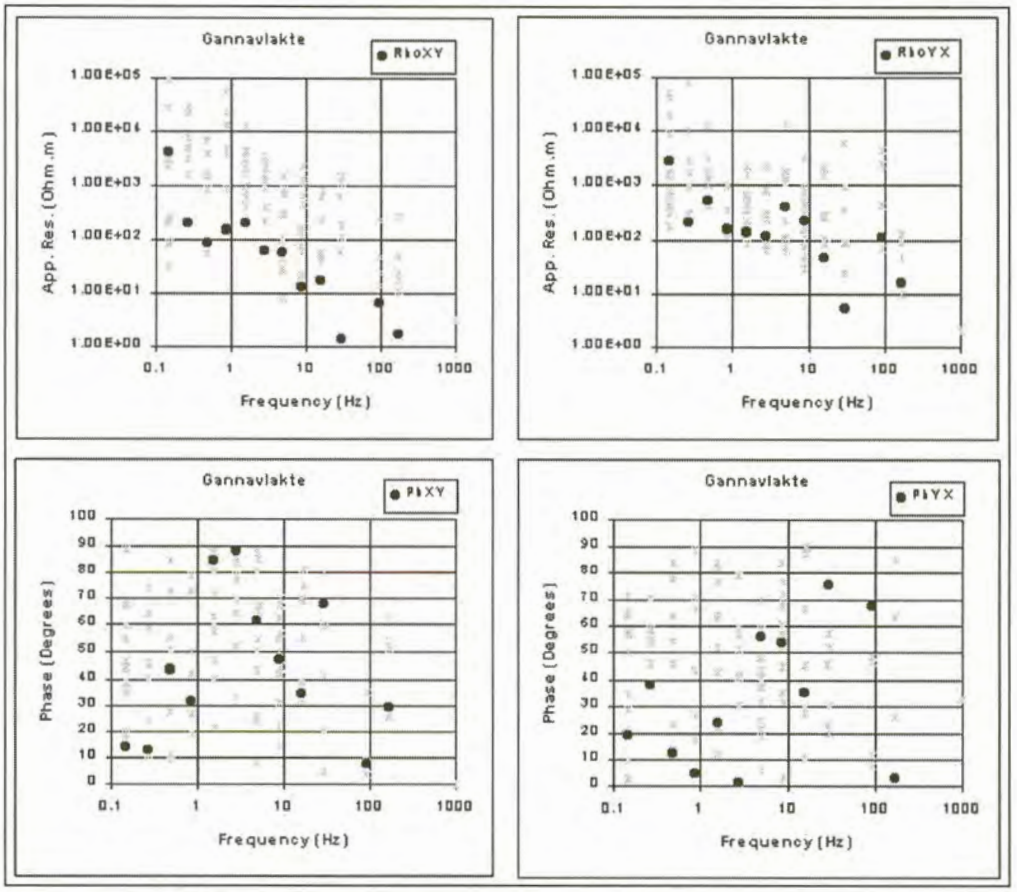

Figure 6.15(b). Curves estimated for Gannavlakte using L_1 norm reduction.

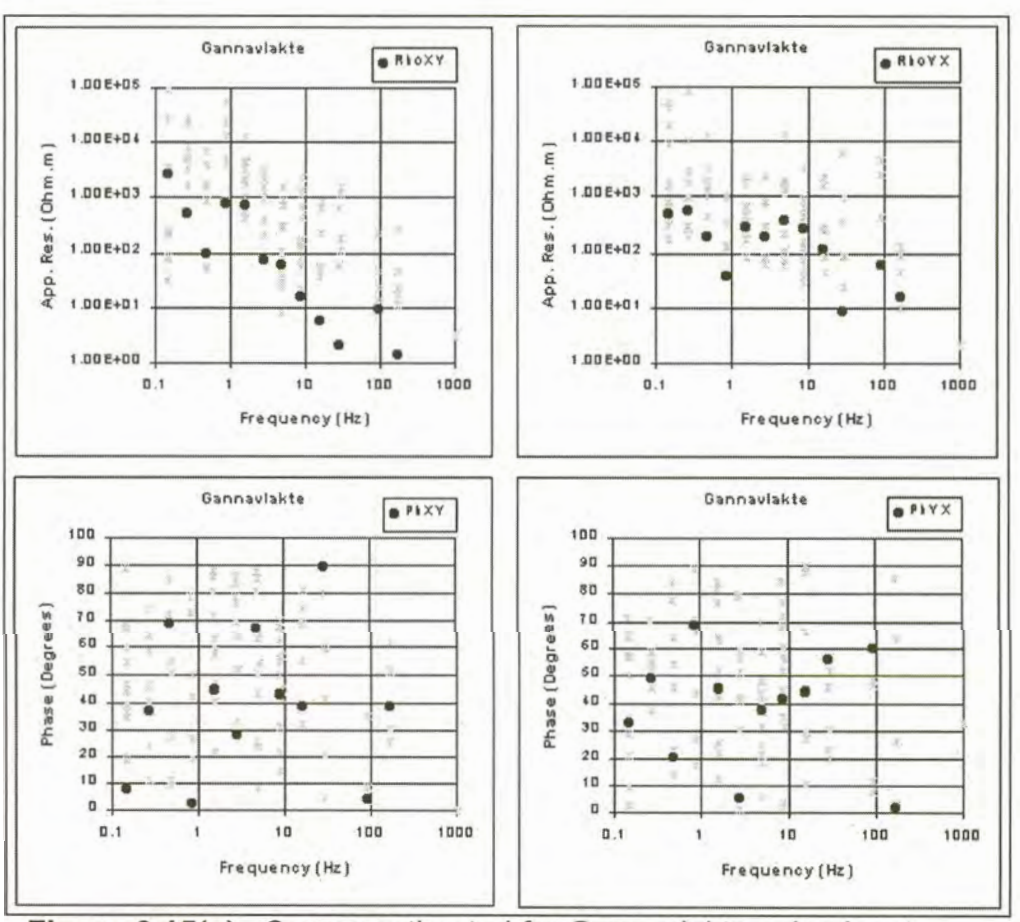

Figure 6.15(c). Curves estimated for Gannavlakte using least squares reduction.

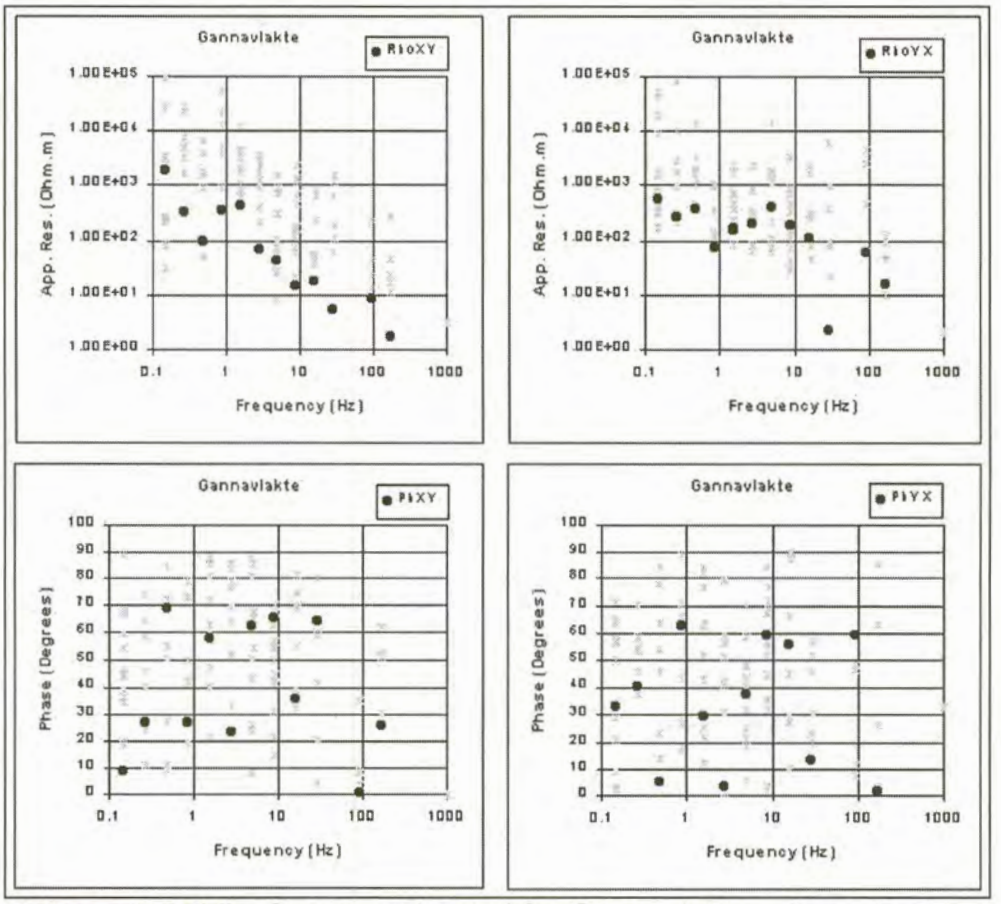

Figure 6.15(d). Curves estimated for Gannavlakte using robust M-estimation.

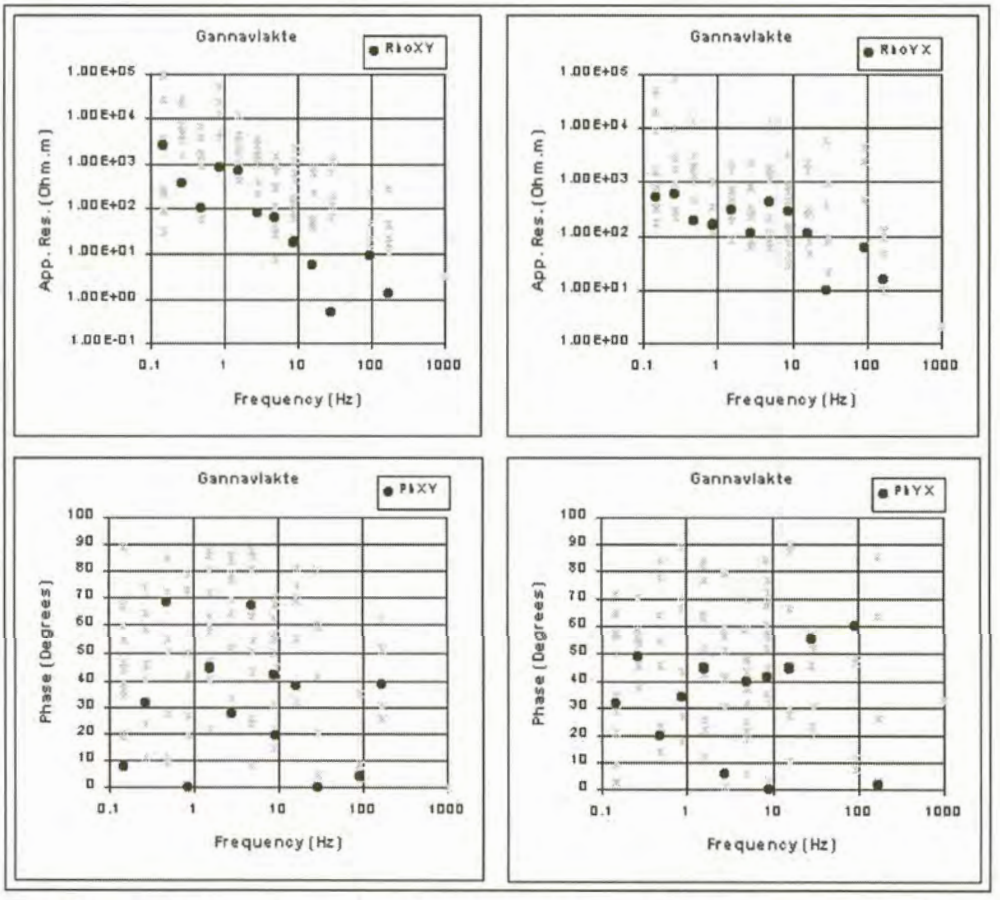

Figure 6.15(e). Curves estimated for Gannavlakte using adaptive L_p norm reduction (Sposito et al., 1983).

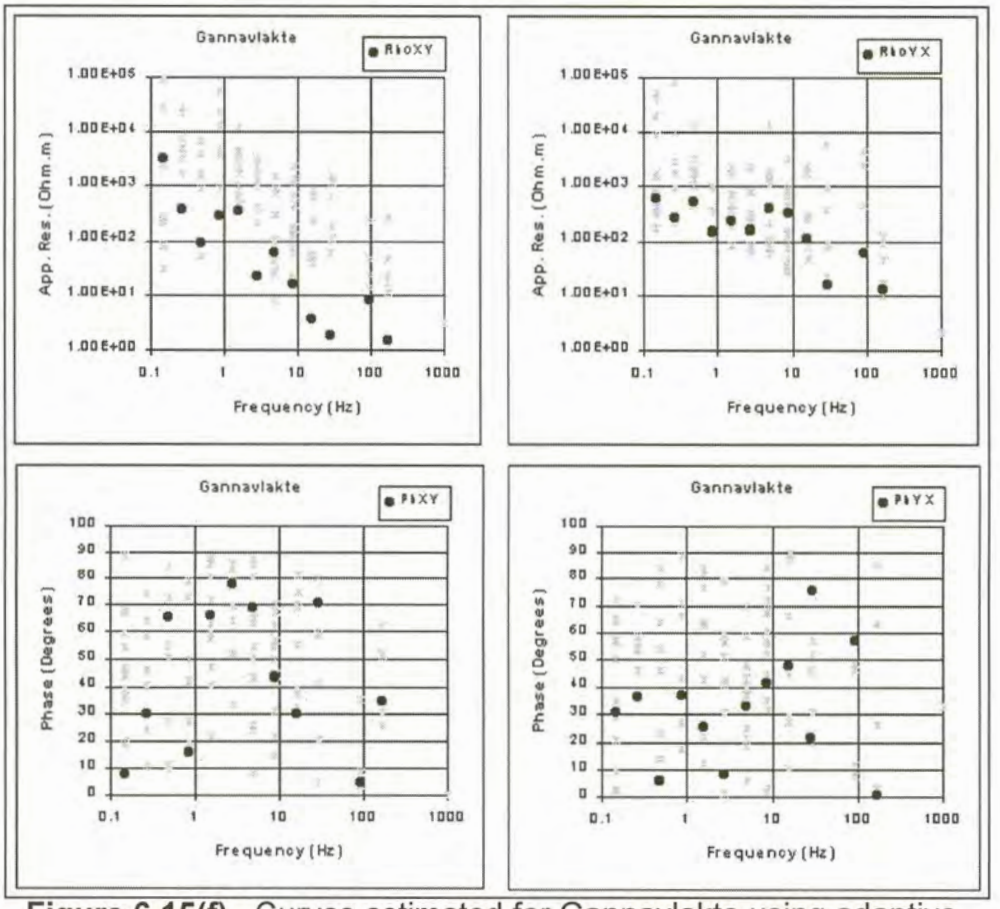

Figure 6.15(f). Curves estimated for Gannavlakte using adaptive L_p norm reduction (Money et al., 1982).

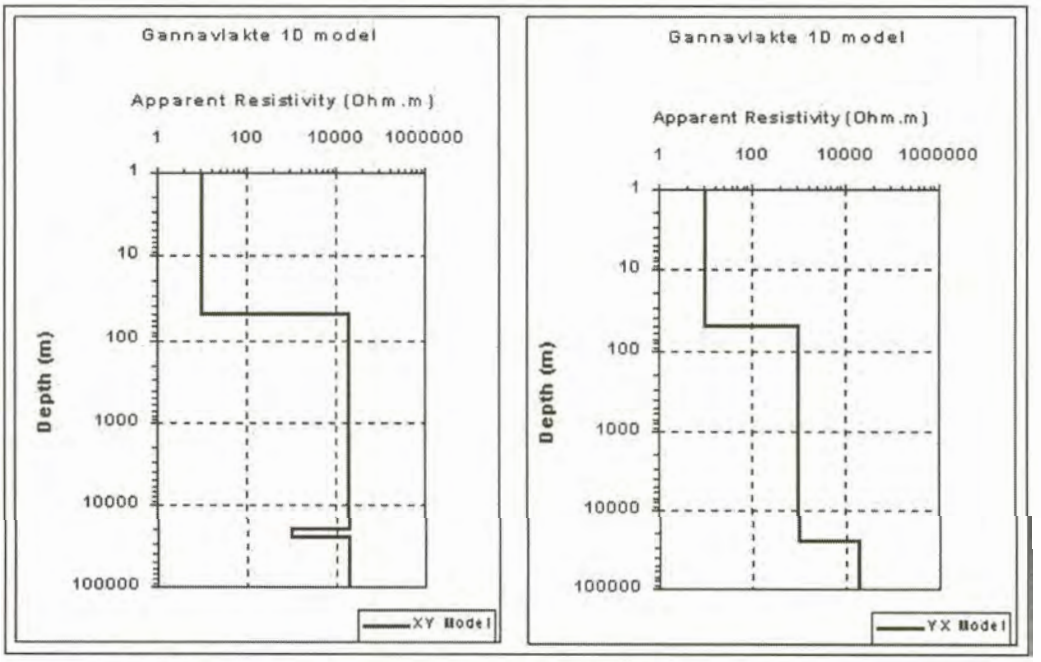

Figure 6.16. One dimensional models for Gannavlakte.

6.3.8. Albany

Figure 6.17(a) shows the data obtained at his station. Data were collected at a large range of frequencies, from 0.01 Hz to 1000 Hz. Although the quality of the apparent resistivity data are very good, the impedance phases are extremely scattered.

Results of statistical reduction

For data in the xy-direction the robust M-estimation technique yields the best results. In general curves fitted for this direction are of lower quality than for the yx-direction. The adaptive L_p norm using Sposito's equation gives the best curve for the ρ_{yx} data (Figure 6.17(e)). The L1 norm gives the worst results, especially at low frequencies (Figure 6.17(b)).

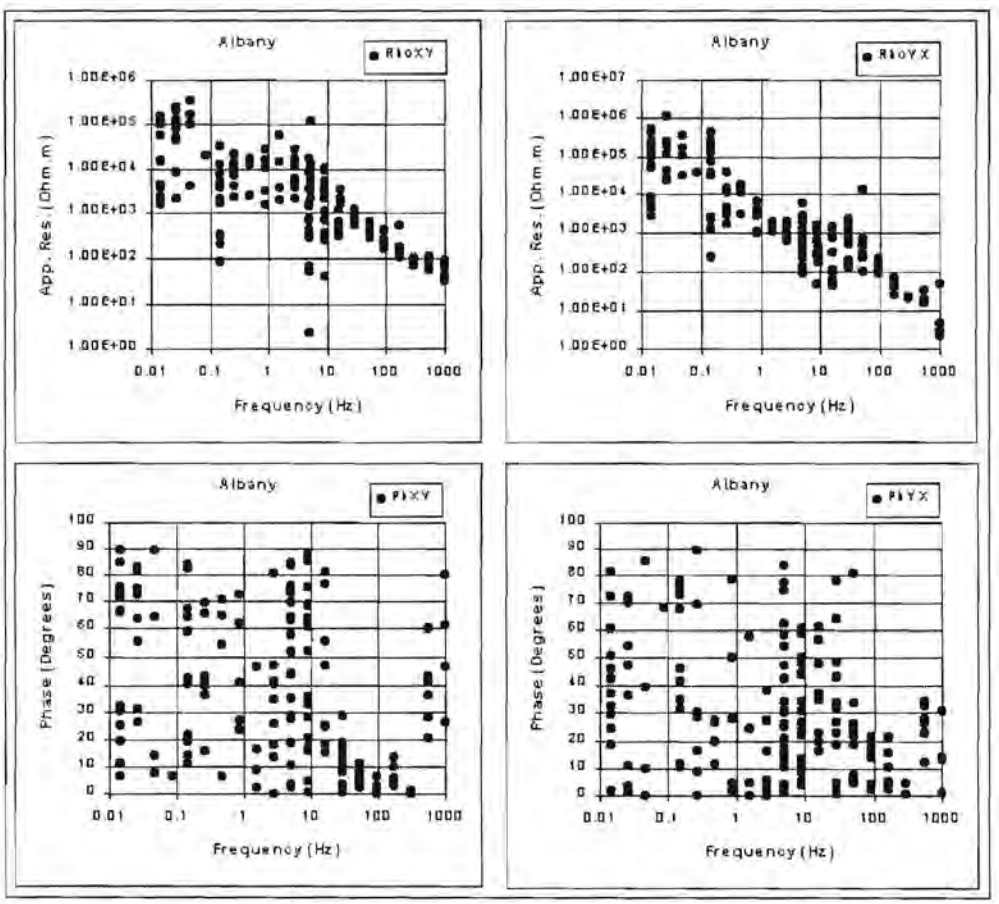

Figure 6.17(a). Apparent resistivity and impedance phase versus frequency curves for Albany.

Interpretation

In the xy-direction the apparent resistivity increases with decreasing frequency. At approximately 2 Hz the curve turns and the resistivities start to decrease, but below 0.1 Hz it increases again. The curve for the yx-direction starts out similar to the ρ_{xy} curve, but between 30 Hz and 1 Hz it flattens out. Below 1 Hz it increases again with decreasing frequency. Figure 6.18 shows the one-dimensional models calculated for these curves.

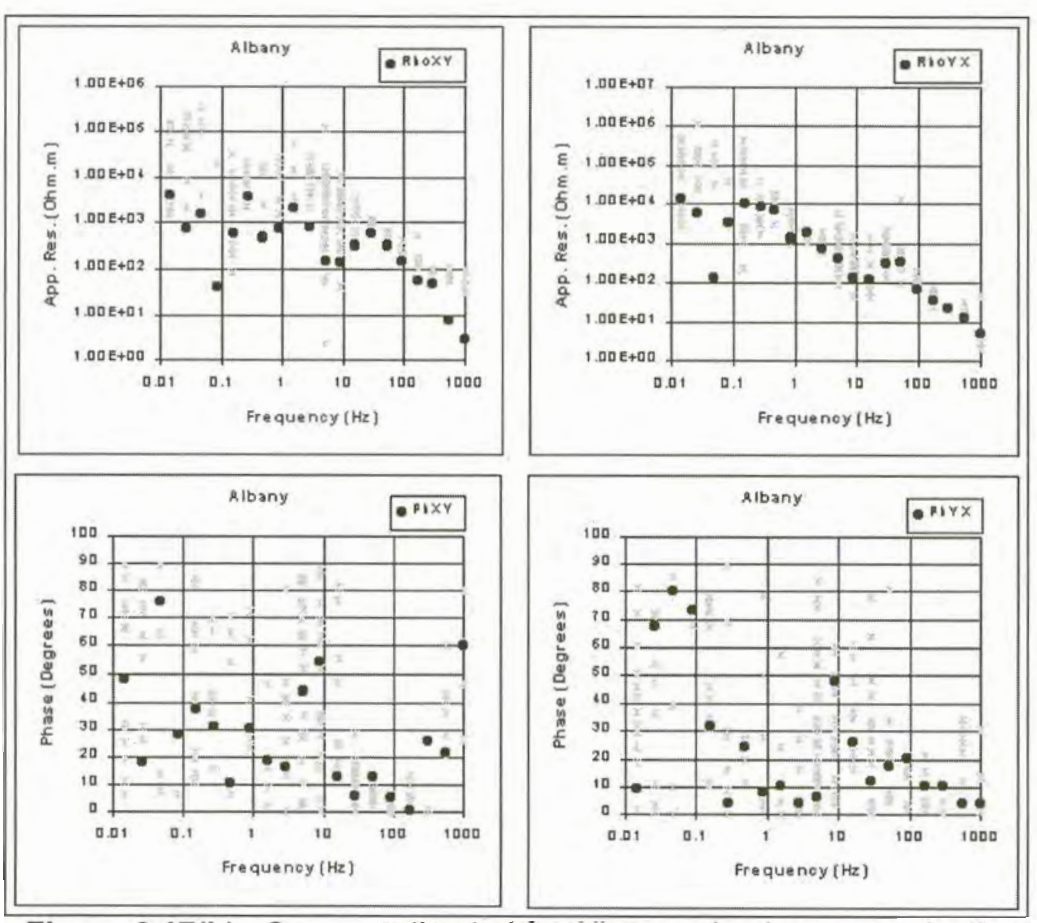

Figure 6.17(b). Curves estimated for Albany using L_1 norm reduction.

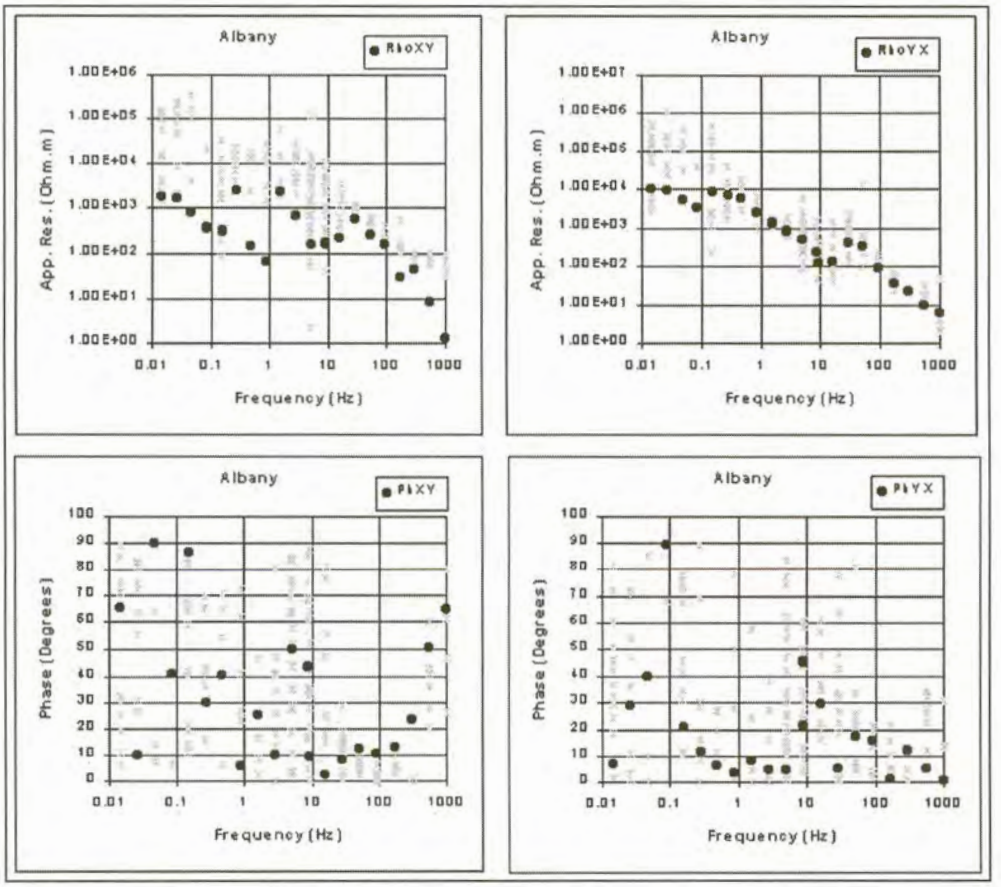

Figure 6.17(c). Curves estimated for Albany using least squares reduction.

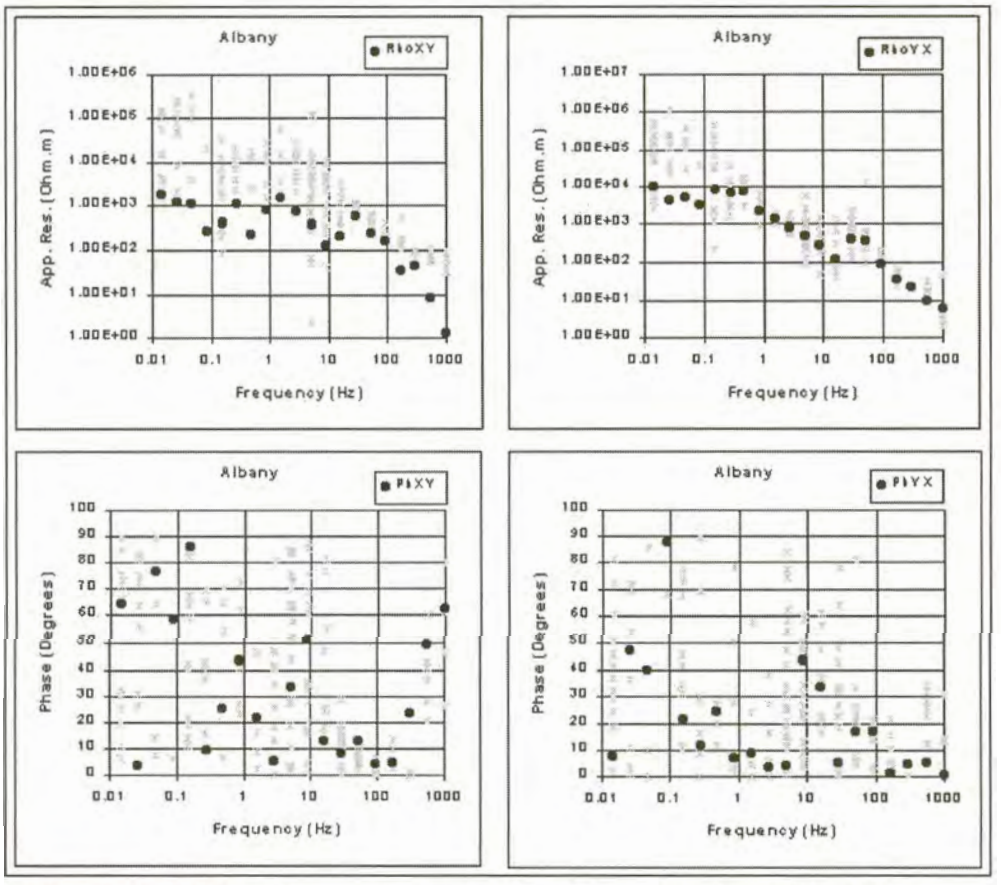

Figure 6.17(d). Curves estimated for Albany using robust M-estimation.

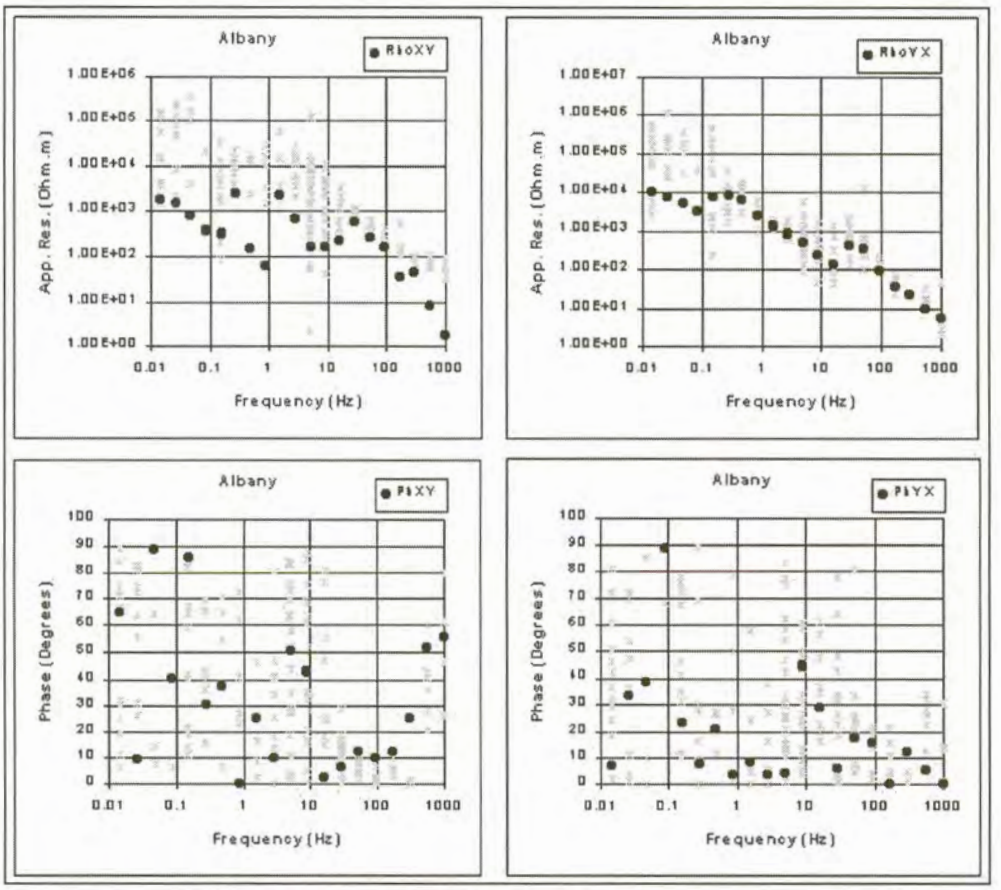

Figure 6.17(e). Curves estimated for Albany using adaptive L_p norm reduction (Sposito et al., 1983).

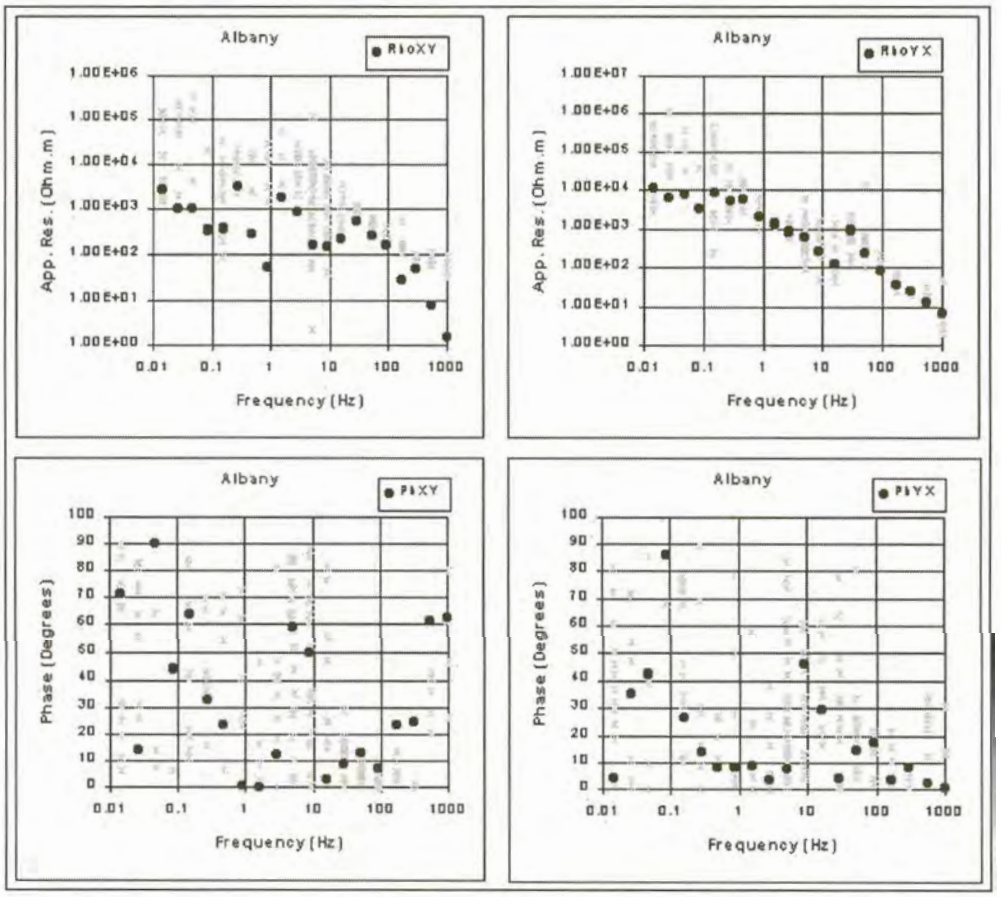

Figure 6.17(f). Curves estimated for Albany using adaptive L_p norm reduction (Money et al., 1982).

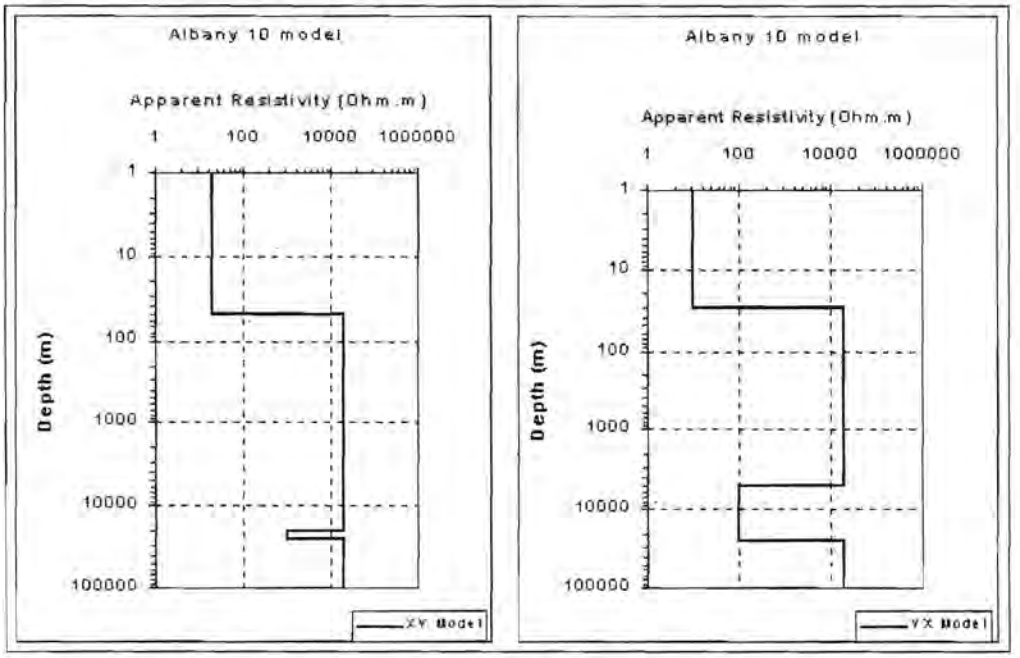

Figure 6.18. One dimensional models for Albany.

6.3.9. Uizip

Only a small amount of data were gathered at this station. Data were obtained between 0.01 Hz and 100 Hz (Figure 6.19). Impedance phase data in the xy-direction are of moderate quality.

Results of statistical reduction

The robust M-estimation technique yields the best results for both the xy- and yx-direction data (Figure 6.19(d)). The adaptive L_p norm methods failed to converge at most of the frequencies (Figures 6.19 (e) and (f)).

Interpretation

Data in the two directions are very similar at lower frequencies. Resistivities decrease with increasing frequency. The ρ_{xy} curve starts to turn just below 10 Hz while the ρ_{yx} curve turns at 1 Hz. The difference in the one-dimensional models (Figure 6.20) shows that the underlying geology is anisotropic.

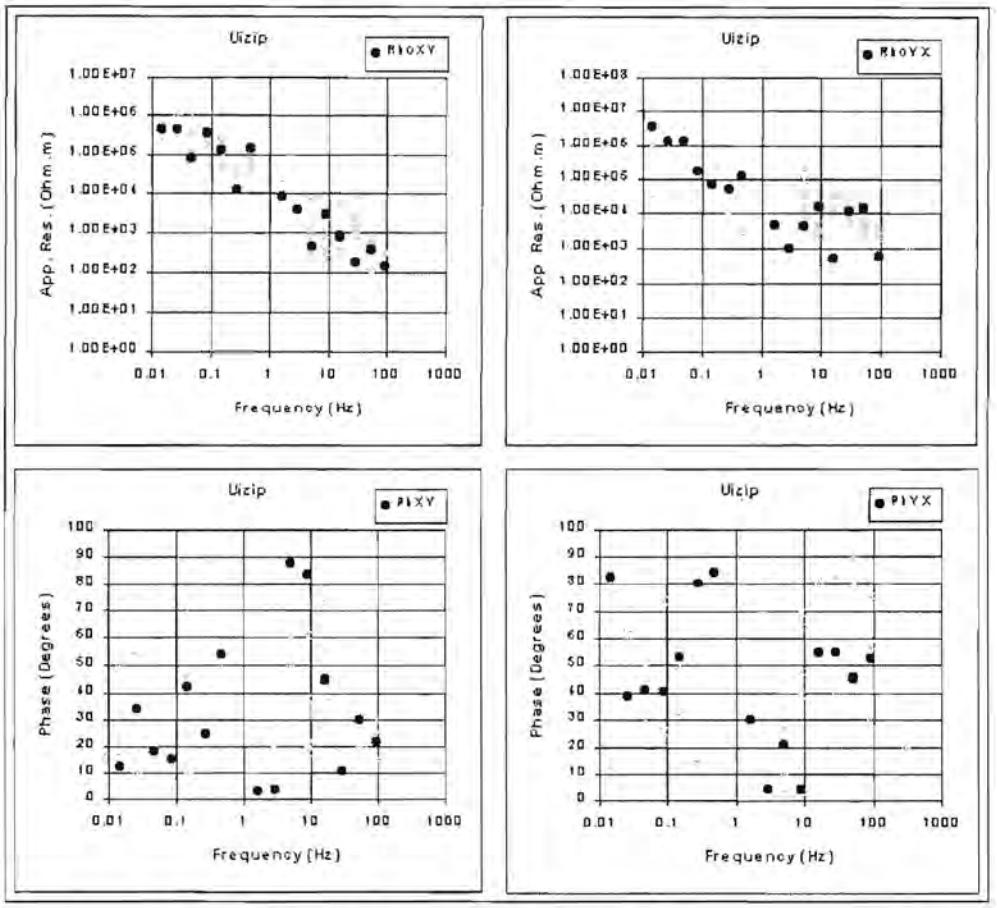

Figure 6.19(c). Curves estimated for Uizip using least squares reduction.

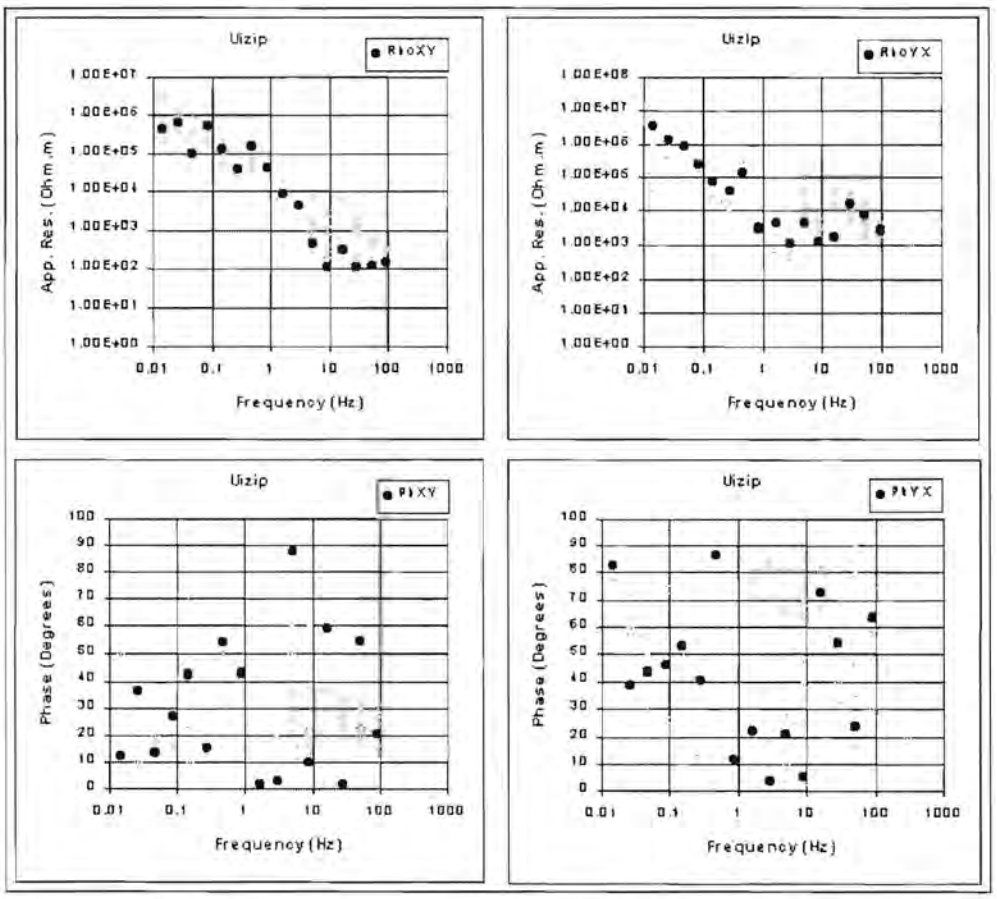

Figure 6.19(d). Curves estimated for Uizip using robust M-estimation.

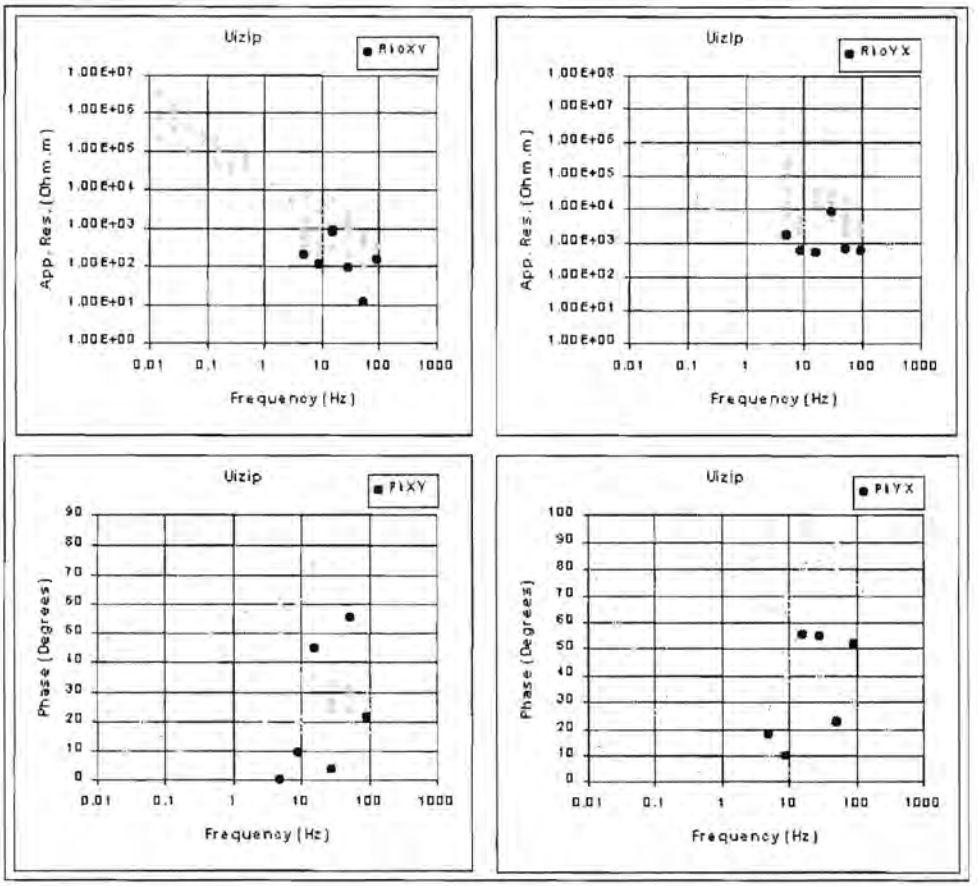

Figure 6.19(e). Curves estimated for Uizip using adaptive L_p norm reduction (Sposito et al., 1983).

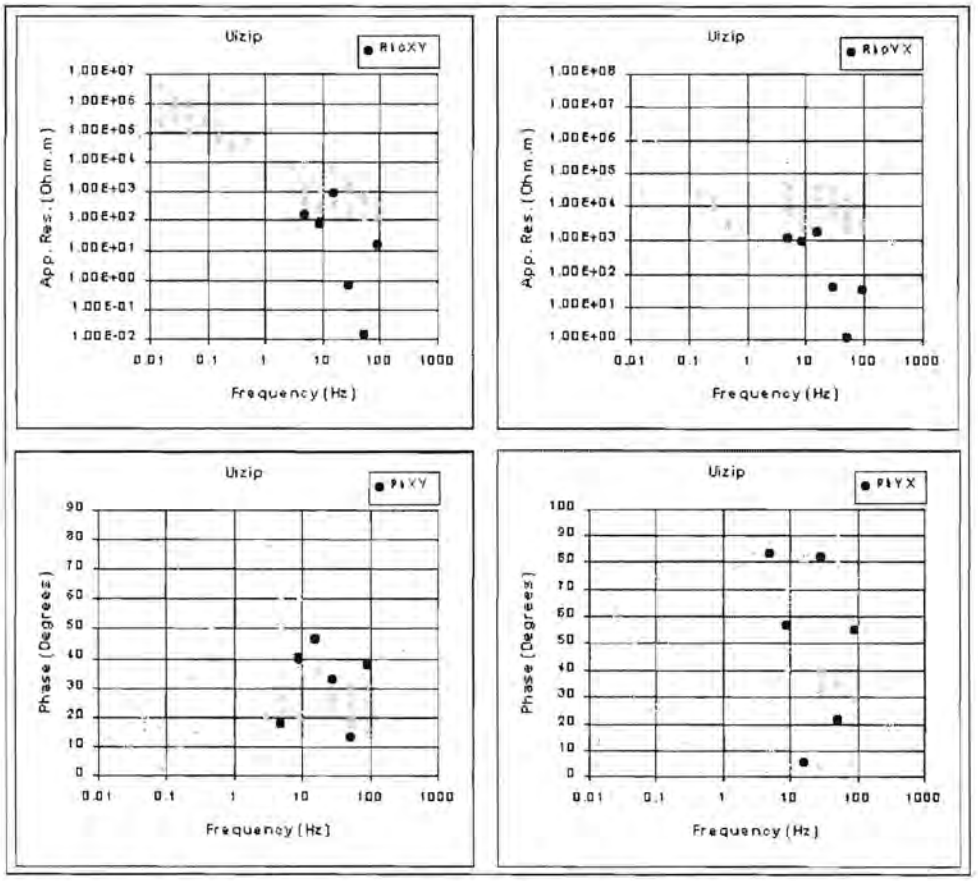

Figure 6.19(f). Curves estimated for Uizip using adaptive L_p norm reduction (Money et al., 1982).

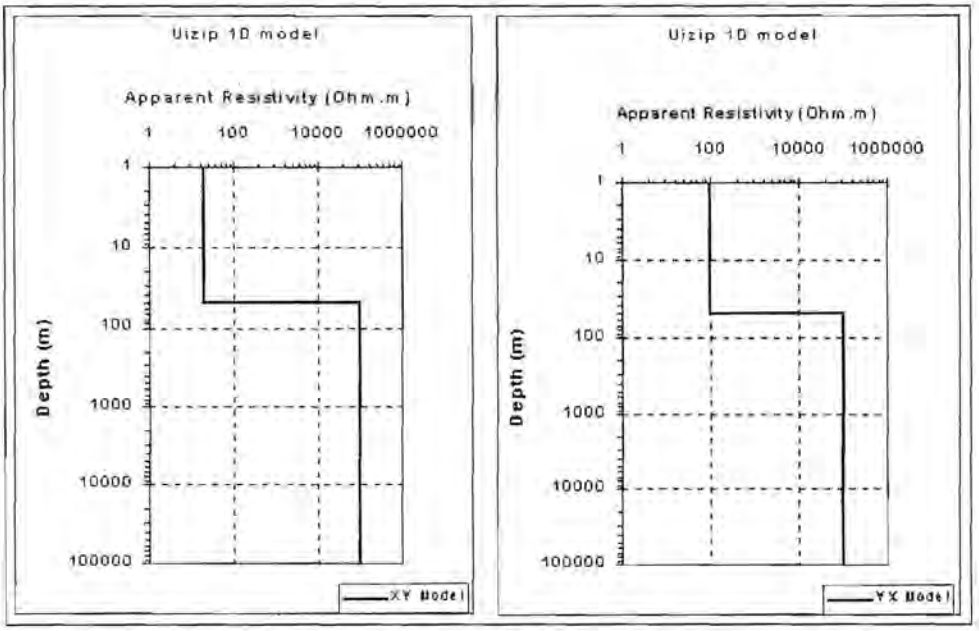

Figure 6.20. One dimensional models for Uizip.

6.3.10. Upington

Most of the data collected at this station fall in the higher frequency range. Below 5 Hz the amount of data drastically decreases (Figure 6.21(a)). Data in the yx-direction are more scattered than in the xy-direction.

Results of statistical reduction

The L1-, L2 norms and robust M-estimation methods give good results in the xy-direction. At lower frequencies the adaptive L_p norm techniques failed to converge, probably as a result of the lack of data at these frequencies. The quality of the curves fitted through the ρ_{yx} data is not very good. The robust M-estimation technique resulted in the best curve.

Interpretation

For both directions, the data result in high resistivity values at high frequencies. The resistivity curves increase a little before starting to turn at 5 Hz. In the xy-direction the curve stays flat until roughly 0.3 Hz where

the resistivities start to increase again. For the yx-direction the values already start to increase at 1Hz.

One dimensional models for this station are shown in Figure 6.22.

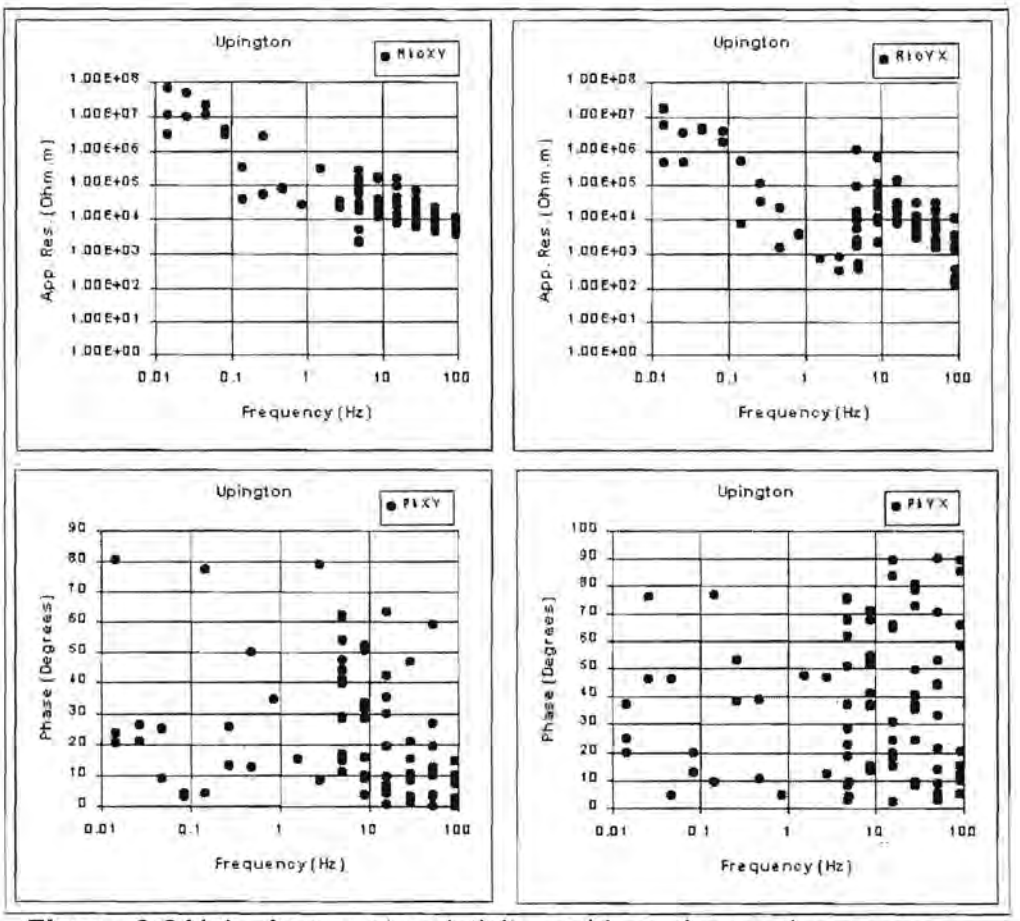

Figure 6.21(a). Apparent resistivity and impedance phase versus frequency curves for the Upington station.

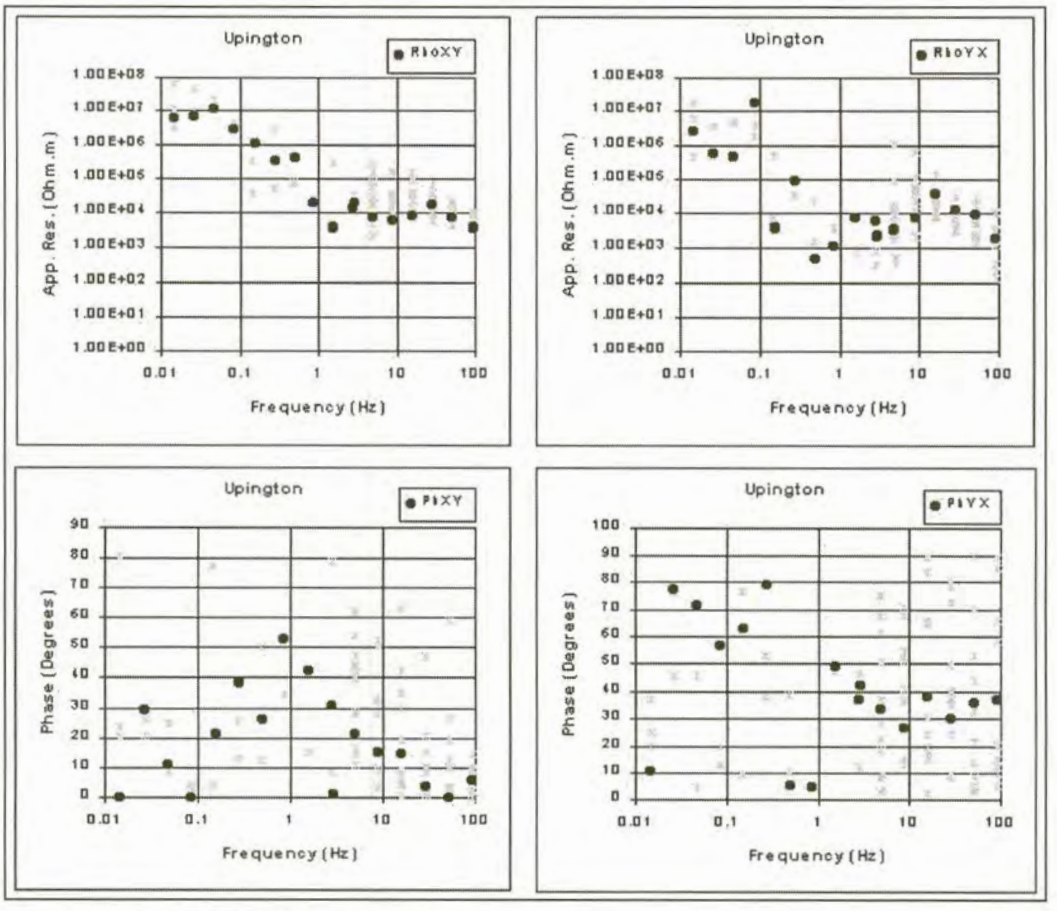

Figure 6.21(b). Curves estimated for Upington using L_1 norm reduction.

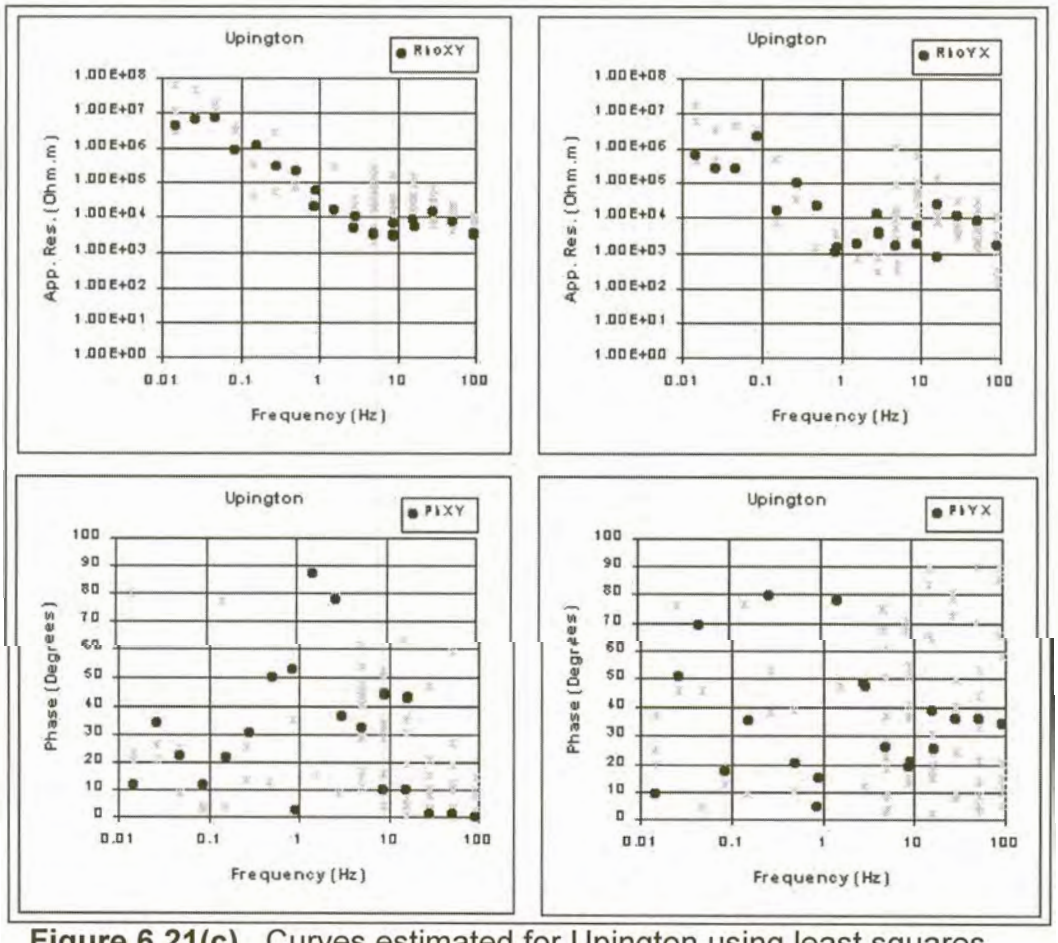

Figure 6.21(c). Curves estimated for Upington using least squares reduction.

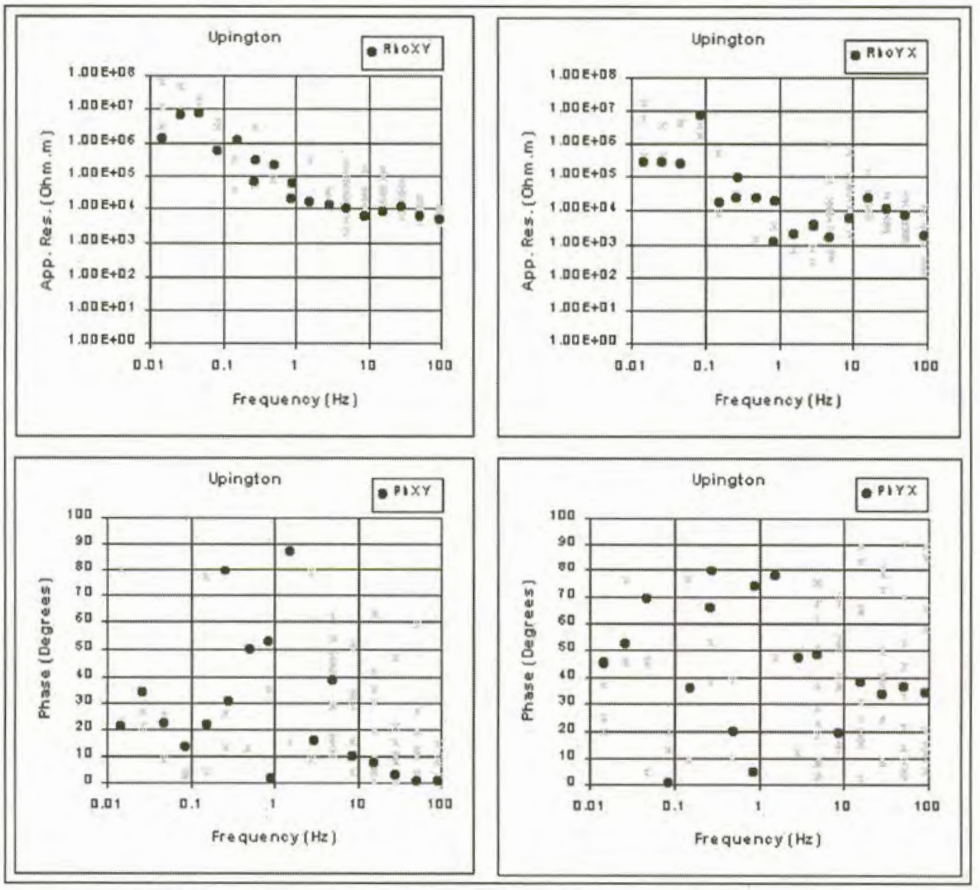

Figure 6.21(d). Curves estimated for Upington using robust M-estimation.

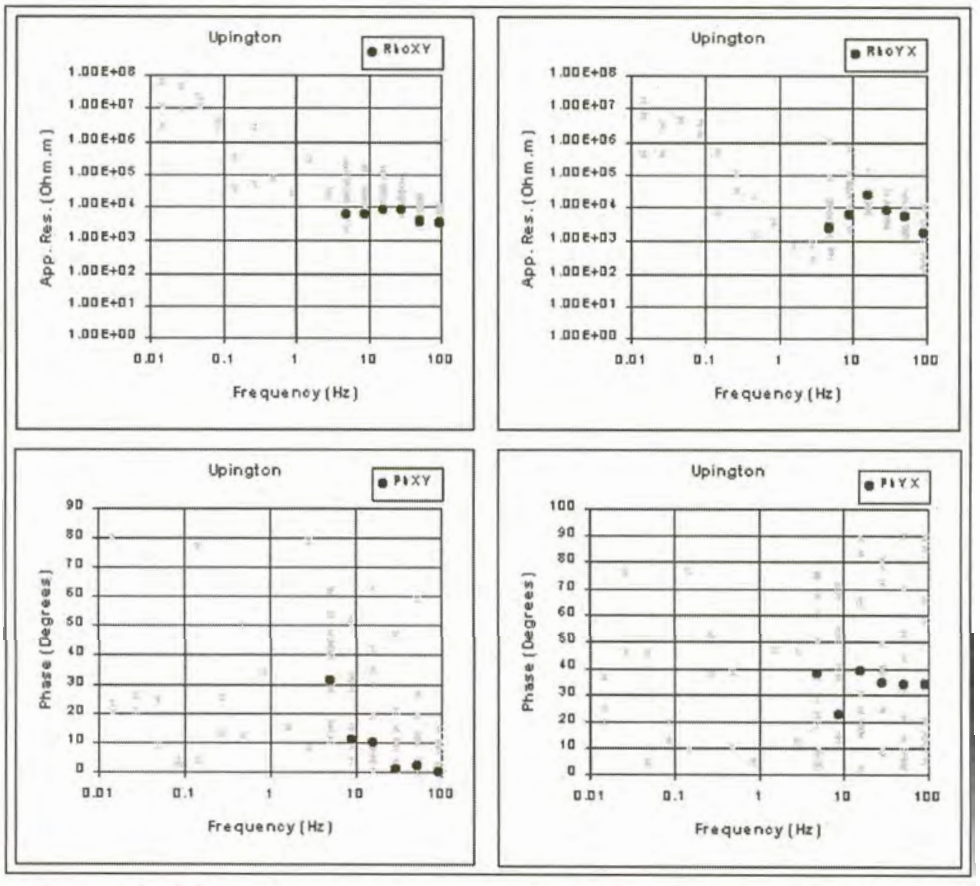

Figure 6.21(e). Curves estimated for Upington using adaptive L_p norm reduction (Sposito et al., 1983).

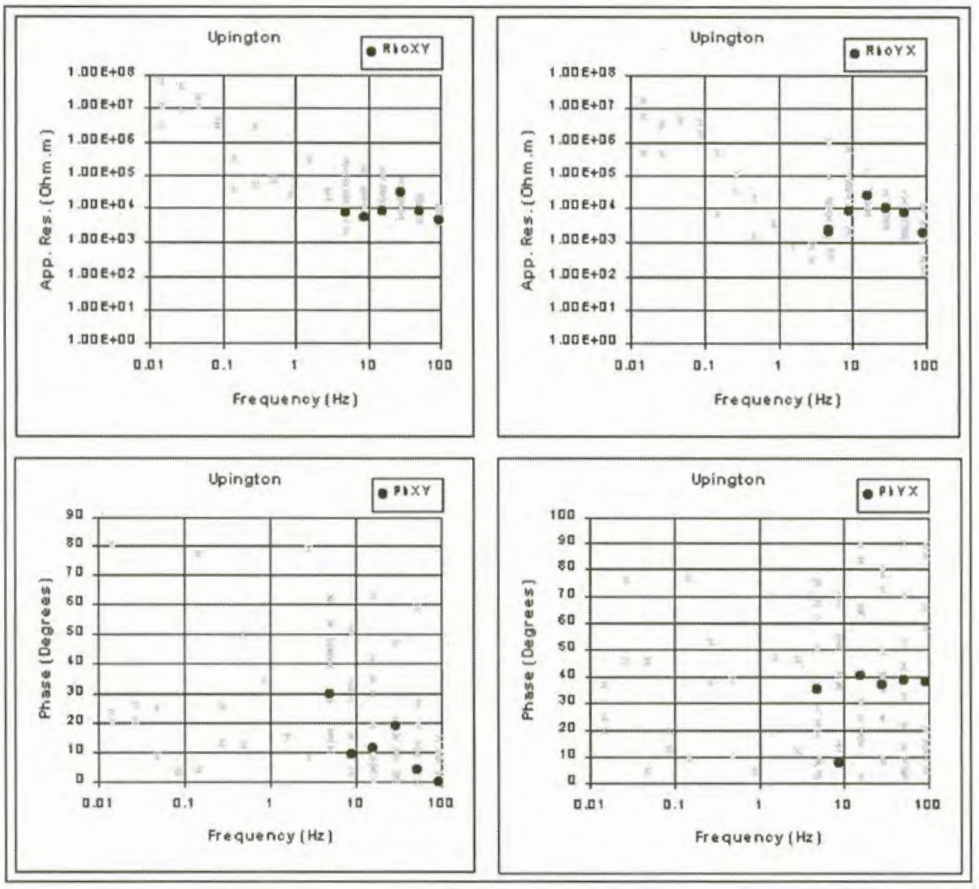

Figure 6.21(f). Curves estimated for Upington using adaptive L_p norm reduction (Money et al., 1982).

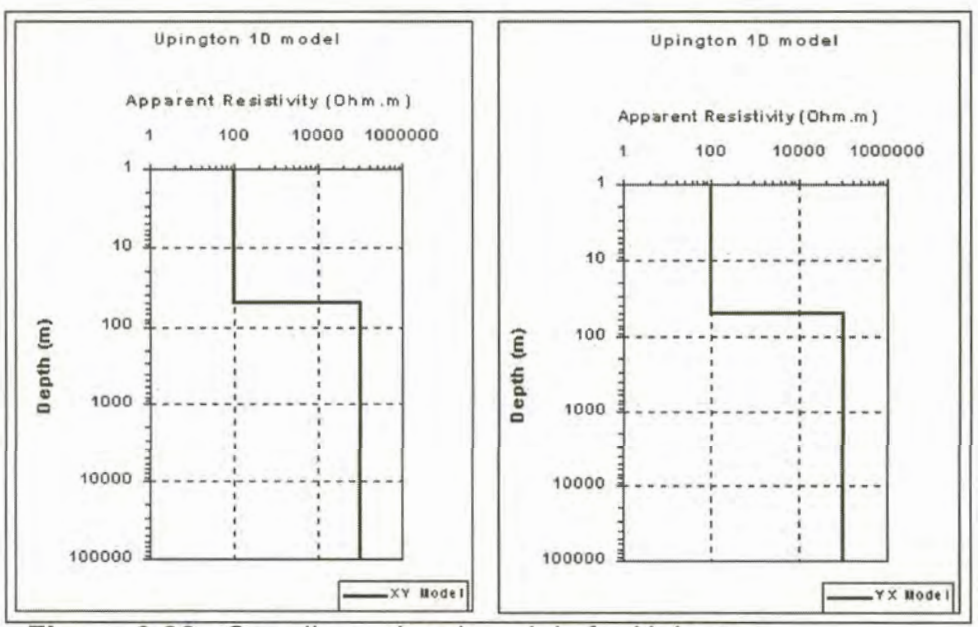

Figure 6.22. One dimensional models for Upington.

6.3.11. Dyason's Klip

An electrode spacing of 150m was used at this station. The distance between the local and remote stations was 450m. Data in the yx-direction are more scattered than data in the xy-direction (Figure 6.23(a)). The quality of the phase data in both directions are extremely poor.

Results of statistical reduction

The curves fitted through the ρ_{xy} data differ quite substantially depending on the reduction technique used. None of the methods yielded curves that fitted the data between 0.3 Hz and 5 Hz. The least squares (Figure 6.23(c)) and robust M-estimation (Figure 6.23(d)) methods produce curves that indicate the presence of a conductor between 1 and 10 Hz while the adaptive L_p norm (Sposito et al., 1983) (Figure 6.23(e)) yielded a curve that is close to being a straight line.

The curves calculated in the yx-direction approximates the data more closely. The adaptive L_p norm techniques (Figures 6.23(e) and (f)) yield very bad results at frequencies above 1 Hz due to a lack of data. It seems as though least squares minimisation (Figure 6.23(c)) produce the best result.

Interpretation

Apparent resistivities start in the vicinity of 1000 Ohm.m at high frequencies and increase with depth. Between 0.1Hz and 2 Hz the ρ_{xy} curve seems to flatten out somewhat before increasing again at lower frequencies. In the yx-direction the resistivity stay nearly constant at high frequencies and starts to increase from 1 Hz and lower. From the data and one-dimensional models (Figure 6.24) it can be interpreted that the underlying earth is more isotropic at greater depths, but become more inhomogeneous at shallower depths.

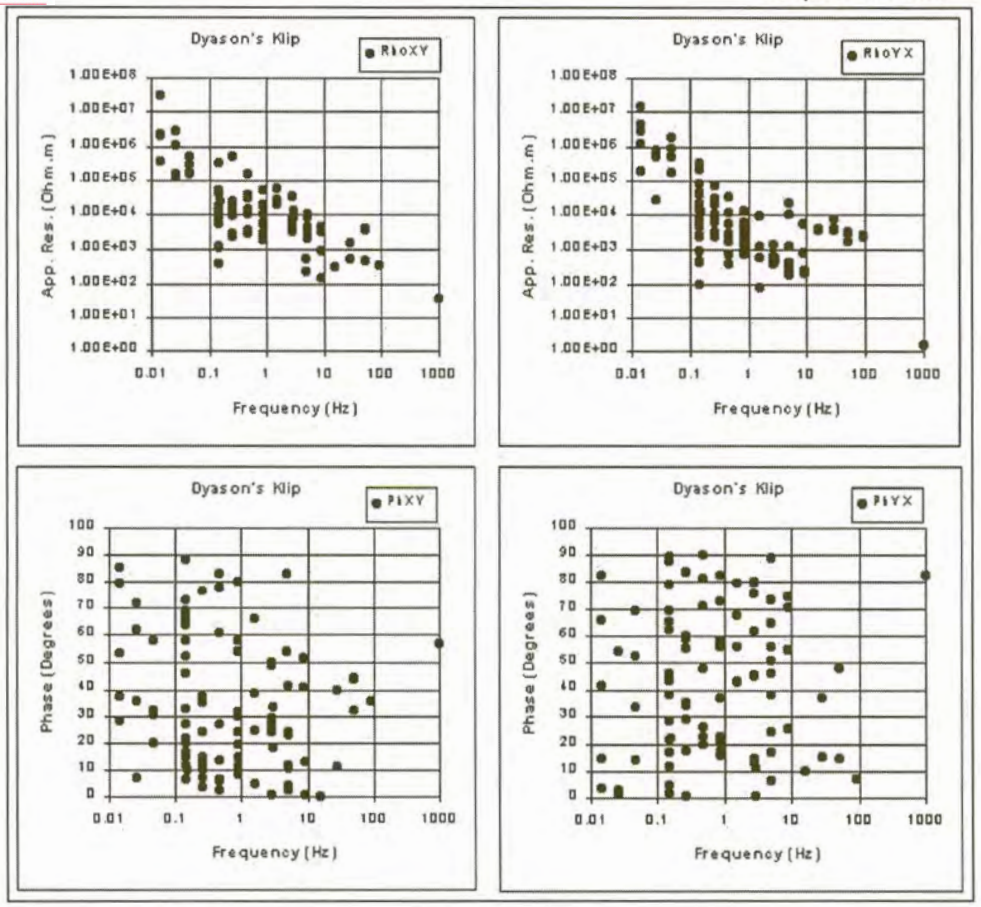

Figure 6.23(a). Apparent resistivity and impedance phase versus frequency curves for Dyason's Klip.

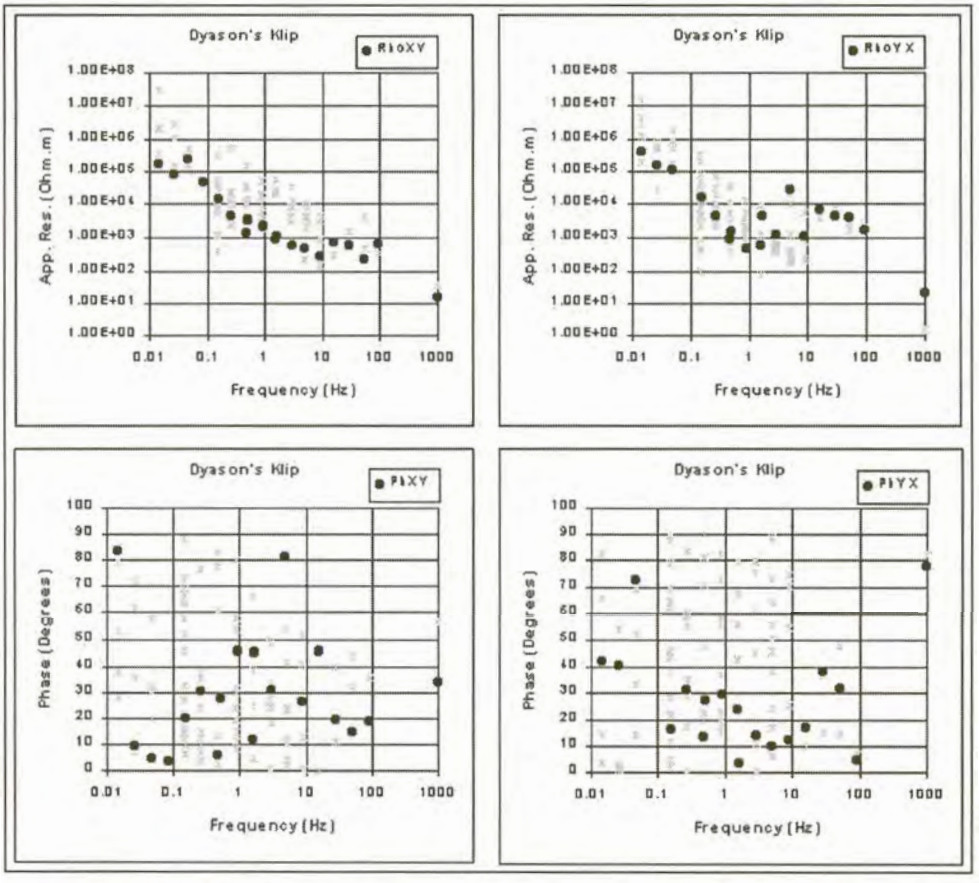

Figure 6.23(b). Curves estimated for Dyason's Klip using L_1 norm reduction.

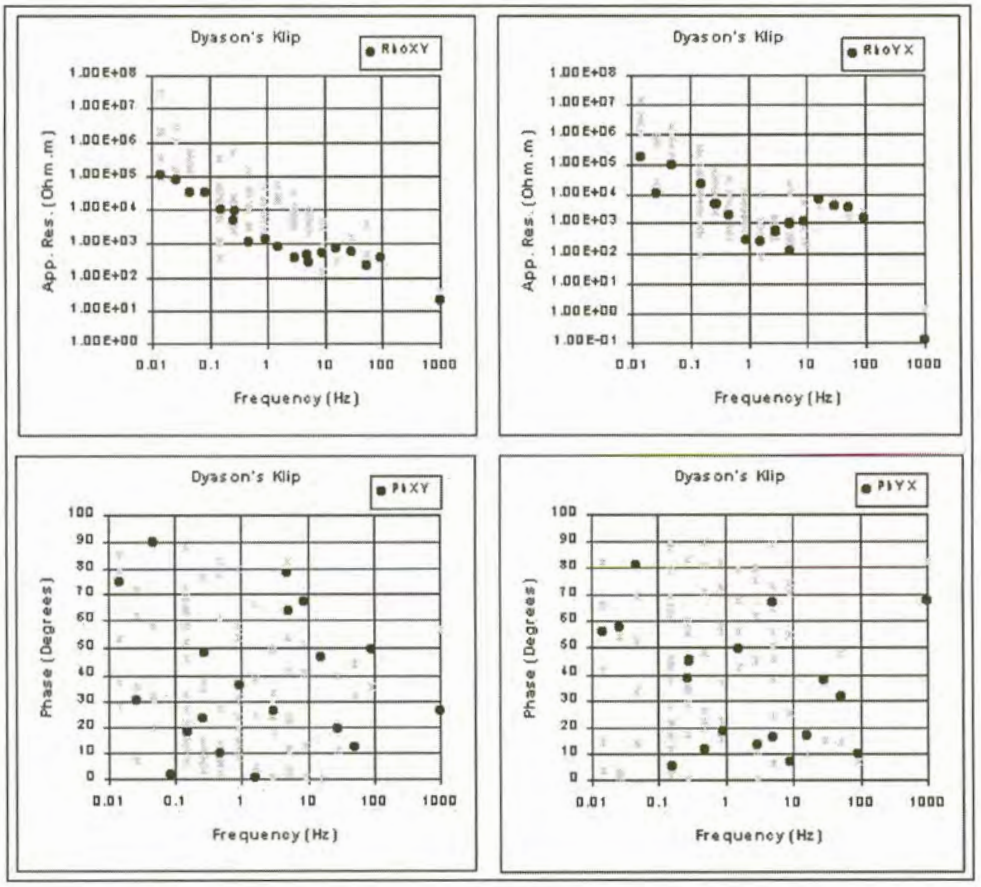

Figure 6.23(c). Curves estimated for Dyason's Klip using least squares reduction.

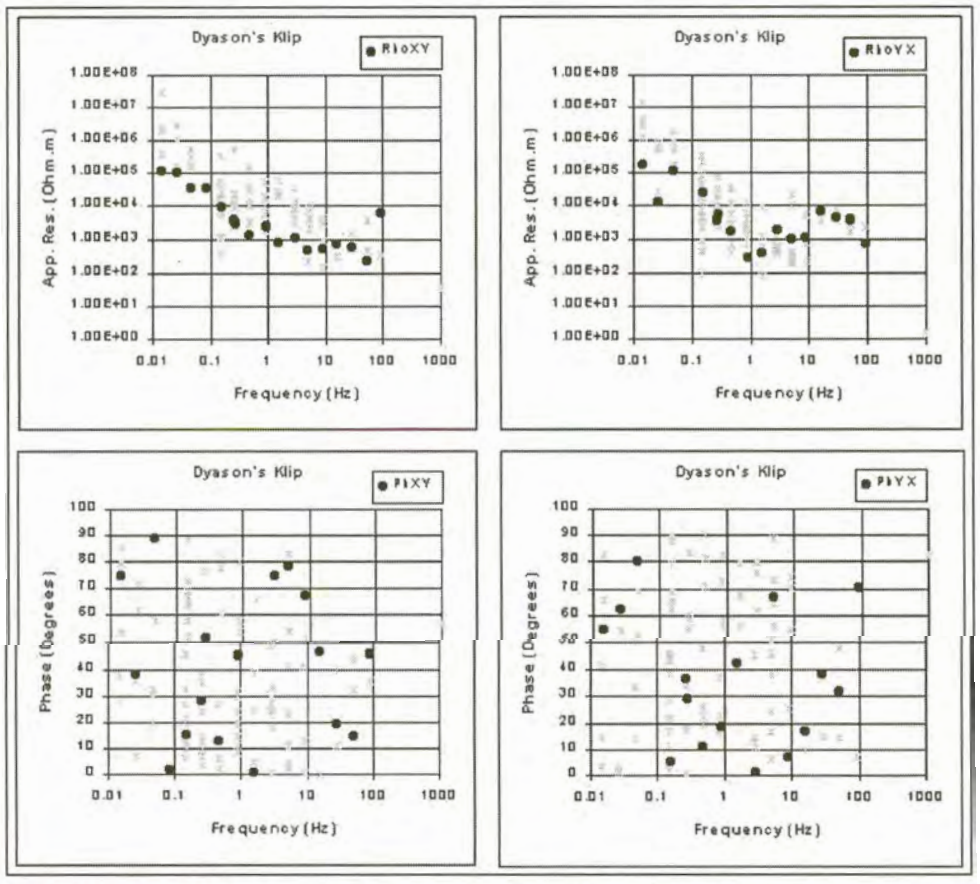

Figure 6.23(d). Curves estimated for Dyason's Klip using robust M-estimation.

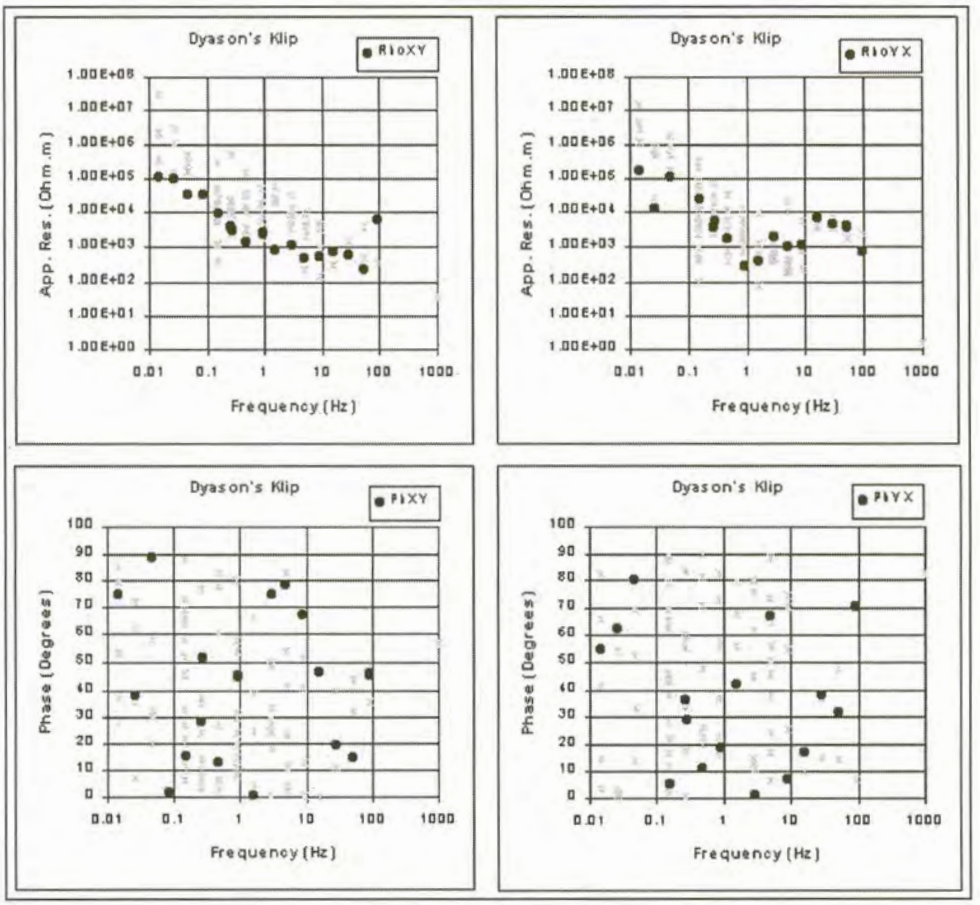

Figure 6.23(e). Curves estimated for Dyason's Klip using adaptive L_p norm reduction (Sposito et al., 1983).

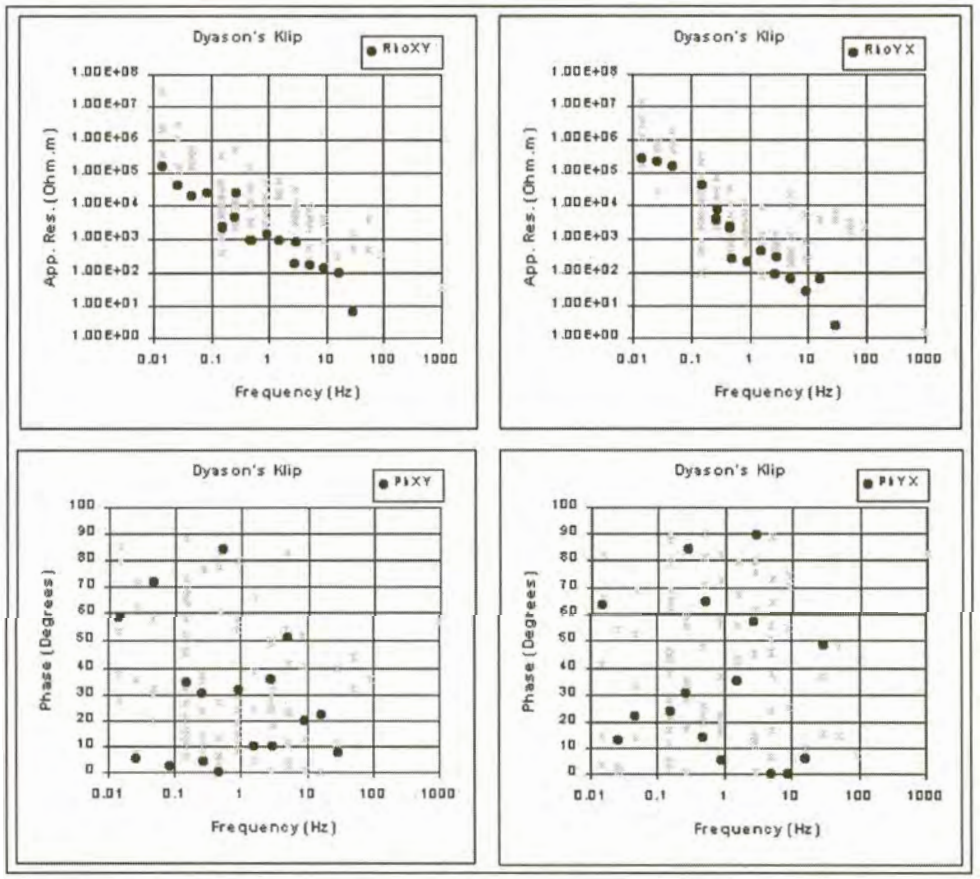

Figure 6.23(f) Curves estimated for Dyason's Klip using adaptive L_p norm reduction (Money et al., 1982).

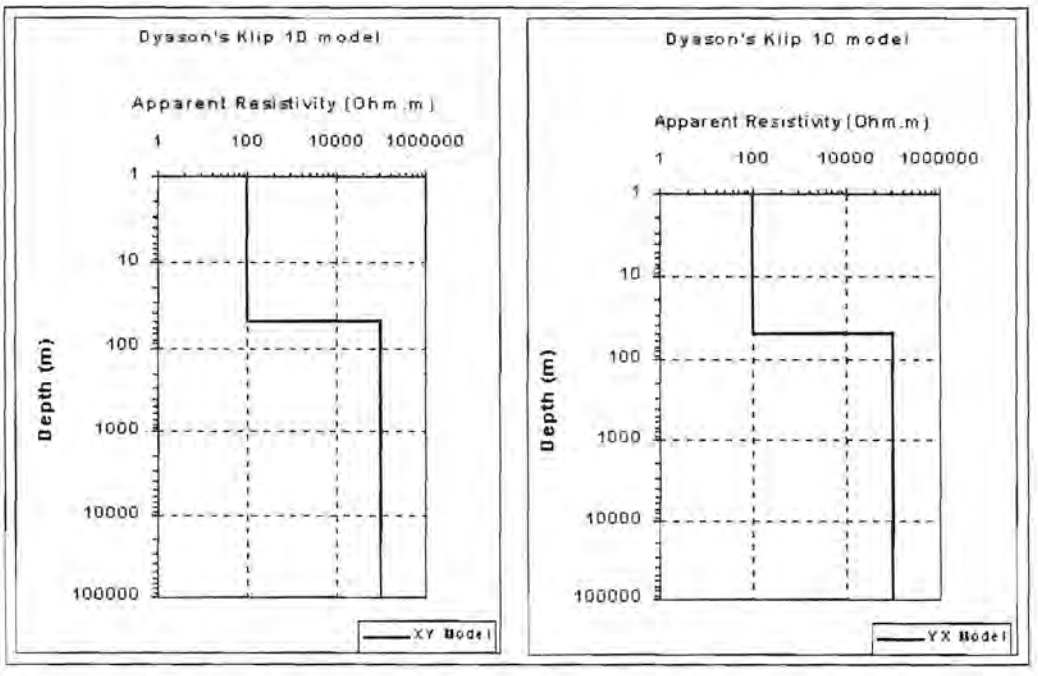

Figure 6.24 One dimensional models for Dyason's Klip.

6.4. TWO DIMENSIONAL MAGNETOTELLURIC MODEL

Figure 6.25 shows the two dimensional magnetotelluric model constructed along the Sishen-Keimoes line. The highly resistive material (20 000 Ωm) represents the basement material. A conductive zone (100 Ωm) separates the basement rocks from less resistive (6700 Ωm) material. It may be caused by conductive seafloor material wedged between resistive cratonic material in the east and a more fractured terrain in the west.

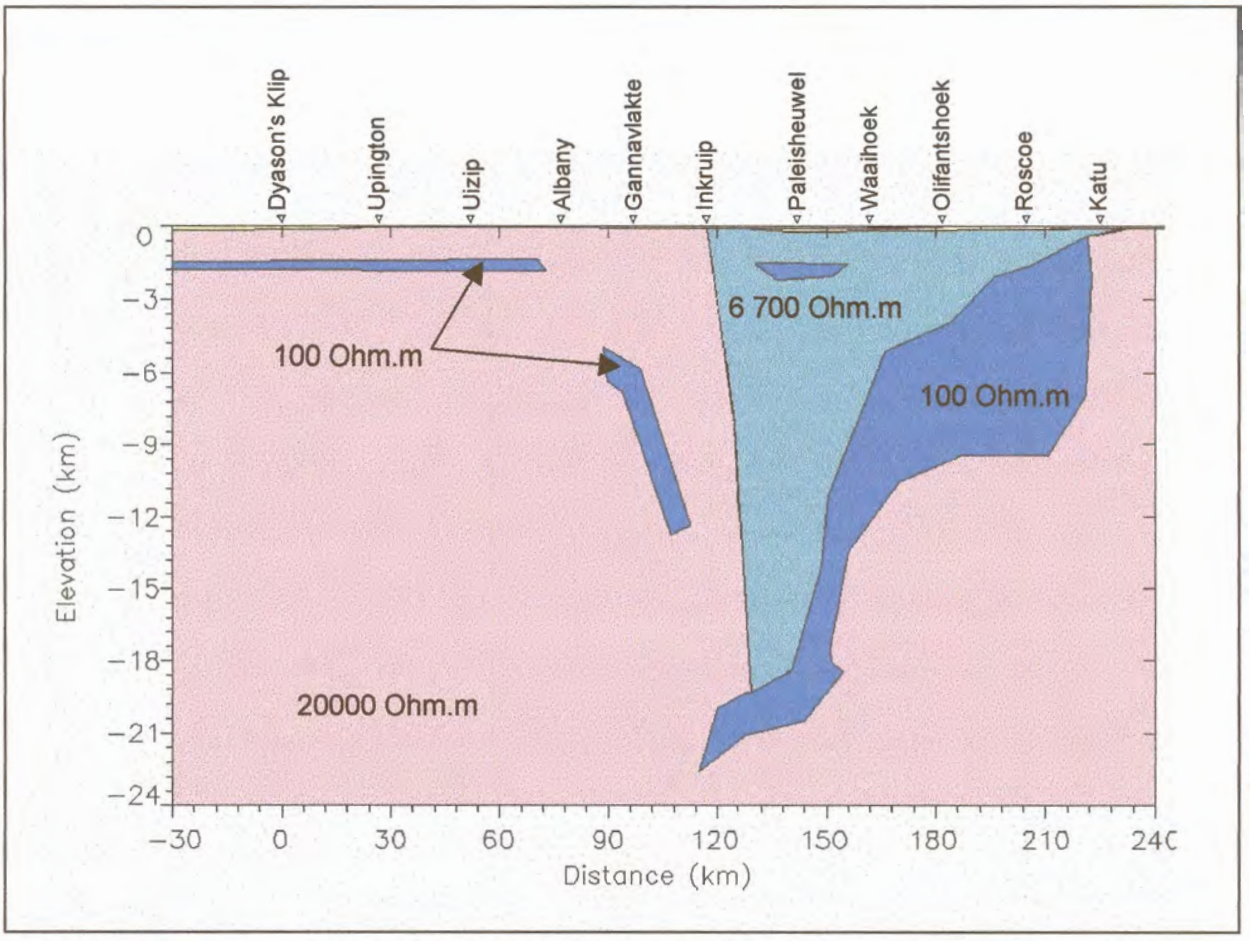

Figure 6.25. Two dimensional model constructed from the magnetotelluric data.

6.5. GRAVITY DATA

Gravity data covering the region of interest (Figure 6.26) were extracted from the regional gravity data set that covers the whole of South Africa. The data were collected at roughly one station every 10 – 12 km^2. Additional measurements were made every 0.5 km along the seismic route. Gravity measurements were conducted with La Coste and Romberg gravimeters and elevations were determined by micro-barometers. Bouguer anomaly values were calculated assuming a mean density of 2670 kg/m^3. The measurements were tied to the International Gravity Standardisation Net values (Morelli et al., 1974) and were referred to the gravity formula based on the 1967 geodetic reference system (Moritz, 1968). A maximum error in a regional Bouguer

anomaly value is calculated by combining an inaccuracy of ~ 2m (~4 gravity units) in the barometrically determined elevation with a maximum error in the observed gravity of 2 g.u. and a positional error of 150m in a north south direction (1 g.u.). This worst case error amounts to approximately 7 g.u.

The data are not terrain corrected since the area is mostly flat. Isostatic equilibrium exists in this area.

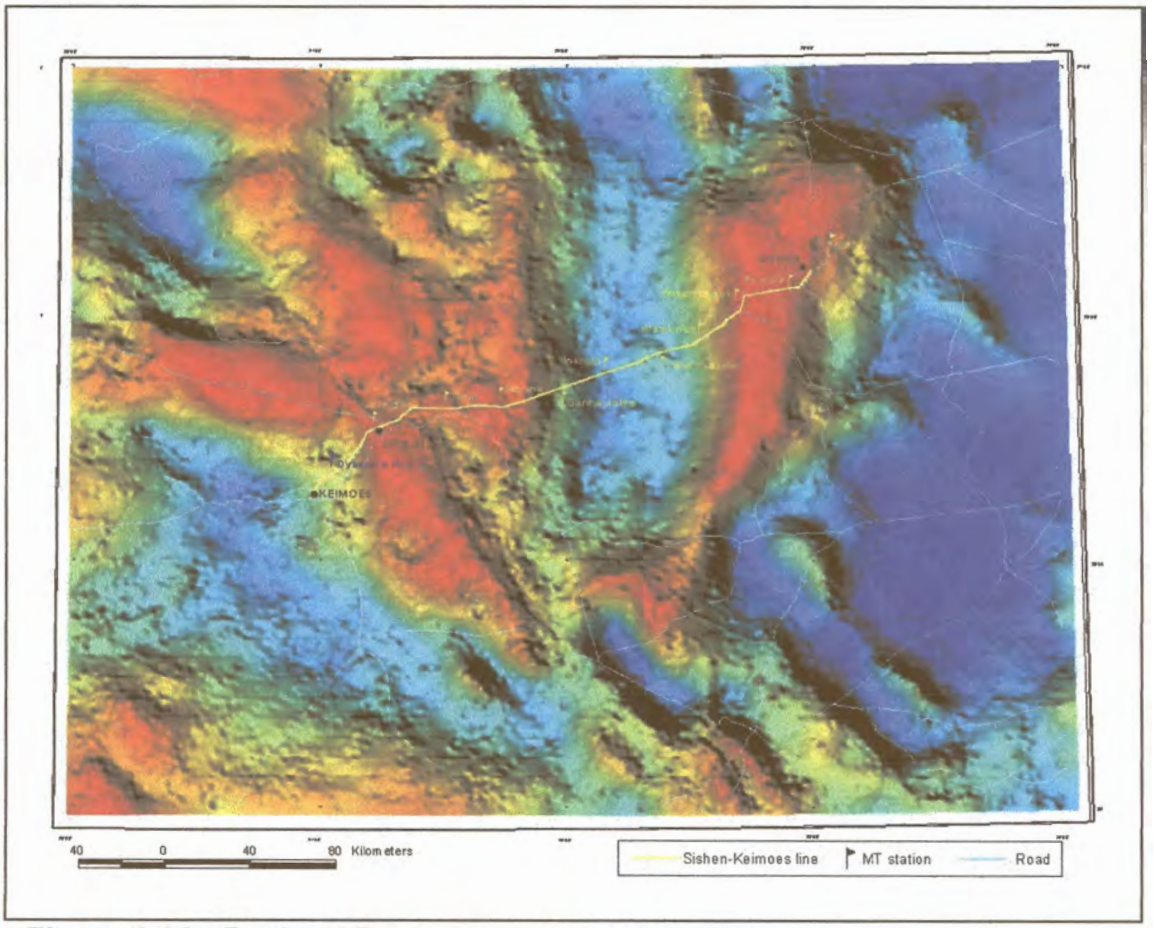

Figure 6.26. Regional Bouguer anomaly map.

Bouguer values were extracted along the road between Sishen and Keimoes and modelled (Figure 6.27). A regional field representing a horizontal line through the minimum of the Bouguer anomaly values was removed. This line would reflect the Bouguer values if only granitic crust of 2670 kg/m^3 was present.

The model shows a thick succesion of dense material in the east. Dense material of the Transvaal and underlying Ventersdorp Supergroups can only

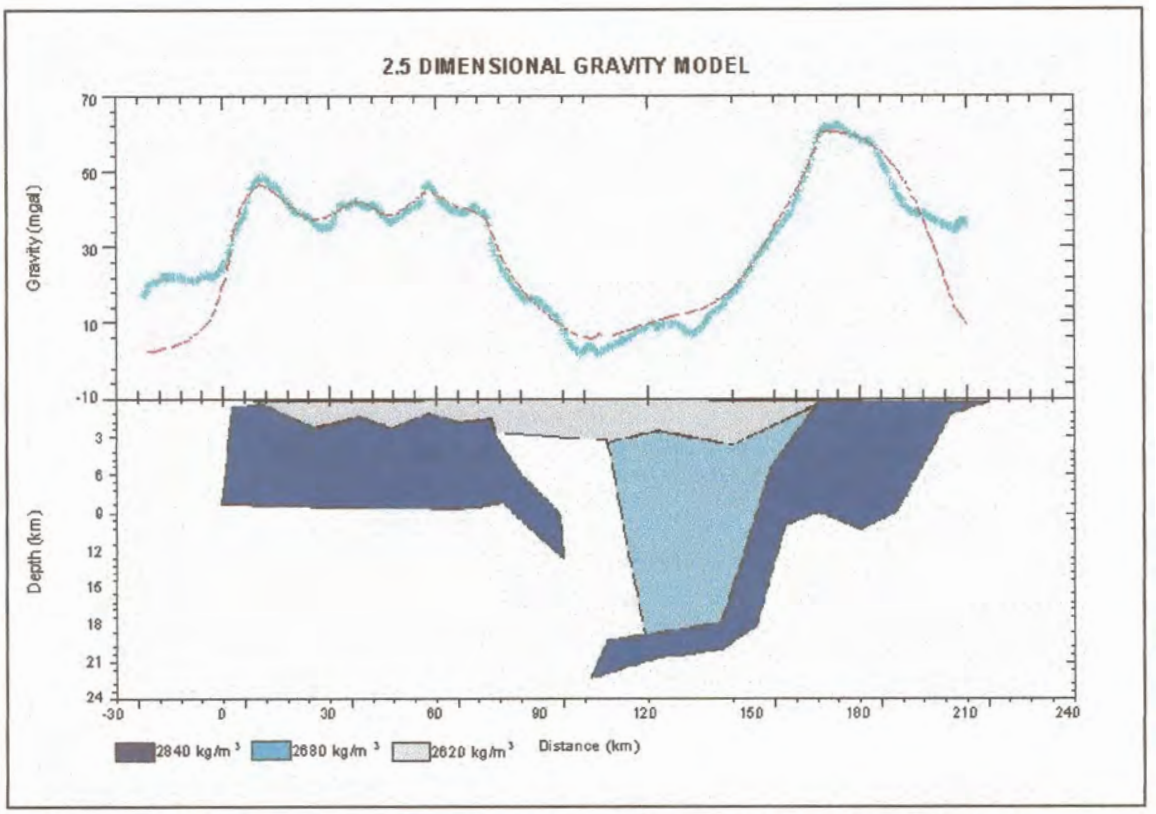

Figure 6.27. Two dimensional model constructed from the gravity data.

account for approximately the top five kilometres of this dense unit. The 2680 kg/m^3 material to the west of the dense body can be attributed to the metamorphosed Kheis basement, or dense units in the granitic Kheis material. A dense body in the west correlates with metamorphosed material belonging to the Namaqua Metamorphic Complex. Olifantshoek Supergroup sediments may constitute the less dense cover.

6.6. MAGNETIC DATA

The aeromagnetic data (Figure 6.28) was collected at a height of 100 ± 15 metres and a 1 km line spacing. The cycling time of the magnetometer was 1 second that, at an aircraft speed of 250 km/h amounts to a total magnetic field measurement about every 63m.

Highly magnetic banded iron formation and jaspillite of the Transvaal Supergroup are partly responsible for the prominent anomaly in the east (Figure

6.29). Similar to the gravity model, the causative body extends to a much greater depth that can be explained by the known geology. The 0.008 cgs units in the centre may be greenstones of the Wilgenhoudtsdrif Group. A highly magnetic body in the west cannot be explained by the mapped geology and is probably related to the Namaqua Metamorphic Complex.

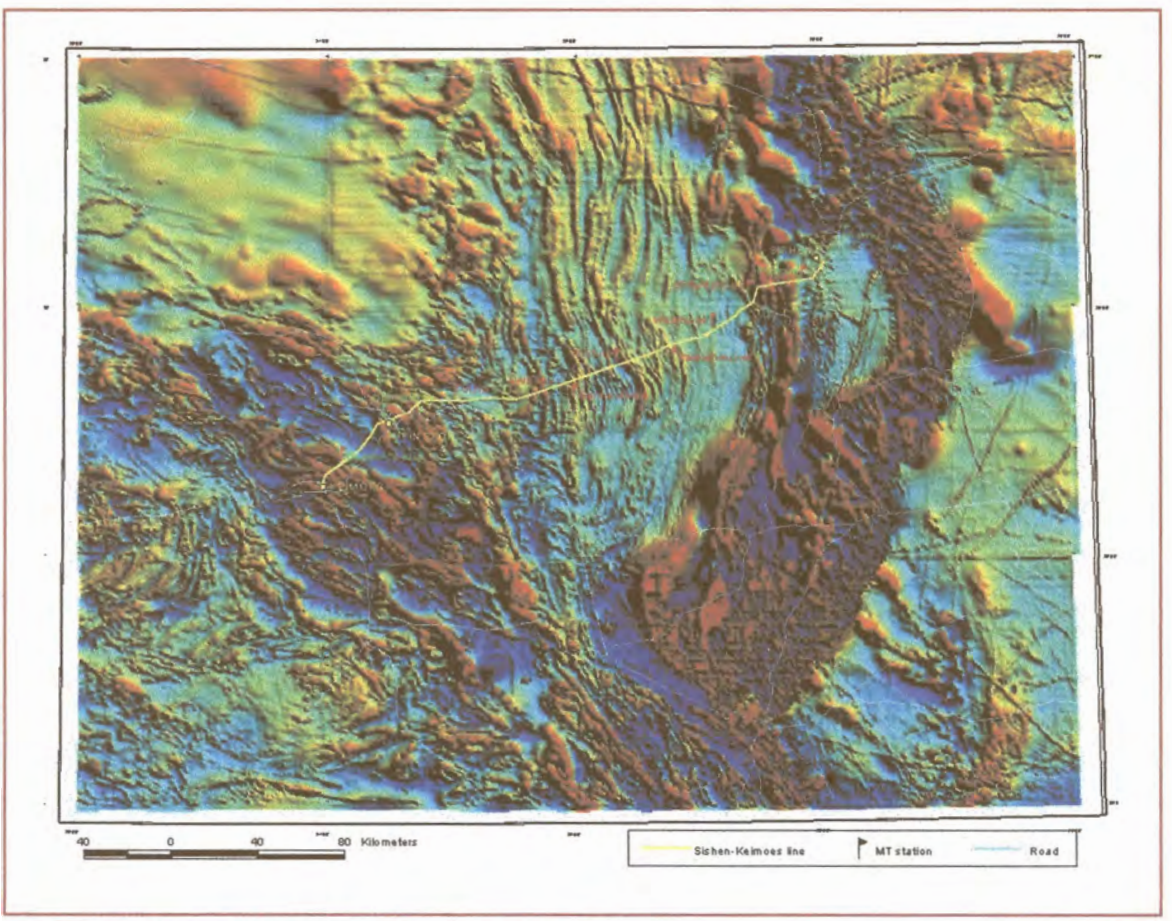

Figure 6.28. Total field aeromagnetic data.

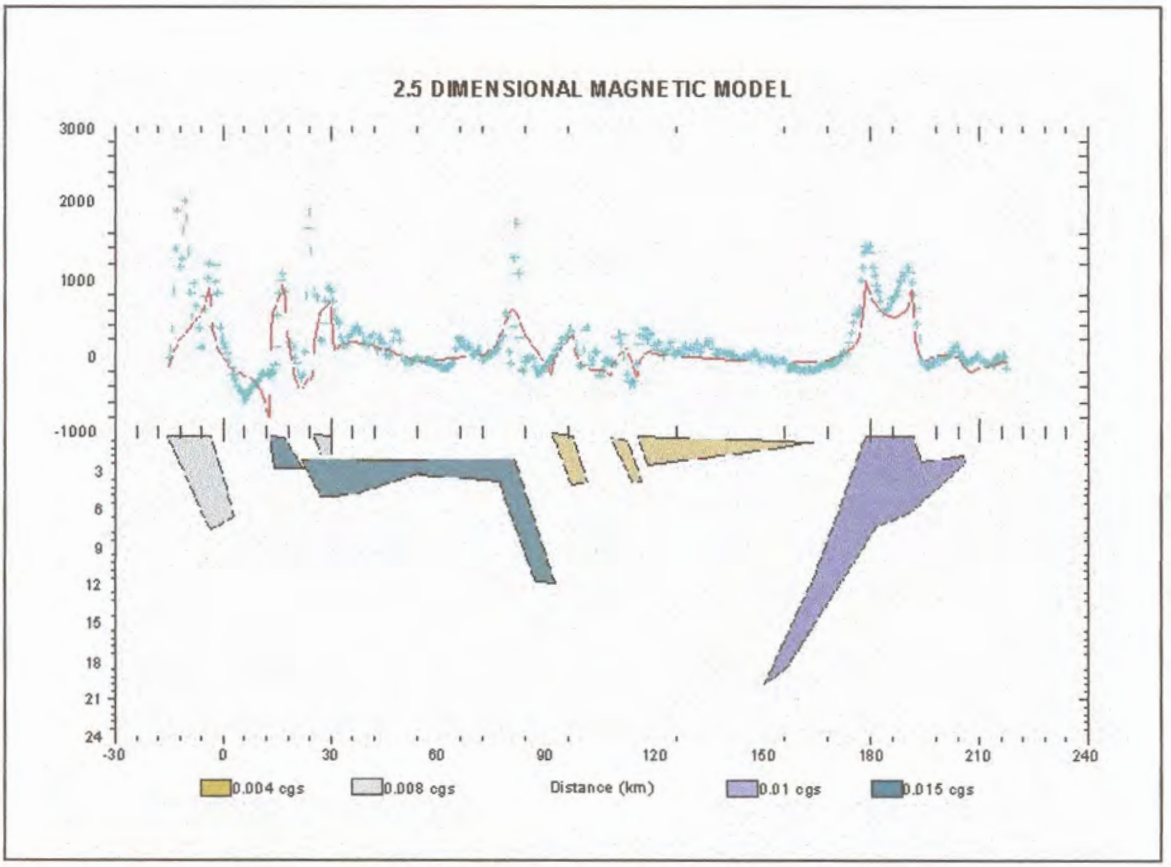

Figure 6.29. Two dimensional model constructed from the magnetic data.

6.7. DEEP REFLECTION SEISMICS

Figure 6.30 shows the migrated deep reflection seismic line recorded between Sishen and Keimoes. The major reflectors are highlighted. The distinct package of dipping reflectors visible on the eastern side of the record can only partially be explained by the Ventersdorp and Transvaal Supergroups. Elongated lens-like reflector packages may indicate thrusting at the edge of the Kaapvaal Craton. Doubling of the crustal layers by thrusting could explain the extensive reflector package. Alternative explanations may be a layered intrusion or an ophiolitic complex introduced by thrusting. Moving westward there is a dramatic decrease in the number of reflectors, and those that do occur dip in the opposite direction. These reflectors may be related to the boundary between the accreted Kheis Province in the east and the Rehoboth and Namaqua Terranes in the west.

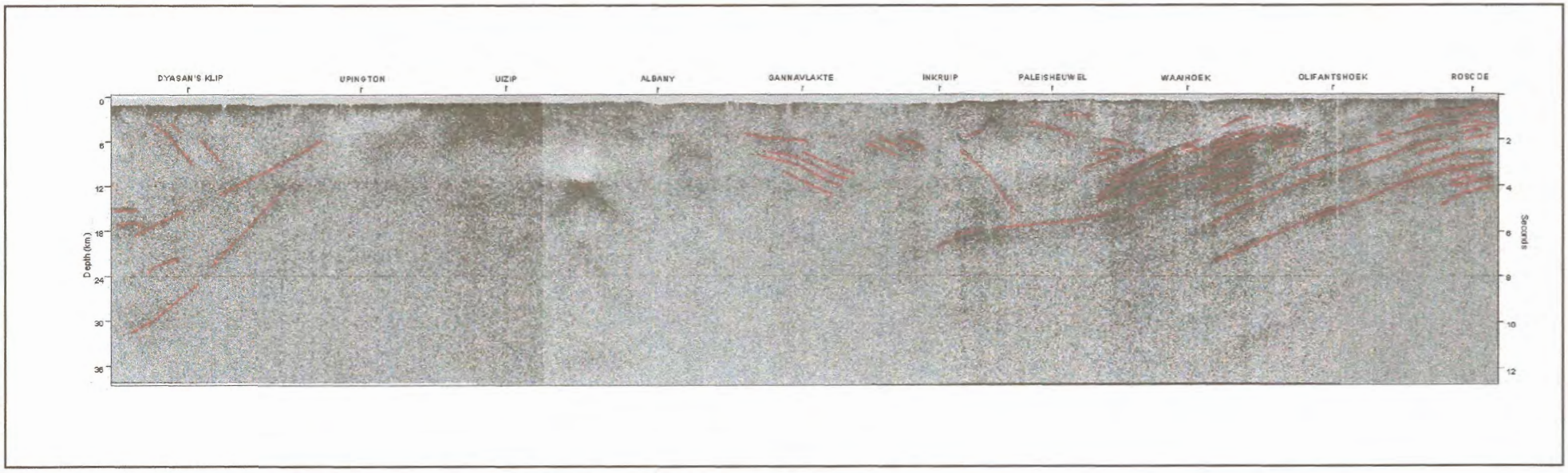

Figure 6.30. Deep reflection seismic section along the Sishen – Keimoes line.

6.8. SYNTHESIS

Considering all the geophysical interpretations we observe the following going from east to west :

(1) The westward dipping reflectors in the east correlate very well with the dense and conductive bodies present on the gravity and MT models. The top halve of the magnetic unit coincides with the dense and conductive bodies.
(2) The 2680 kg/m^3 and 6 700 ohm.m bodies west of the dense, conductive material coincide and their western edges line up with an eastward dipping reflector. We also note the absence of magnetic material in this area at greater depths.
(3) The top part of the dense body in the west correlates with highly magnetic material. At the eastern edge of the dense body, an eastward dipping lobe correlates with a similarly sloping part of the magnetic unit, conductive material and seismic reflectors.
(4) Shallow magnetic and conductive material overlap in the area between Paleisheuwel and Waaihoek.

Lense-shaped reflectors in the eastern reflective package may point to thrusting that took place at the western edge of the Kaapvaal Craton. Thrusting could result in stacking that would explain the thickness of the reflector sequence. Changes in the characteristics of the seismic, gravity and magnetotelluric data west of these reflectors are attributed to the transition to a different crustal terrane. The dense, conductive material that coincides with the reflective package therefore possibly demarcates the boundary between the Kheis Tectonic Province and the Kaapvaal Craton. This material is interpreted to be an ophiolitic sequence emplaced into an accretionary wedge that formed between the Kheis and Kaapvaal Craton during a proposed collisional event (1.75 Ga).

The eastward dipping dense, conductive material and reflectors west of the Kheis Province may similarly be accounted for by subducted seafloor material at the western edge of the Kheis Province. Very little is known about the period

between the Kheis and Namaqua events and whether accretion took place during this period. An explanation for the dense material to the west of the Kheis Terrane is that it constitutes again obducted seafloor material. The outcropping Jannelsepan ultramafic schists are probably a manifestation of this dense unit. Alternatively, these bodies may be explained by material that intruded into weak or fractured zones in the Kheis basement.

CHAPTER 7

CONCLUSIONS

7.1. COMPARISON OF DIFFERENT STATISTICAL REDUCTION TECHNIQUES

Applying different statistical reduction techniques to magnetotelluric data collected at eleven stations in the Northern Cape yielded disappointing results in many instances. The following points were noticed:

- For bad quality data, robust M-estimation and the adaptive L_p norm technique using Sposito et al's (1983) equation to calculate the value of p gave better results than L_1 -, L_2 – and adaptive L_p norm (using Money et al's (1982) equation) methods. Robust M-estimation was, however, superior in most of the cases albeit by a very small margin.
- For better quality data, all techniques gave similar results, with robust M-estimation and the adaptive L_p norm technique using Sposito et al's (1983) equation to calculate the value of p again somewhat better.
- The adaptive L_p norm method technique using Money's equation to calculate the value of p generally gave very bad results.

The effectiveness of the statistical techniques is dependent on the quality of the data. It is important to point out that the quality of the data used in the study was not always very good. Data were collected in batches between 1991 and 1998. During this period the acquisitioning system was in its main developmental phase and improvements were continuously made in an attempt to minimise electrical noise introduced by the equipment. The quality of data collected most recently (stations Albany, Uizip, Upington and Dyason's Klip) is significantly better than data collected earlier. As a consequence, statistical reduction techniques yielded better results for these stations.

7.2. COMPARISON OF MT RESULTS WITH RESULTS FROM OTHER GEOPHYSICAL METHODS

The magnetotelluric method was able to detect a conductive body that coincides with the western edge of a reflector package recorded on deep seismic reflection data. Bouguer anomaly data show a dense body at the same location. The magnetotelluric data provided valuable additional information that concurred with the other geophysical data and aided in gaining a better understanding of the geological structure of the area.

Given the high cost associated with deep reflection seismic surveys, it might be economically viable to do a magnetotelluric survey in addition to eg. gravity and magnetic surveys prior to embarking on a seismic survey. In this way areas of special interest may be identified and more intensive geophysical investigations can be localised to these areas. A magnetotelluric survey costs in the region of R10 000 a station.